Numerical Analysis of Collision Models in 2D Particulate Flow

---

Dissertation
zur Erlangung des Grades eines
Doktors der Naturwissenschaften

Der Fakultät für Mathematik der
Technischen Universität Dortmund
vorgelegt von

Kamran Usman

Numerical Analysis of Collision Models in 2D Particulate Flow

Kamran Usman

Dissertation eingereicht am: 07. 07. 2013
Tag der mündlichen Prüfung: 09. 10. 2013

Mitglieder der Prüfungskommission

Prof. Dr. Stefan Turek (1. Gutachter, Betreuer)
Prof. Dr. Dmitri Kuzmin (2. Gutachter)
Prof. Dr. Christian Meyer
Prof. Dr. Matthias Röger
Dr. Abderrahim Ouazzi

Dedicated to my loving parents

Acknowledgements

I am sincerely grateful to my supervisor Prof. Dr. Stefan Turek, for his support, encouragement, and motivation throughout my research work which enabled me to develop an understanding of the subject. As my teacher and mentor, he guided me into the wonderful world of scientific research. I am greatly indebted for his availability, inspiration, criticism and optimism while keeping an enjoyable working atmosphere. His professional and editorial advice was essential for the completion of this thesis. I thank him for sharing with me his unstoppable taste for turning ideas into practical innovations.

I would like to express my appreciation to R. Münster, D. Anca and Dr. D. Wan. They paved the way for me during the initial phase of my PhD studies to deepen my understanding of the particulate flow problems and implementation of the numerical techniques to treat such problems.

Reflecting back on this enjoyable and painful PhD journey, my experience at TU Dortmund would not have been such a pleasurable one without the presence of all the people working here. I would like to express my heartiest regards and blessings to people like S. Buijssen, C. Becker for administrative support, B. S. Hosseini and M. Klinger for sharing and bearing me in same room time to time and all those people who helped, supported and accompanied. I would also like to thank Dr. D. Kuzmin for offering series of lecture on CFD related topics and his availability and willingness for discussions. My thanks will go also to Dr. A. Ouazzi and Dr. M. Razzaq who shared wonderful thoughts on scientific and non scientific topics and for there thought provoking discussions on academic as well as socio-political issues radiantly.

I am unable to find appropriate words to say thanks to my parents. They emphasized, took care and provided an atmosphere so that I can spent my time on education, sports and tourism equally. They are always with me in every endeavour, without their moral support and patience it would have been much harder to keep up the motivation to finish this thesis.

Finally, I would like to express my gratitude to the Higher Education Commission (HEC) of Pakistan for providing the funding for my PhD project and giving me an opportunity to work in a scientific atmosphere.

Dortmund, July 06, 2013

Kamran Usman

Contents

1

Introduction

Solid particles in liquids (fluids) can be found in many natural processes such as interaction of the offshore structures with the ocean current, mixing and sedimentation in estuary, wind blown sand particles in deserts or dust particles in air, lava flow etc. Slurry flow, paper pulp, food products and dust particle clogging have a wide range of applications from the industrial point of view. Inhaled smoke particles, particle transport, dispersion, filtration, melting and solidification, aggregate formation, particle deposition from petroleum fluid flow and peristaltic transport of solid particles in fluid during biological processes have been the subject of a great amount of research with contributions coming from engineering, chemistry, biology, physics and mathematics. Particulate flows are quite hard to simulate from a numerical point of view as they require, in many cases, frequent generation and deformation of the computational grids when the particle boundaries are complex and changing (rotating and translating) over time. For the case with large number of particles, the interaction between fluid and particles and inter-particle collisions gives further complexity to the problem.

Numerous algorithms have been developed for the numerical solution of particulate flows such as penalty based methods [47], discrete element models (DEM) [34, 35, 40], population balance based models [7, 12], distributed Lagrange multiplier (DLM) fictitious domain methods [18, 38, 50] and level-set methods [36, 39]. Such problems can be broadly classified into two families. The first one is an Eulerian approach in which a fixed mesh (or a mesh independent of particles) is used. This mesh covers the whole domain occupied by the fluid. One popular example of such an approach is the distributed Lagrange multiplier (DLM)/fictitious domain methods proposed by Glowinski, Joseph and coauthors [18]. The second type is based on a Lagrangian approach such that a moving mesh follows the motion of the boundary of the particles in fluid. This approach is referred to as Arbitrary Lagrangian Eulerian (ALE) [21, 31, 43, 44, 57, 61]. Eulerian approaches have a big advantage over Lagrangian approaches because the mesh remains unchanged, saving/decreasing the CPU cost per time step (less computational effort is required) and saves the expensive mesh generation, but the resulting accuracy is often not clear. Therefore, in all the methods, the overall aim is to deal with the moving boundaries in the fluid successfully such that the numerical approximation is sufficiently high and the computational cost is also acceptable at the same time.

In Eulerian approaches, the fluid-particle domain is based on a (FEM [11, 17]) background grid. The Newton-Euler equations model the motion of the solid particles. Boundary conditions applied at the interface between the fluid and the particles are treated as an additional constraint to the governing Navier-Stokes equations and the fluid domain is extended into the whole domain covering both fluid and particle domains. The FBM is started with a coarse mesh which may additionally contain the geometrical details of the solid particles and the boundary parametrization describing particles as well with regard to the boundary conditions. Hence, the particles are treated as interior objects and are solved iteratively in all solution steps. FBM allows the computational domain to remain fixed and does not require remeshing with time allowing it to be handled independently from the flow features [55, 60].

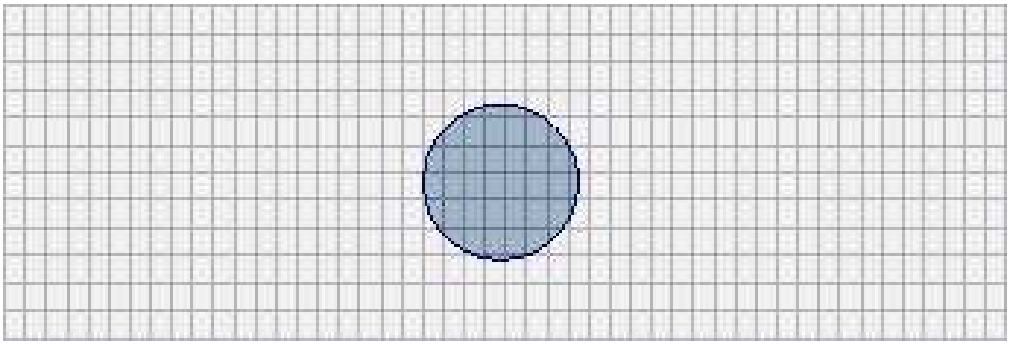

Figure 1.1: A circular particle in the fluid domain using an Eulerian grid.

Contrary to the Eulerian approaches, the ALE approach consists of a Lagrangian step such that the computational grid moves with the fluid-particle interface. The mesh is modified and remapped near the interface by allowing the mesh nodes to move with respect to the fluid and then is finally replaced with a new mesh and the whole solution is transferred to the new mesh. The grid is kept fixed away from the interface and the moving boundaries are tracked by the Lagrangian motion of the mesh nodes near the interface [21, 41, 42, 57].

The DEM [40] approach is also used for the computation of granular flow, powder mechanics, soil and rock mechanics. In DEM granular materials are treated as a collection of independent elements interacting with each other using different models for cohesive forces. The DEM is also closely related to molecular dynamics (MD). For example, in the case of granular materials the properties of the particles and their interaction laws are collectively used in the DEM approach which form a dissipative many-particle system. In DEM, constitutive relations are derived to describe the micro-macro transition of the macroscopic (granular) material considered as a continuum [28].

Another method to model bubbles or droplets in solvent, aggregate formation and adhesive particles is the Population balance model [3], combined with CFD [52], which was proposed by Smoluchowski in 1917. In this method a rate equation for particles collision is defined which leads actually to a mass balance problem [7, 12].

In case of more than one particle in the fluid, a collision model is required to prevent particles from inter-penetrating each other. Collisions or near-collisions between the particles produce severe difficulties in the direct simulation of particulate flows. Even if particles are very near to each other then the cost of simulation is significantly increased, because for the simulation of particle-particle interaction mechanisms in a direct manner, the flow fields have to be resolved accurately in the narrow gap between the converging particle surfaces. In Lagrangian approaches the corresponding element size has to be reduced which leads to extremely small elements and thus increases the number of unknowns to be solved for. Numerical problems are likely to occur in such simulations when two or more particles get very close to each other, i.e. the mesh has to be refined in the gap zone between the particles, making it computationally expensive. To handle this problem numerically, different collision models have been proposed in the literature. Such as repulsive force models [59], lubrication collision models [33], conservation collision models (conservation of linear momentum and kinetic energy) [63], stochastic collision models (physical properties of the particle) [51], semi-experiential collision models, etc.

Out of the many methods to compute particulate flows such as discussed above, based on an embedding of the solid particles in a global domain which is covered by a background Cartesian mesh [20] and the other class of methods which uses a conforming mesh of the fluid domain [22, 30], faces the problem of particle overlapping and makes the computations difficult to simulate and expensive. In [22], the mesh is refined in the neighborhood of the approaching particles to approximate the lubrication forces with high accuracy.

Indeed, for regular external forces there cannot be any particle-particle contact in finite time, as the particle-particle force between two smooth objects separated by a viscous fluid acts as $-\frac{\varepsilon'}{\varepsilon}$ [32, 45], where ε is the distance. A commonly used strategy to keep the particles apart consists in adding short range repulsive forces between the approaching particles, which prevents particles to overlap [18]. Those methods have proved to be very efficient and behave quite satisfactorily in many situations, but they require fine tuning of some numerical parameters to control the minimal distance between the bodies. One example of this method is the collision model proposed by Maury [33] which gives a first order approximation of the lubrication forces exerted by the fluid in the inter-particle gap. Wan and Turek have also used a repulsive force collision model [59] to keep the particles at a safety distance in particulate flow simulations. Mostly, these repulsive force collision models introduce new constraints on the time step, the distance between particles and some depends on physical properties of the fluid and particles. One approach presented by Maury [32] in which the minimal distance between particles is controlled by running a minimization procedure (at each time step) on a global functional of the particle positions, such that the corresponding minimal distance is greater than a preset safety distance $\varepsilon > 0$. This method has proved to be very efficient even for the case of large number of particles.

1.1. Motivation and Research Objectives

The present work was motivated by the necessity to handle particle collisions in the direct simulation of particulate flow. In direct simulations, particles are treated individually, and the Navier-Stokes equations are solved separately in the domain occupied by the fluid. Many methods which have been proposed to compute such flows face the problem of body overlapping. Particularly in case of a large number of particles, it becomes difficult to maintain the particles at some distance and to estimate a minimal collision force such that this force does not behaves unrealistically and at the same time this collision force should also be respectful of the underlying physics. Additionally, in case of a large number of particles in the fluid, the interaction between fluid and particles as well as the collisions between particles become more complex and the simulation becomes highly expensive to compute and difficult to keep particles from overlapping. Our aim is to investigate

different collision models for the particulate flow which can prevent the particle collisions as well as these collision models do not affect/disturb the physical behavior of the particulate flow.

1.2. Thesis Contributions

The contributions made to the thesis comprise of examining, analyzing and validation of collision models in particulate flow problems. After the analysis of different collision models using MATLAB, these collision models were coupled and integrated into the software FEATFLOW [53] and tested using benchmark problem. Comparison regarding the efficiency of the different collision models is described running some tests. These collision models were modified for the case of non-circular particles (general shape particles). Later many applications for the particulate flow were simulated including many particles sedimentation, particles in Annulus and particles in Driven cavity.

1.3. Thesis Outline

In the following, we give a brief overview of each chapter and summarize the arrangement of different parts of the thesis.

In Chapter 2, the governing equations for the coupled system of fluid and particles are given. The motion of the particles in the fluid is described using the Newton-Euler equations. An overview to find the hydrodynamic forces and the particle-particle and particle-wall forces acting on the particle are presented. Finally, we explain some techniques to deal with the non-circular particles.

Collision models which were investigated and examined in the work are discussed in Chapter 3 to deal with the collision of particles in the fluid. Repulsive force collision model and a lubrication collision model (distance based and velocity based) are described. A minimization method to find the new velocities of the particles after collision is given. The extension of the minimization procedure to get a sticky particle model is also explained. In the end, a collision model based on the conservation of linear momentum is discussed.

The fictitious boundary method (FBM) to couple the fluid and particle system is discussed in Chapter 4. A strategy to integrate boundary conditions with FBM and calculation of hydrodynamic forces acting on the particle is explained. A flow chart diagram is presented to show the whole FBM steps.

After analyzing and examining the collision models the characteristics and results of these models are presented in Chapter 5. Two circular particles, many circular particles, general shape particles, particles in an Annulus and particles in a lid driven cavity are simulated and results are presented.

Conclusion and future work for the thesis is presented in Chapter 6.

2

Mathematical Modeling

In this chapter, we will discuss the mathematical modeling for the governing Navier-Stokes equations along with the moving particles in the fluid. The equations for the hydrodynamic forces acting on the particle and the collision forces arising due to the particle-particle and particle-wall interactions will be discussed.

Consider N particles of mass M_i $(i = 1, ..., N)$ in an incompressible fluid with density ρ_f and viscosity ν. We denote $\Omega_f(t)$ as the domain occupied by the fluid and $\Omega_i(t)$ as the domain occupied by the ith particle at time t.

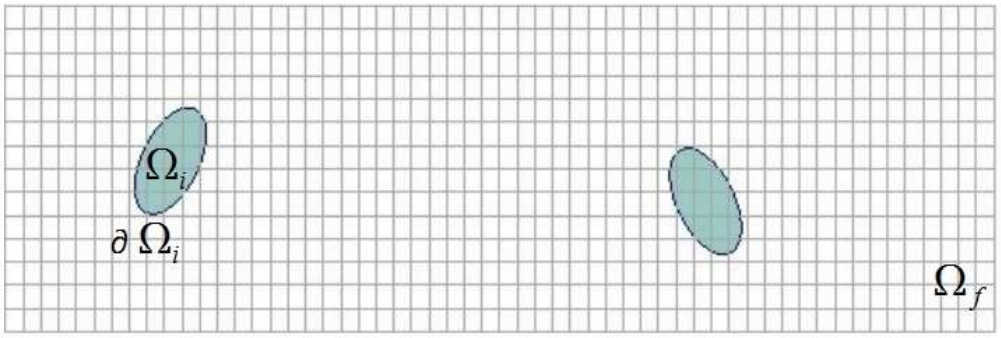

Figure 2.1: Rigid moving particles in fluid.

2.1. The incompressible Navier-Stokes Equation

2.1.1. Model of incompressible flow

The Navier-Stokes equations for the fluid in $\Omega_f(t)$ can be written as [2, 25, 54, 62]

$$\rho_f \left(\frac{\partial \mathbf{u}}{\partial t} + \mathbf{u} \cdot \nabla \mathbf{u} \right) - \nabla \cdot \sigma = 0, \quad \nabla \cdot \mathbf{u} = 0 \quad \forall t \in (0, T) \tag{2.1.1}$$

where σ is the total stress tensor in the fluid phase, given by

$$\sigma = -p\mathbf{I} + \mu_f \left[\nabla \mathbf{u} + (\nabla \mathbf{u})^T \right]. \tag{2.1.2}$$

Here, p is the pressure, $\mathbf{u}$ the fluid velocity and $\mathbf{I}$ is the identity tensor. Let us denote $\Omega_T = \Omega_f(t) \cup \{\Omega_i(t)\}_{i=1}^N$ as the entire computational domain which is independent of t. We can impose Dirichlet- and Neumann-type boundary conditions on the outer boundary $\Gamma = \partial\Omega_f(t)$. We denote $\Omega_f = \Omega_f(t)$ and $\Omega_i = \Omega_i(t)$ dropping t in all the following notations, since these quantities are always depending on t.

2.2. Solid Particles in Fluid - Multiphase Flow

2.2.1. Model of particle motion

Particles in the fluid can translate and rotate due to the forces acting on them such as the gravity, hydrodynamic forces and collision forces due to particle-particle or particle-wall interactions [58]. The Newton-Euler equations that govern the motion of each particle are [58, 65]

$$M_i \frac{d\mathbf{U}_i}{dt} = (\Delta M_i)\mathbf{g} + \mathbf{F}_i + \mathbf{F}_i', \quad \mathbf{I}_i \frac{d\omega_i}{dt} + \omega_i \times (\mathbf{I}_i \omega_i) = T_i \tag{2.2.1}$$

where $\mathbf{U}_i$ denotes the translational velocities and ω_i denotes the angular velocities of the ith particle. $\Delta M_i = M_i - M_f$ gives the mass difference between the mass of particle M_i and the mass of the fluid M_f occupying the same volume, $\mathbf{g}$ is the gravity, $\mathbf{F}_i'$ are the particle-particle and particle-wall collision forces. Particles are assumed to be smooth and no tangential collision forces are acting on them. $\mathbf{F}_i$ denotes the resultant of the hydrodynamic drag/lift forces and T_i, the torque about the center of mass of the ith particle. The position $\mathbf{X}_i$ and angle θ_i of the ith particle can be obtained by the integration of the following kinematic equations [58, 59],

$$\frac{d\mathbf{X}_i}{dt} = \mathbf{U}_i, \quad \frac{d\theta_i}{dt} = \omega_i. \tag{2.2.2}$$

The velocity $\mathbf{u}(\mathbf{X})$, for any $\mathbf{X} \in \overline{\Omega}_i$, can be found by applying no-slip boundary conditions at the interface $\partial\Omega_i$ between the fluid and the ith particle, and is given by [58, 59]

$$\mathbf{u}(\mathbf{X}) = \mathbf{U}_i + \omega_i \times (\mathbf{X} - \mathbf{X}_i). \tag{2.2.3}$$

2.3. Hydrodynamic forces acting on the particle

The hydrodynamic drag and lift forces acting on the ith particle can be found by [45]

$$\mathbf{F}_i = (-1)\int_{\partial\Omega_i} \sigma \cdot \mathbf{n} d\Gamma_i, \quad T_i = (-1)\int_{\partial\Omega_i} (\mathbf{X} - \mathbf{X}_i) \times (\sigma \cdot \mathbf{n}) d\Gamma_i \tag{2.3.1}$$

where σ is the total stress tensor in the fluid phase defined by Equation (2.1.2), $\mathbf{X}_i$ is the position of the mass center of the ith particle, $\partial\Omega_i$ is the boundary of the ith particle, $\mathbf{n}$ is the unit normal vector on the boundary $\partial\Omega_i$ pointing outward of the flow region.

2.4. Collision Forces on the particle

The sum of all the repulsive forces acting on the ith particle due to other particles and the boundary/wall can be expressed by [57]

$$\mathbf{F}_i^{'} = \sum_{j=1, j\neq i}^{N} \mathbf{F}_{ij}^{P} + \mathbf{F}_i^{W} \tag{2.4.1}$$

where $\mathbf{F}_{ij}^{P}$ are the forces on the ith particle due to other particles and $\mathbf{F}_i^{W}$ is the repulsive force on the ith particle due to the wall. The methodology of finding these repulsive forces on each particle will be discussed in the following chapters.

2.5. Non-circular particles

Non-circular particles and particles of irregular shape in the fluid make complications due to their shape and requires extra numerical effort and certain features to be calculated for their representation. Collision models also need modifications for the calculation of collision forces acting on the surface of the non-circular particles.

2.5.1. Particle representation

Circular particles can be represented easily using their center and radius. Similarly some regular shapes such as elliptical, square and rectangular shaped particles can also be represented using basic quantities (center, radius/length and angle/orientation).

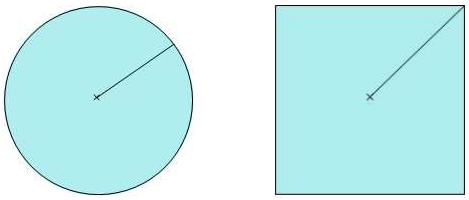

(a) Circle (b) Square

Figure 2.2: Regular shape particles

We consider the general shape particles as polygons. The particle surfaces are represented using a collection of data points which form the vertices of the polygon as shown in the Figure 2.3.

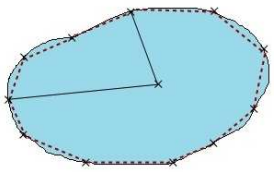

Figure 2.3: Irregular shape particle

Quantities such as center of mass, radius, volume and moment of inertia have to be calculated for the dynamics of the particles in the fluid. We describe the methods for the calculation of these quantities for the polygons in the next subsection.

2.5.2. Particle geometry

Let us consider a closed polygon with N vertices (x_i, y_i), $i = 0, ..., N-1$ such that $(x_0, y_0) = (x_N, y_N)$. We denote (X_c, Y_c) as the center of mass, A_p as the area and I_p as the moment of inertia of the polygon.

- *Radius:*
  R_{max} denotes the maximum of the distance between the center of mass and the vertices of the polygon and R_{min} denotes the minimum of the distance between the center of mass and the vertices of the polygon.

- *Area:*
  The area is given by [9]
  $$A = \frac{1}{2}\sum_{i=0}^{N-1}(x_i y_{i+1} - x_{i+1} y_i). \tag{2.5.1}$$

- *Center of mass:*
  The center of mass can be calculated using [9, 29]
  $$X_c = \frac{1}{6A}\sum_{i=0}^{N-1}(x_i + x_{i+1})(x_i y_{i+1} - x_{i+1} y_i), \tag{2.5.2}$$
  $$Y_c = \frac{1}{6A}\sum_{i=0}^{N-1}(y_i + y_{i+1})(x_i y_{i+1} - x_{i+1} y_i). \tag{2.5.3}$$

- *Moment of Inertia:*
  The moment of inertia is given by [9, 29]
  $$I_p = \int r^2 dm = \sum_i r_i^2 dm_i, \tag{2.5.4}$$
  where m is the mass of the body, r_i is the distance between the point mass dm_i (the mass m is divided into small point masses dm_i) and the axis of rotation.

3

Collision Models

If there are two or more particles in the fluid, a collision model is needed to prevent the particles from inter-penetrating each other [5, 8, 48, 64]. Theoretically, smooth particle-particle or wall-particle collisions cannot take place in finite time in the continuous system since the viscous fluid in the gap zone of colliding particles exerts repulsive forces (or lubrication forces) which prevents these particle collisions [19, 20]. However numerical errors occurring in the numerical simulations can cause the particles to have contact or even overlap each other. Special precautions are required to avoid particles contact or overlap when the gap becomes extremely small. In order to simulate the particle-particle interaction mechanism, the flow in the narrow gap between approaching particles has to be accurately resolved and collisions during numerical simulations present severe difficulties in the direct simulation of particulate flow since it can increase the cost of simulation. The corresponding element size has to be reduced which leads to extremely small elements and thus increases the number of unknowns to be solved for.

For the sake of simplicity, it is assumed that the particle collisions are smooth. In numerical calculations, the overlapping of particles can occur which raises the problem of different rigid body constraints to be applied at the same velocity node. Overlapping of the particles is not a correct physical phenomenon and can also cause diverging calculations. To avoid this problem, Glowinski, Joseph and coauthors [19, 20] proposed a repulsive force model in which particle surface is kept at a distance of more than one element size away from each other, by adding an artificial short range repulsive force. Singh, Joseph and coauthors [50] proposed a repulsive force collision model in which particles can even overlap slightly and the constraint of the rigid body that is closer to the velocity node having an overlap of two different rigid bodies is applied. Mostly, repulsive force collision models require the choice of stiffness parameters to restrict the magnitude of the repulsive forces and still there is no accurate theory to determine the exact values of these parameters. Diaz-Goano and Minev [13] proposed a collision strategy making the repulsive forces independent of the choice of the stiffness parameter. In this model, the repulsive forces are applied only if the distance between particles is less than a threshold value which is calculated as a function of the particle and the mesh size in such a way that the minimum distance between particles is still maintained.

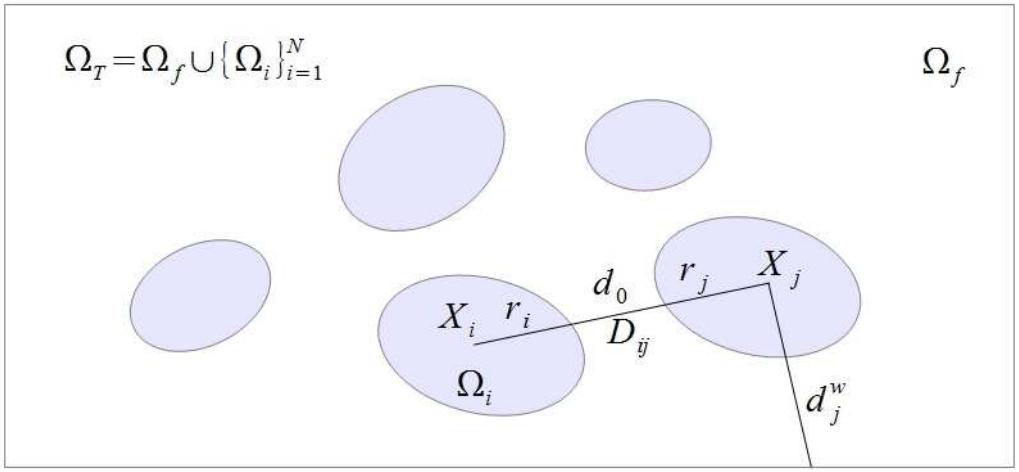

Figure 3.1: Particle-particle and particle-wall collisions inside the fluid domain.

We have investigated and analyzed different collision models in particulate flow. Before integrating these collision models within the CFD code, we have tested them using Matlab for the characteristics, efficiency, implementation and comparison. In this chapter, we will present results for the collision of particles in the absence of fluid, considering pure dry collisions. In the subsequent chapters, we will show how to combine and use these collision models with the fluid flow and simulate the particulate flow.

Firstly, the case of two circular particles is discussed. Later, we will simulate many circular particles. The collision models are then extended for the case of general shape particles.

3.1. Repulsive Force Collision Model (Model 1)

We examine a collision model (see [59]), in which a new method of short range repulsive forces has been introduced which can prevent particles from reaching too close as well as it can also deal with the case of overlapping when numerical errors bring the particles very close to each other.

3.1.1. Introduction

In this model, first of all the separation distance between the particles is checked. If the distance is less than a threshold value, then the repulsive force is activated. This force is calculated iteratively so that both particles move in the normal direction, along the line that passes through the centers of mass of both particles such that the minimum distance between particles is still maintained.

3.1.2. Model problem

For the particle-particle collisions, the repulsive force depends on the radii of the particles and the distance between their centers and is determined as (see Figure 3.1)

$$\mathbf{F}_{ij}^P = \begin{cases} 0 & \text{for } D_{ij} > d_0\,, \\ \frac{1}{\varepsilon_P}(\mathbf{X}_i - \mathbf{X}_j)(d_0 - D_{ij})^2 & \text{for } 0 \le D_{ij} \le d_0\,, \\ \frac{1}{\varepsilon_P'}(\mathbf{X}_i - \mathbf{X}_j)(-D_{ij}) & \text{for } D_{ij} \le 0 \end{cases} \tag{3.1.1}$$

where $D_{ij} = |\mathbf{X}_i - \mathbf{X}_j| - (r_i + r_j)$ is the signed distance between the particles, r_i and r_j are the radii, $\mathbf{X}_i$ and $\mathbf{X}_j$ are the center coordinates of the ith and jth particle, d_0 is the range of the repulsive force, ε_P and ε'_P are small positive stiffness parameters. Usually $d_0 = 0.5 \sim 2.5\Delta h$, where Δh is the mesh size when using the collision model with the fluid flow simulations [59].

The expression for the repulsive forces in Equation (3.1.1) deals with three cases, i.e. no collision, getting very close, and slightly overlapping.

Remark: The values for the stiffness parameters ε_P and ε'_P are such that they do not cause a discontinuity or singularity. For example, for sufficiently viscous fluid where $d_0 \simeq \Delta h$ and ρ_i/ρ_f is of order 1 (ρ_i is the particle density and ρ_f is the fluid density), then we can take $\varepsilon_P \simeq (\Delta h)^2$ and $\varepsilon'_P \simeq \Delta h$ in the calculations.

3.1.3. Numerical scheme

- *Calculate distance between particles:*
  First of all the distance between the particles is calculated. If the distance is smaller than a fixed value $d_\circ$, then the repulsive forces are activated.

- *Compute particle's repulsive force:*
  The repulsive forces are calculated by using equation (3.1.1).

- *Update the velocity and position of the particle:*
  Velocities and position of the particles are updated after the calculation of repulsive forces by,

$$\mathbf{V}^{n+1} = \mathbf{V}^n + h(\mathbf{F}^{n+1} + \mathbf{f}^{n+1})/m$$

$$\mathbf{X}^{n+1} = \mathbf{X}^n + h\mathbf{V}^{n+1}$$

  where h is the time-step, m mass of the particle, $\mathbf{F}$ represents the repulsive forces and $\mathbf{f}$ represents the body forces acting on the particle such as gravity.

3.1.4. Numerical results

Results for the collision of 2 particles are presented. Initially, the particles are at $(0.0, 0.5)$ and $(0.12, 0.8)$. The acceleration due to gravity is $g = 9.8$, the particle diameter is 0.2, density of the particle is 1.25 and, hence, the mass of the particle is $m = 0.04$. The first particle is released from rest and the second (upper) particle is given an initial vertical velocity $v = -0.25$ so that the particles can collide during they fall. The width and height of the channel is 3 and 4, respectively. The particles are falling in the absence of fluid and we consider here pure dry collisions.

We present results for the time step of 0.00075, which is neither too large nor too small for the analysis of falling particles and their collisions.

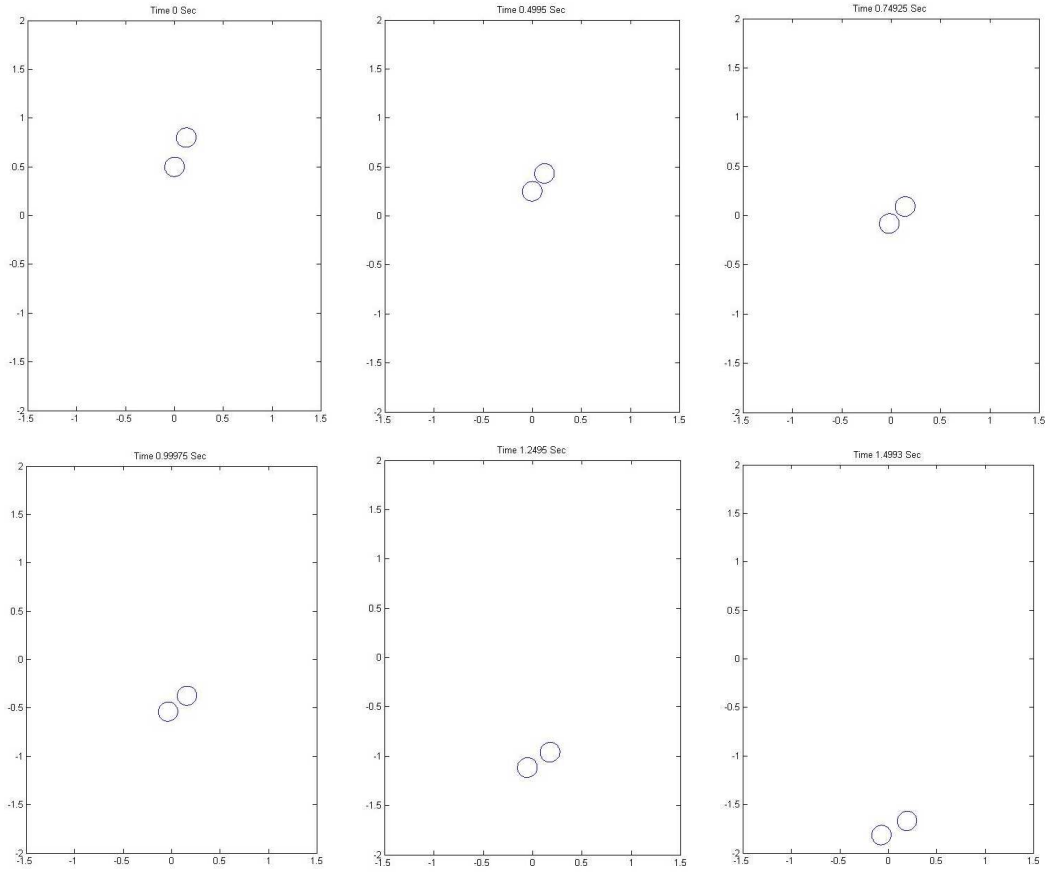

Figure 3.2: Simulation of 2 particles moving under gravity at t = 0.0, t = 0.5, t = 0.75, t = 1.0, t = 1.25 and t = 1.5

The time history of two particles falling and colliding.

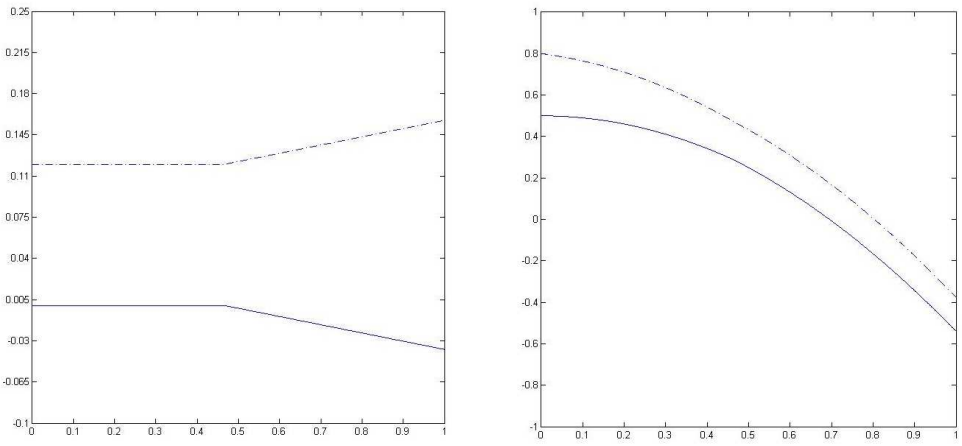

Figure 3.3: x-coordinate and y-coordinate of 2 particles w.r.t. time.

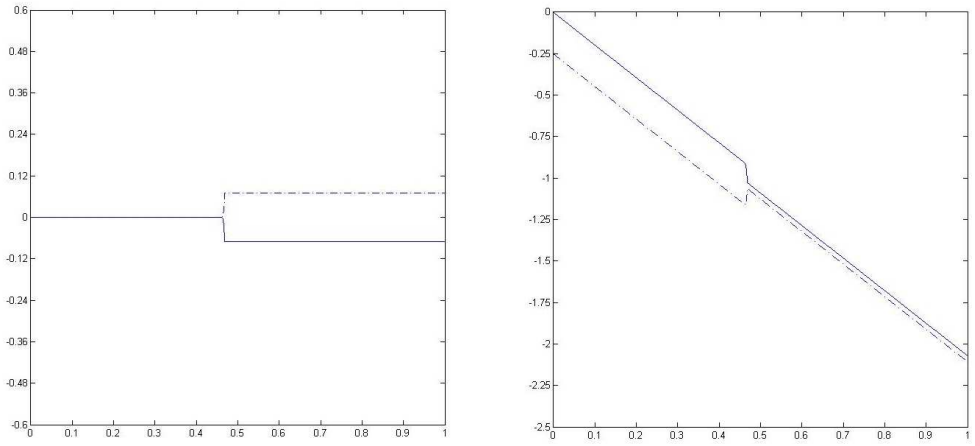

Figure 3.4: u-component and v-component of the translational velocity of 2 particles w.r.t. time.

The solid line represents the first particle and the dashed line represents the second particle. Figure 3.3 (left) shows the x-coordinate of the center of the two particles and similarly, figure 3.3 (right) shows the y-coordinate of the center of the two particles. Figure 3.4 (left) shows the u-component of velocity of the two particles and similarly, figure 3.4 (right) shows the v-component of velocity of the two particles.

As the particles fall, they come closer to each other. When the inter-particle distance reduces to a fixed value $d_\circ$, the collision forces are activated and the particles are again separated such that they do not collide and keep on falling.

3.1.5. Characteristics

Some of the characteristics of this collision model are as follows:

1. The repulsive force depends on the distance of the bodies from each other and is activated as soon as the distance is below a certain threshold value $d_\circ$. More precisely, the repulsive force is a function of the distance.

2. In computations, bodies can overlap instead of the collision model. The definition of the repulsive force is extended in the case of overlapping.

3. The lubrication force is independent of the body forces (gravity, hydrodynamic forces).

4. Each particle is treated individually i.e. one by one computation of the repulsive force is required for each particle in an iterative way.

3.1.6. Conclusion

As soon as the distance drops below a threshold value, the collision forces are activated. The time-step has to be reduced while particles get too close. In case of large number of particles, it is hard to avoid body overlap. The repulsive force depends directly on the distance between the particles, and the force decreases as the distance between the particles decreases which can allow the particles to overlap in certain situations and hence the extended definition of force in case of overlapping is necessary. In the next model we will discuss a repulsive force model which depends inversely on the distance between particles. So, the force increases with the decrease in distance between the particles which seems to be more practical for collision models.

3.2. Repulsive Force Collision Model (Model 2)

B. Maury, in [33], introduced a lubrication model to treat the particle collisions in the fluid. This method computes the repulsive forces as the lubrication forces between particles in fluid when the inter particle distance is very small.

3.2.1. Introduction

This collision model is based on the lubrication phenomenon that when two moving surfaces are close enough to each other, a Poiseuille-type flow develops in the gap zone of the surfaces which produces high stress values. These lubrication forces are dissipative in nature and are opposite to the relative motion of the surfaces. If the bodies are steady then they experience no force.

3.2.2. Model problem

The proposed model is based on the lubrication phenomenon such that the magnitude of the normal forces acting on the two approaching surfaces can be found by

$$|\mathbf{F}| = \tilde{\mu}\frac{|\mathbf{v}|}{d} \tag{3.2.1}$$

where d is the distance between the surfaces, $\mathbf{v}$ the relative velocity and $\tilde{\mu}$ depends on the geometry of the surface and the fluid viscosity. Similarly a force orthogonal to $\mathbf{F}$ due to the shear motion of the surfaces is given by

$$|\mathbf{F}^{\perp}| = \tilde{\mu}^{\perp}|\mathbf{v}|ln\left(\frac{d_{\circ}}{d}\right) \tag{3.2.2}$$

where $d_{\circ}$ is the minimum distance between the surfaces.

For the case of two particles having centers $\mathbf{X}_i$ and $\mathbf{X}_j$, with $D_{ij} = |\mathbf{X}_i - \mathbf{X}_j| - (r_i + r_j)$ as the signed distance, the lubrication force $\mathbf{F}_i = -\mathbf{F}_j$ can be calculated by [45],

$$\mathbf{F}_i = -\mathbf{F}_j = -\kappa(D_{ij})\left[(\dot{\mathbf{X}}_i - \dot{\mathbf{X}}_j)\cdot\mathbf{e}_{ij}\right]\mathbf{e}_{ij} - \kappa^{\perp}(D_{ij})\left[(\dot{\mathbf{X}}_i - \dot{\mathbf{X}}_j)\cdot\mathbf{e}_{ij}^{\perp}\right]\mathbf{e}_{ij}^{\perp} \tag{3.2.3}$$

where $\mathbf{e}_{ij}$ is the unit vector along the line through the center of particles. The functions κ and $\kappa^{\perp}$ are defined as

$$\kappa(d) = \tilde{\mu}\frac{1}{d},\ \kappa^{\perp}(d) = \tilde{\mu}^{\perp} ln\frac{d_{\circ}}{d}, \tag{3.2.4}$$

where $\tilde{\mu} = 6\pi\mu r_i^2 r_j^2/(r_i + r_j)^2$ for two circular particles with radii r_i and r_j in fluid with viscosity μ [27]. The functions κ and $\kappa^{\perp}$ vanish if the distance between particles is greater than $d_{\circ}$.

3.2.3. Numerical scheme

- *Calculate distance between particles:*
  First of all the distance between the particles is calculated. If the distance is smaller than a fixed value $d_{\circ}$, then the repulsive forces are activated.

- *Compute particle's repulsive force:*
  The repulsive forces are calculated by using equation (3.2.3).

- *Update the velocity and position of the particle:*
  Velocities and position of the particles are updated after the calculation of repulsive forces by,

$$\mathbf{V}^{n+1} = \mathbf{V}^n + h(\mathbf{F}^{n+1} + \mathbf{f}^{n+1})/m$$

$$\mathbf{X}^{n+1} = \mathbf{X}^n + h\mathbf{V}^{n+1}$$

  where h is the time-step, m mass of the particle, $\mathbf{F}$ represents the repulsive forces and $\mathbf{f}$ represents the body forces acting on the particle such as gravity.

3.2.4. Numerical results

Results for the collision of 2 particles are presented in the same way as before. Initially, the particles are at $(0.0, 0.5)$ and $(0.12, 0.8)$. The acceleration due to gravity is $g = 9.8$, the particle diameter is 0.2, density of the particle is 1.25 and, hence, the mass of the particle is $m = 0.04$. The first particle is released from rest and the second (upper) particle is given an initial vertical velocity $v = -0.25$ so that the particles can collide during they fall. The width and height of the channel is 3 and 4, respectively. The particles are falling in the absence of fluid and we consider here pure dry collisions.

We present results for the time step of 0.00075.

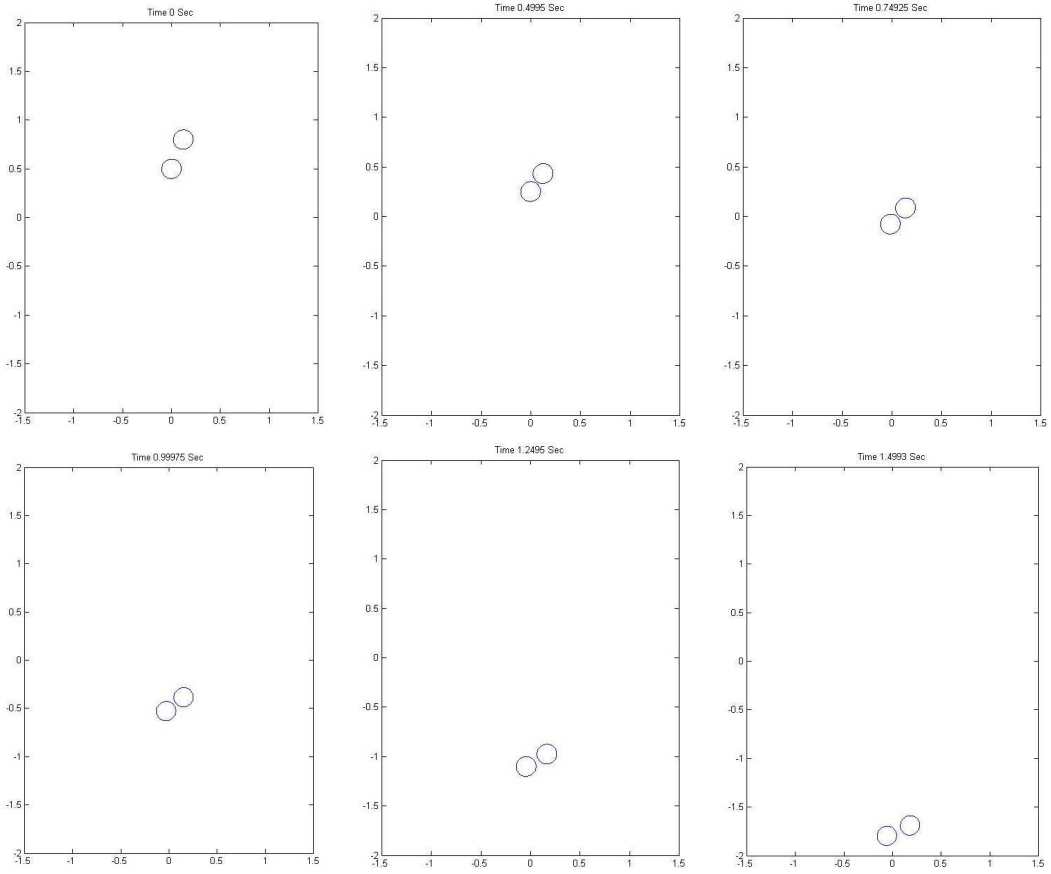

Figure 3.5: Simulation of 2 particles moving under gravity at t = 0.0, t = 0.5, t = 0.75, t = 1.0, t = 1.25 and t = 1.5

The time history of two particles falling and colliding.

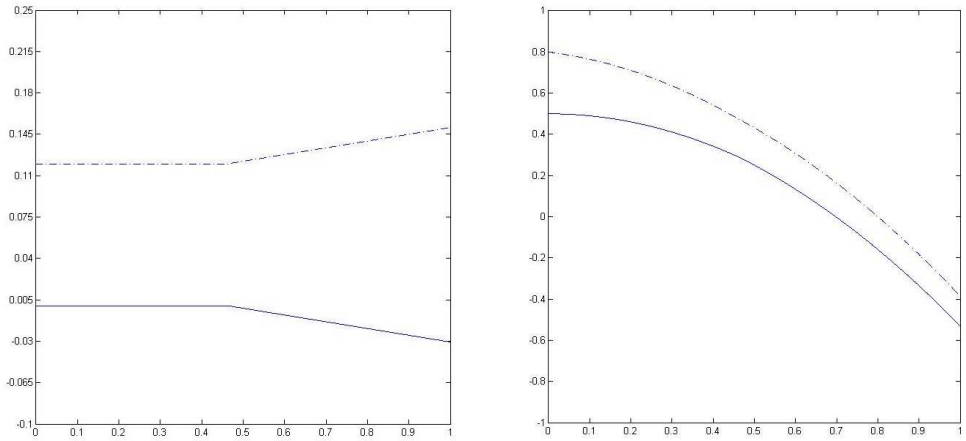

Figure 3.6: x-coordinate and y-coordinate of 2 particles w.r.t. time.

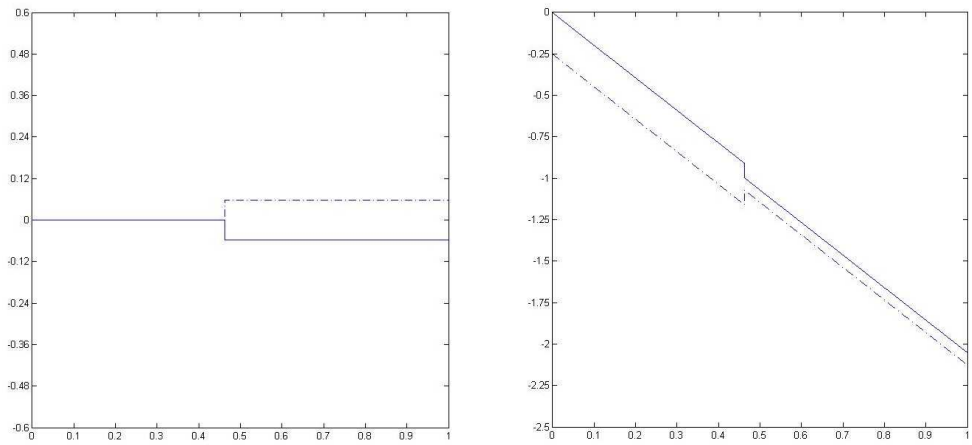

Figure 3.7: u-component and v-component of the translational velocity of 2 particles w.r.t. time.

The solid line represents the first particle and the dashed line represents the second particle. Figure 3.6 (left) shows the x-coordinate of the center of the two particles and similarly, figure 3.6 (right) shows the y-coordinate of the center of the two particles. Figure 3.7 (left) shows the u-component of velocity of the two particles and similarly, figure 3.7 (right) shows the v-component of velocity of the two particles.

This model again gives almost the same result for the two falling particles and does not show any significant difference compared to the previous collision model (Model 1) during the collision process. The particles separate afterward.

3.2.5. Characteristics

Some of the characteristics of this collision model are as follows:

1. The repulsive force opposes the relative motion, and if the bodies are steady then there is no force. In other words, the repulsive force is a function of the velocity and position.

2. In computations, bodies can overlap. It is therefore necessary to extend the definition of D_{ij} which takes negative values as soon as the particles i and j overlap.
3. We have supposed that κ and $\kappa^{\perp}$ are functions of the distance such that they vanish when d is greater than a fixed value $d_{\circ}$.
4. In numerical simulations we take the value of $d_{\circ}$ equal to the characteristic size of the particles.
5. The lubrication force is independent of the body forces (gravity, hydrodynamic forces).
6. We keep the close particles artificially at a fixed small distance ε in order to get realistic configurations.
7. Each particle is treated individually i.e. one by one computation of the repulsive force is required for each particle in an iterative way.

3.2.6. Conclusion

As soon as the distance drops below a certain value, the corresponding quantity for distance calculation is activated, and forces on particles are obtained with high accuracy. The time step has to be reduced while particles get too close. The repulsive force increases with the decrease in distance between the particles and hence depends inversely on the distance. In case of large numbers of particles, it is hard to avoid body overlap. For a large number of sedimenting particles, the forces from the surrounding particles increase with more and more particles sediment and this can lead to a large force acting on the sandwiched particles. This large force can even cause the sandwiched particles to overlap.

3.3. Collision Model Based on a Minimization Procedure (Model 3)

In this collision model, Maury [32] proposed a numerical scheme to compute the new velocities for colliding particles using a minimization procedure. The method is based on the global computation of the new velocities for the particles in fluid. These new velocities are found by solving a Lagrangian functional with the constraint based on the distance between particles which has to be greater than a threshold value $d_{\circ} > 0$.

3.3.1. Introduction

The advantage of this method is that it controls the minimal distance between particles by treating the positions in a global way, unlike the one by one computations of the repulsive forces between the particles. This scheme can avoid the particle overlaps during particulate flow simulations which other schemes do not guarantee in case of a large number of particles. This method is not consistent from the energy point of view [32] regardless of the fact that it is very robust even for the case of large time steps and multiple contacts. We can consider the collisions as inelastic collisions, since the nature of the lubrication forces between particles in a viscous fluid is dissipative.

3.3.2. Model problem

Let us consider the system of N solid particles with centers $\mathbf{X}_i$, radii r_i and masses m_i. The signed distance between particles i and j is defined as,

$$D_{ij}(\mathbf{X}) = |\mathbf{X}_j - \mathbf{X}_i| - (r_i + r_j). \tag{3.3.1}$$

The value of D_{ij} goes to negative as soon as particles i and j overlap. Then the new velocities of the particles are found by solving the following minimization problem

$$\min \frac{1}{2}|\mathbf{V}-\mathbf{U}-hM^{-1}\mathbf{f}|_M^2 \tag{3.3.2}$$

subject to the following constraint

$$D_{ij}+h(\mathbf{U}_j-\mathbf{U}_i)\cdot\mathbf{e}_{ij}\geq 0 \tag{3.3.3}$$

where $|\mathbf{v}|_M^2=\mathbf{v}^T M\mathbf{v}$, $\mathbf{V}_i$ is the new velocity, $\mathbf{U}_i$ is the old velocity of the ith particle, $\mathbf{f}$ are the body forces acting on the particle such as the gravity, h is the time step and $\mathbf{e}_{ij}$ is the unit vector along the line through the center of the particles. The corresponding Lagrangian functional can be written as

$$\mathbf{L}(\mathbf{V},\lambda)=\frac{1}{2}|\mathbf{V}-\mathbf{U}-hM^{-1}\mathbf{f}|_M^2-\sum_{1\leq i<j\leq N}\lambda_{ij}(D_{ij}+h(\mathbf{U}_j-\mathbf{U}_i)\cdot\mathbf{e}_{ij}). \tag{3.3.4}$$

Equation (3.3.4) can be solved using the method of Lagrange multipliers to get the new velocities of the particles.

Example: 2-particles

For simplicity , we can write for the case of two particles

$$\mathbf{X}=(\mathbf{X}_1,\mathbf{X}_2),\quad \mathbf{V}=(\mathbf{V}_1,\mathbf{V}_2),\quad \mathbf{f}=(\mathbf{f}_1,\mathbf{f}_2)$$

where $\mathbf{X}_i=(x_i,y_i)$, $\mathbf{V}_i=(u_i,v_i)$, $\mathbf{f}_i=(f_i,g_i)$, $\mathbf{e}_{ij}=(e_{ij}x,e_{ij}y)$, $i=1,2$. Using equation (3.3.2) and equation (3.3.3), we get a system of five linear equations:

$$\tilde{u}_1=u_1+\frac{h}{m_1}[f_1-\lambda_{12}\cdot e_{12x}]$$

$$\tilde{u}_2=u_2+\frac{h}{m_2}[f_2+\lambda_{12}\cdot e_{12x}]$$

$$\tilde{v}_1=v_1+\frac{h}{m_1}[g_1-\lambda_{12}\cdot e_{12y}]$$

$$\tilde{v}_2=v_2+\frac{h}{m_2}[g_2+\lambda_{12}\cdot e_{12y}]$$

$$(\tilde{u}_2-\tilde{u}_1)\cdot e_{12x}+(\tilde{v}_2-\tilde{v}_1)\cdot e_{12y}=-D_{12}/h.$$

Solving the above equations we get the new velocities for both particles simultaneously. In matrix form, we can write

$$\begin{bmatrix} 1 & 0 & 0 & 0 & e_{12x}\cdot\alpha_1 \\ 0 & 1 & 0 & 0 & -e_{12x}\cdot\alpha_2 \\ 0 & 0 & 1 & 0 & e_{12y}\cdot\alpha_1 \\ 0 & 0 & 0 & 1 & -e_{12y}\cdot\alpha_2 \\ -e_{12x} & e_{12x} & -e_{12y} & e_{12y} & 0 \end{bmatrix}\begin{bmatrix}\tilde{u}_1\\ \tilde{u}_2\\ \tilde{v}_1\\ \tilde{v}_2\\ \lambda_{12}\end{bmatrix}=\begin{bmatrix}u_1+\alpha_1\cdot f_1\\ u_2+\alpha_2\cdot f_2\\ v_1+\alpha_1\cdot g_1\\ v_2+\alpha_2\cdot g_2\\ -D_{12}/h\end{bmatrix}$$

where $\alpha_1=h/m_1$ and $\alpha_2=h/m_2$. λ_{ij} is the magnitude of the collision force between the ith and the jth particle. In case of two particles we can only get λ_{12} when particle i and particle j collide. For three particles, we can have λ_{12}, λ_{13} and λ_{23}. Hence, the size of the matrix varies with the number of contact of the particles with each other.

Example: 3-particles

Now we write the matrix form for the case of three particles for a better understanding of the scheme which could then easily be extended to N-particles.

$$\begin{bmatrix} 1 & 0 & 0 & 0 & 0 & 0 & e_{12x}\cdot\alpha_1 & e_{13x}\cdot\alpha_1 & 0 \\ 0 & 1 & 0 & 0 & 0 & 0 & -e_{12x}\cdot\alpha_2 & 0 & e_{23x}\cdot\alpha_2 \\ 0 & 0 & 1 & 0 & 0 & 0 & 0 & -e_{13x}\cdot\alpha_3 & -e_{23x}\cdot\alpha_3 \\ 0 & 0 & 0 & 1 & 0 & 0 & e_{12y}\cdot\alpha_1 & e_{13y}\cdot\alpha_1 & 0 \\ 0 & 0 & 0 & 0 & 1 & 0 & -e_{12y}\cdot\alpha_2 & 0 & e_{23y}\cdot\alpha_2 \\ 0 & 0 & 0 & 0 & 0 & 1 & 0 & -e_{13y}\cdot\alpha_3 & -e_{23y}\cdot\alpha_3 \\ -e_{12x} & e_{12x} & 0 & -e_{12y} & e_{12y} & 0 & 0 & 0 & 0 \\ -e_{13x} & 0 & e_{13x} & -e_{13y} & 0 & e_{13y} & 0 & 0 & 0 \\ 0 & -e_{23x} & e_{23x} & 0 & -e_{23y} & e_{23y} & 0 & 0 & 0 \end{bmatrix} \begin{bmatrix} \tilde{u}_1 \\ \tilde{u}_2 \\ \tilde{u}_3 \\ \tilde{v}_1 \\ \tilde{v}_2 \\ \tilde{v}_3 \\ \lambda_{12} \\ \lambda_{13} \\ \lambda_{23} \end{bmatrix} = \begin{bmatrix} u_1+\alpha_1\cdot f_1 \\ u_2+\alpha_2\cdot f_2 \\ u_3+\alpha_3\cdot f_3 \\ v_1+\alpha_1\cdot g_1 \\ v_2+\alpha_2\cdot g_2 \\ v_3+\alpha_3\cdot g_3 \\ -D_{12}/h \\ -D_{13}/h \\ -D_{23}/h \end{bmatrix}$$

The above system of equations is solved by using simple Gaussian elimination method with partial pivoting in the software FEATFLOW [53].

Remark 1: For the case of n-particles, there can be a maximum of $n\frac{(n-1)}{2}$ number of contacts and correspondingly we can get $n\frac{(n-1)}{2}$ different λ_{ij}'s. The system of equations in this case will consist of $2n+n\frac{(n-1)}{2}$ components.

Remark 2: For the case of large numbers of particles, we get matrices with large entries and direct methods are not much suitable for the solution. Therefore, we can use other iterative methods for the fast solution of the system of equations such as the basic iterative methods or some advanced methods like Krylov subspace methods [6, 46].

3.3.3. Numerical scheme

- *Calculate distance between particles:*
  First of all the distance between the particles is calculated. If the distance is smaller than a fixed value $d_\circ$, then the minimization algorithm is activated.

- *Compute new particle's velocity:*
  The velocities are calculated by solving the minimization problem as shown in equation (3.3.4).

- *Update the velocity and position of the particle:*
  The positions of the particles are updated after the calculation of new velocities by,

$$\mathbf{X}^{n+1} = \mathbf{X}^n + h\mathbf{V}^{n+1}$$

  where h is the time-step.

3.3.4. Numerical results

Results for the collision of 2 particles are presented in the same way as before. Initially, the particles are at $(0.0, 0.5)$ and $(0.12, 0.8)$. The acceleration due to gravity is $g = 9.8$, the particle diameter is 0.2, density of the particle is 1.25 and, hence, the mass of the particle is $m = 0.04$. The first particle is released from rest and the second (upper) particle is given an initial vertical velocity $v = -0.25$ so that the particles can collide during they fall. The width and height of the channel is 3 and 4, respectively. The particles are falling in the absence of fluid and we consider here pure dry collisions.

We present again results for the time step of 0.00075.

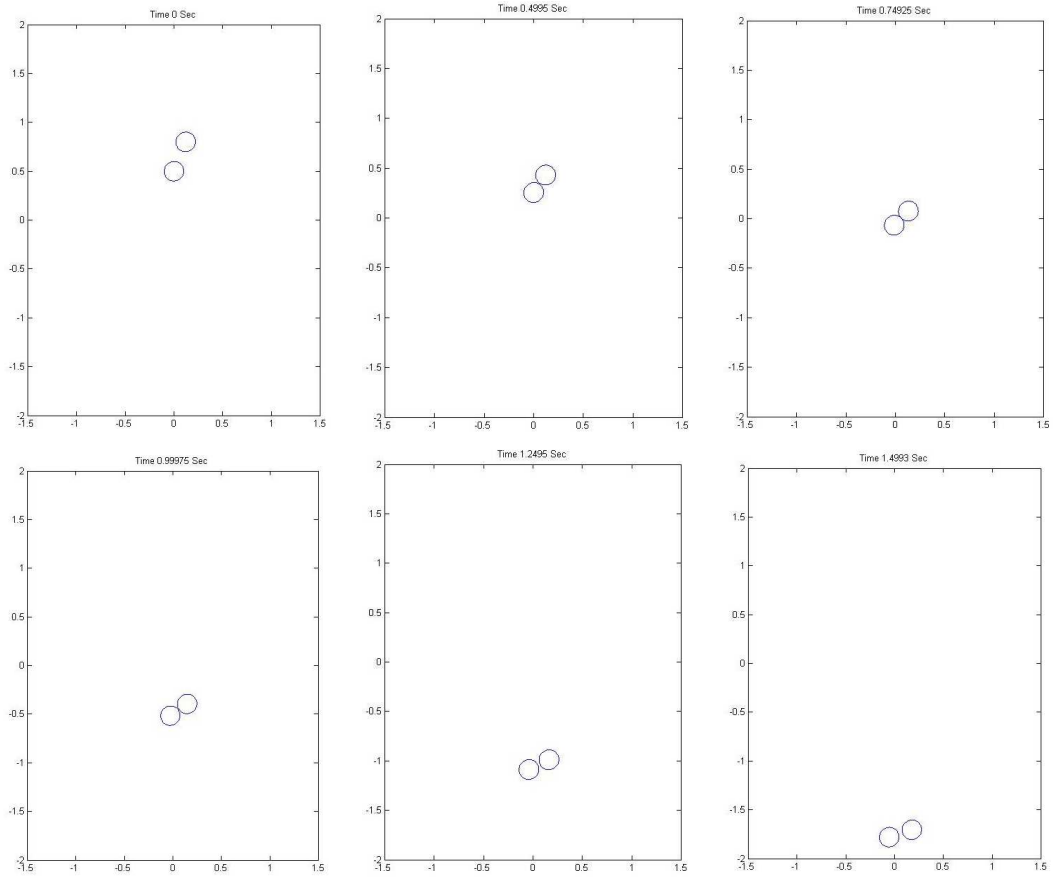

Figure 3.8: Simulation of 2 particles moving under gravity at t = 0.0, t = 0.5, t = 0.75, t = 1.0, t = 1.25 and t = 1.5

The time history of two particles falling and colliding.

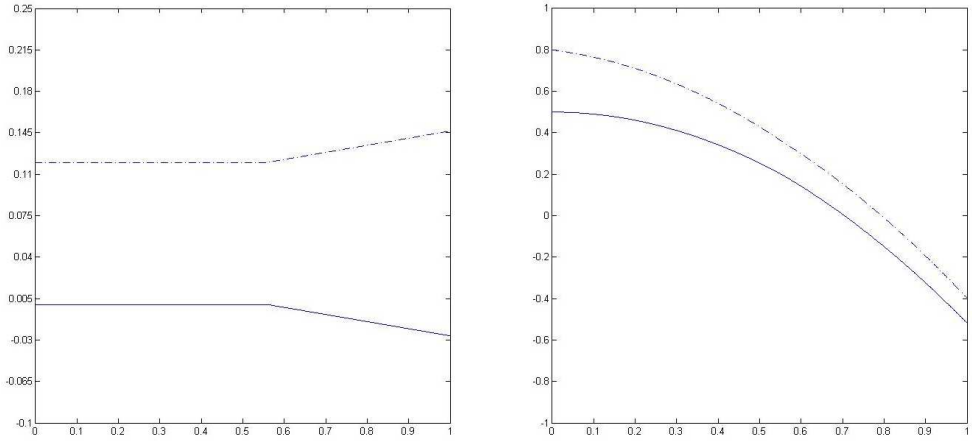

Figure 3.9: x-coordinate and y-coordinate of 2 particles w.r.t. time.

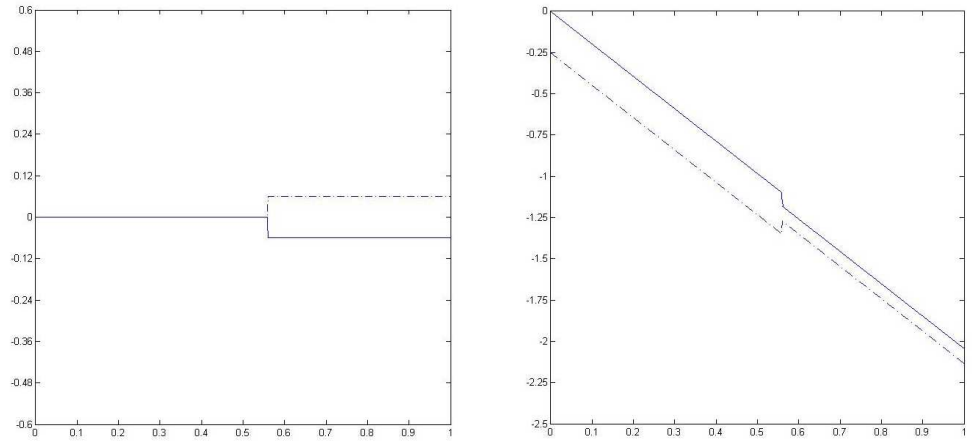

Figure 3.10: u-component and v-component of the translational velocity of 2 particles w.r.t. time.

The solid line represents the first particle and the dashed line represents the second particle. Figure 3.9 (left) shows the x-coordinate of the center of the two particles and similarly, figure 3.9 (right) shows the y-coordinate of the center of the two particles. Figure 3.10 (left) shows the u-component of velocity of the two particles and similarly, figure 3.10 (right) shows the v-component of velocity of the two particles.

The two falling particles give similar results as compared with the results of collision model 1 and collision model 2. The particles separate during the collision process and keep on falling.

3.3.5. Characteristics

Some of the characteristics of this collision model are as follows:

1. Considering the nature of the collisions between the particles in a viscous fluid as dissipative we call it inelastic collisions.

2. All particles contacts which can occur during a time step are handled globally. The particles are not treated individually, i.e., one by one computation of the repulsive force for each

particle is not required.

3. The computed new velocities are dependent on the body forces.

4. The scheme is stable and robust and produces feasible configurations, even for large time steps.

5. The new velocities can be obtained as a solution to the system $AX = B$.

6. For a two dimensional case and for n-particles, there are $2n + n(n-1)/2$ number of equations to be solved at each time step.

3.3.6. Conclusion

Motion of the particles is computed with a non-elastic impact law. This scheme is very stable and robust (even for large time steps) and specially suitable to control the minimum distance between the solid particles in particulate flow. However, solvers to deal with larger matrices (arising due to large number of particles) require further investigation in future.

3.4. Sticky or Gluey Particle Model (Model 4)

In viscous fluids, the colliding/contacting particles can stick together and can form a bundle of many particles [10]. Maury and Lefebvre proposed a modification to the collision model proposed by Maury [32], and developed a sticky/gluey particle model (agglomeration model) to compute the motion of the solid particles moving in a viscous fluid [27].

3.4.1. Introduction

In this model, first of all the new velocities of the particles are found by using the minimization procedure described in [32]. Then there is a check for the sticking and un-sticking of the particles as a further step.

3.4.2. Model problem

Let us consider the system of N solid particles with centers $\mathbf{X}_i$, radii r_i and masses m_i. The Lagrangian formulation for the calculation of new intermediate velocities for the particles, described in subsection (3.3), can be written as

$$\mathbf{L}(\overline{\mathbf{V}}, \lambda) = \frac{1}{2}|\overline{\mathbf{V}} - \mathbf{U} - hM^{-1}\mathbf{f}|_M^2 - \sum_{1 \le i < j \le N} \lambda_{ij}(D_{ij} + h(\mathbf{U}_j - \mathbf{U}_i) \cdot \mathbf{e}_{ij}) \tag{3.4.1}$$

where $D_{ij} = |\mathbf{X}_i - \mathbf{X}_j| - (r_i + r_j)$ is the distance between the particles, $\mathbf{V}_i$ is the new velocity, $\mathbf{U}_i$ is the old velocity of the ith particle, $\mathbf{f}$ are the body forces acting on the particle such as the gravity, h is the time step and $\mathbf{e}_{ij}$ is the unit vector along the line through the center of the two particles. From this Lagrangian, we obtain λ^{n+1} and we introduce a new parameter γ, such that

$$\bar{\gamma}^{n+1} = \gamma^n - h\lambda^{n+1}, \tag{3.4.2}$$

and the new velocities of the particle are obtained from the two cases of gamma,

$$\begin{aligned} &\text{if } \bar{\gamma}^{n+1} \leqslant 0, \quad \mathbf{V} = \overline{\mathbf{V}} \text{ and } \gamma^{n+1} = \bar{\gamma}^{n+1}, \\ &\text{if } \bar{\gamma}^{n+1} > 0, \quad \mathbf{V} = \bar{\gamma}^{n+1}/m \text{ and } \gamma^{n+1} = 0. \end{aligned}$$

The particles stick together more firmly as much as γ is negative.

To see this scheme more clearly, we proceed as follows: As λ_{ij} gives the magnitude of the force acting on the ith and jth particle, so we can get $\lambda_{ij} \cdot e_{ij}$ and $\lambda_{ij} \cdot (-e_{ij})$ as the directional force acting on the ith and jth colliding particles. Now

$$\dot{\bar{\gamma}}_i^{n+1} = -\lambda_{ij}^{n+1} \cdot e_{ij} \tag{3.4.3}$$

implies that

$$\bar{\gamma}_i^{n+1} = \gamma_i^n - h\lambda_{ij}^{n+1} \cdot e_{ij}. \tag{3.4.4}$$

We can see from equation (3.4.4) that $\bar{\gamma}_i^{n+1}/m_i$ gives the new velocity of the ith particle, i.e.

$$\bar{\gamma}_i^{n+1}/m_i = \mathbf{V}_i \tag{3.4.5}$$

where m_i is the mass of the ith particle. The two cases of gamma for sticking and un-sticking of the particles can be rewritten in a more comprehensive way as

$$\begin{aligned} &\text{if } \bar{\gamma}_i^{n+1} \leqslant 0, \quad \mathbf{V}_i = \overline{\mathbf{V}}_i \text{ and } \gamma_i^{n+1} = \bar{\gamma}_i^{n+1}, \\ &\text{if } \bar{\gamma}_i^{n+1} > 0, \quad \mathbf{V}_i = \bar{\gamma}_i^{n+1}/m \text{ and } \gamma_i^{n+1} = 0. \end{aligned}$$

Remark 1: $\lambda_{ij} \neq 0$ if and only if there is a possible particle contact, otherwise $\lambda_{ij} = 0$.

Remark 2: Only the particles which are close enough to experience collision ($D_{ij} < d_\circ$), are updated using this scheme and similarly γ is also updated for these particles, respectively.

Remark 3: If $\gamma \leqslant 0$, the particles stick together more firmly and if $\gamma > 0$, the particles un-stick.

3.4.3. Numerical scheme

- *Calculate distance between particles:*
  First of all the distance between the particles is calculated. If the distance is smaller than a fixed value $d_\circ$, then the minimization algorithm is activated.

- *Compute new particle's velocity:*
  The velocities are calculated by solving the minimization problem as shown in equation (3.4.1).

- *Update the velocity and position of the particle:*
  Positions of the particles are updated after the calculation of new velocities by,

  $$\mathbf{X}^{n+1} = \mathbf{X}^n + h\mathbf{V}^{n+1}$$

  where h is the time-step.

3.4.4. Numerical results

Results for the collision of 2 particles are presented in the same way as before. Initially, the particles are at $(0.0, 0.5)$ and $(0.12, 0.8)$. The acceleration due to gravity is $g = 9.8$, the particle diameter is 0.2, density of the particle is 1.25 and, hence, the mass of the particle is $m = 0.04$. The first particle is released from rest and the second (upper) particle is given an initial vertical

velocity $v = -0.25$ so that the particles can collide during their fall. The width and height of the channel is 3 and 4, respectively. The particles are falling in the absence of fluid and we consider here pure dry collisions.

We present results for the time step of 0.00075.

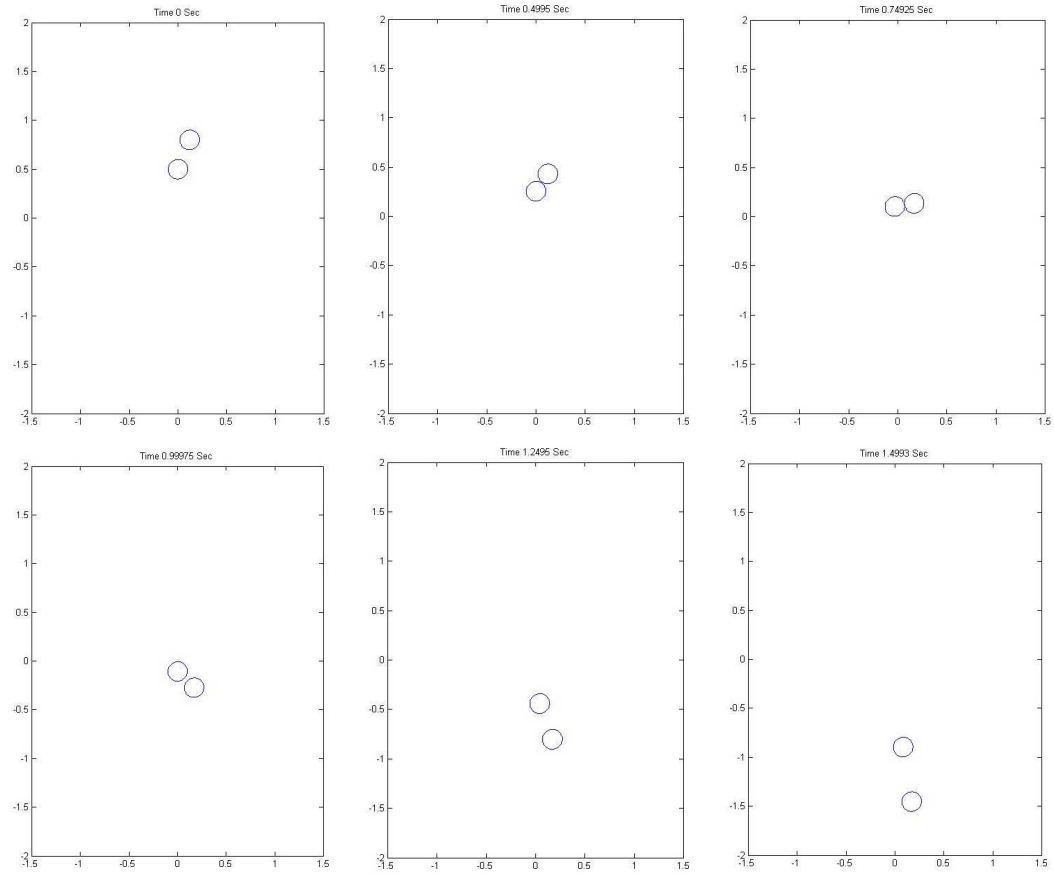

Figure 3.11: Simulation of 2 particles moving under gravity at t = 0.0, t = 0.5, t = 0.75, t = 1.0, t = 1.25 and t = 1.5

The time history of two particles falling and colliding.

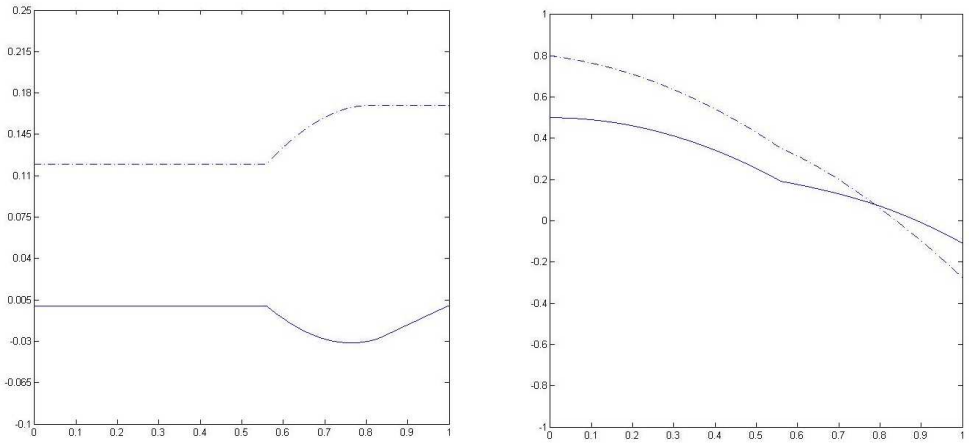

Figure 3.12: x-coordinate and y-coordinate of 2 particles w.r.t. time.

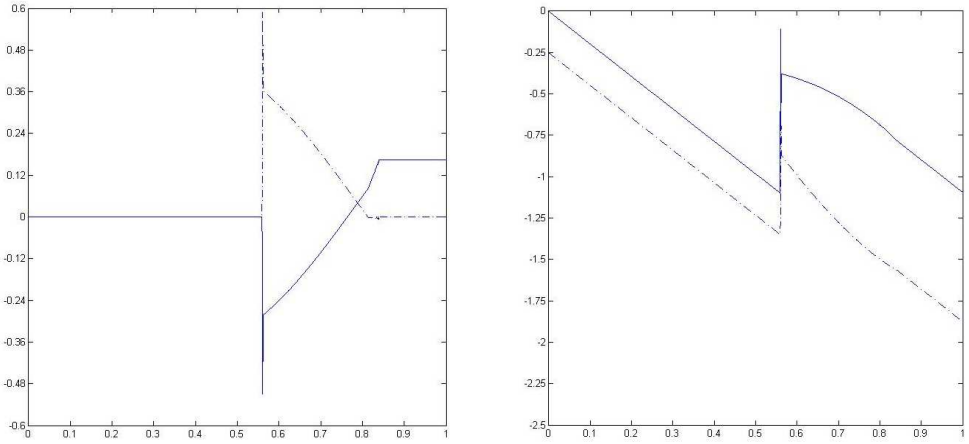

Figure 3.13: u-component and v-component of the translational velocity of 2 particles w.r.t. time.

The solid line represents the first particle and the dashed line represents the second particle. Figure 3.12 (left) shows the x-coordinate of the center of the two particles and similarly, figure 3.12 (right) shows the y-coordinate of the center of the two particles. Figure 3.13 (left) shows the u-component of velocity of the two particles and similarly, figure 3.13 (right) shows the v-component of velocity of the two particles.

This collision model shows very interesting results compared with the previous results of collision models (model 1, model 2 and model 3). During the collision process the particles stick together for some time, the upper particle rolls over the lower particle and later they separate.

3.4.5. Characteristics

Some of the characteristics of this collision model are as follows:

1. This model is a modification of the model described in subsection (3.3).

2. This model relies on two states, i.e. glued or unglued.

3. These states are described by a new variable γ which stands for an adhesion potential. The more γ is negative, the more solids are glued.
4. All the characteristics of the model described in subsection (3.3) are valid for this model.

3.4.6. Conclusion

The scheme simulates collections of gluey particles and is the same as the scheme described in section 3.3 with the modification of sticking and un-sticking as a further step.

3.5. Collision Model Based on Conservation of Linear Momentum (Model 5)

This final collision model, proposed by Ardekani [4], computes the contact force depending on the linear conservation of momentum along the line of centers of the two colliding particles instead of computing the repulsive forces between them.

3.5.1. Introduction

In this approach, when the distance between two particles reaches zero, then the new velocities for the colliding particles are estimated. The coefficient of restitution e_{dc} controls and determines the nature of the collision and the rebound velocity, i.e. inelastic or plastic collision. The advantage of this method is that the linear momentum is conserved for the system of both colliding particles along their line of centers and hence the particle velocity is not updated explicitly preventing numerical instabilities.

3.5.2. Model problem

Consider collision between two smooth particles. The linear momentum in normal direction along their line of centers is conserved for both the particles during collision and they experience the same force in opposite direction. For the tangential direction, the linear momentum is conserved separately for each particle. Hence using the preceding concepts during the collision process [4], we can write

$$U_{np1}^{t_c^+} = \frac{e_{dc}(U_{np2}^{t_c^-} - U_{np1}^{t_c^-})M_{p2}}{M_{p1}+M_{p2}} + \frac{M_{p1}U_{np1}^{t_c^-} + M_{p2}U_{np2}^{t_c^-}}{M_{p1}+M_{p2}}, \tag{3.5.1}$$

$$U_{np2}^{t_c^+} = -\frac{e_{dc}(U_{np2}^{t_c^-} - U_{np1}^{t_c^-})M_{p1}}{M_{p1}+M_{p2}} + \frac{M_{p1}U_{np1}^{t_c^-} + M_{p2}U_{np2}^{t_c^-}}{M_{p1}+M_{p2}}, \tag{3.5.2}$$

where U_n is the normal velocity, t_c is the time at which the collision starts. e_{dc} is the coefficient of restitution and M_p is the mass of the particle. In previous repulsive force collision methods, the repulsive forces depend on the function of distance between particles and they do not guarantee that the particles will not overlap. Moreover, the new velocities after collision and the minimum distance between particles depend on a stiffness parameter. Thus, the particle linear velocities can be calculated as

$$U_{p\alpha} = U_{np\alpha}\, sin\theta + U_{tp\alpha}\, cos\theta \tag{3.5.3}$$

$$V_{p\alpha} = U_{np\alpha}\, cos\theta - U_{tp\alpha}\, sin\theta. \tag{3.5.4}$$

Here, α is the particle index (1 or 2), U_t is the tangential velocity, U_p and V_p are the x-component and y-component of the velocity. This approach can be extended to particulate flow with large number of particles.

3.5.3. Numerical scheme

- *Calculate distance between particles:*
  First of all the distance between the particles is calculated. If the distance is smaller than a fixed value $d_\circ$, then the collision process is activated.

- *Compute new particle's velocity:*
  The velocities are calculated by finding, firstly, the normal velocities from equation (3.5.1) and equation (3.5.2) and then using equation (3.5.3) and equation (3.5.4) to get the linear velocities for both the particles.

- *Update the velocity and position of the particle:*
  Positions of the particles are updated after the calculation of new velocities by

$$\mathbf{X}^{n+1} = \mathbf{X}^n + h\mathbf{V}^{n+1}$$

  where h is the time-step.

3.5.4. Numerical results

Results for the collision of 2 particles are presented in the same way as before. Initially, the particles are at $(0.0, 0.5)$ and $(0.12, 0.8)$. The acceleration due to gravity is $g = 9.8$, the particle diameter is 0.2, density of the particle is 1.25 and, hence, the mass of the particle is $m = 0.04$. The first particle is released from rest and the second (upper) particle is given an initial vertical velocity $v = -0.25$ so that the particles can collide during they fall. The width and height of the channel is 3 and 4, respectively. The particles are falling in the absence of fluid and we consider here pure dry collisions.

We present results for the time step of 0.00075.

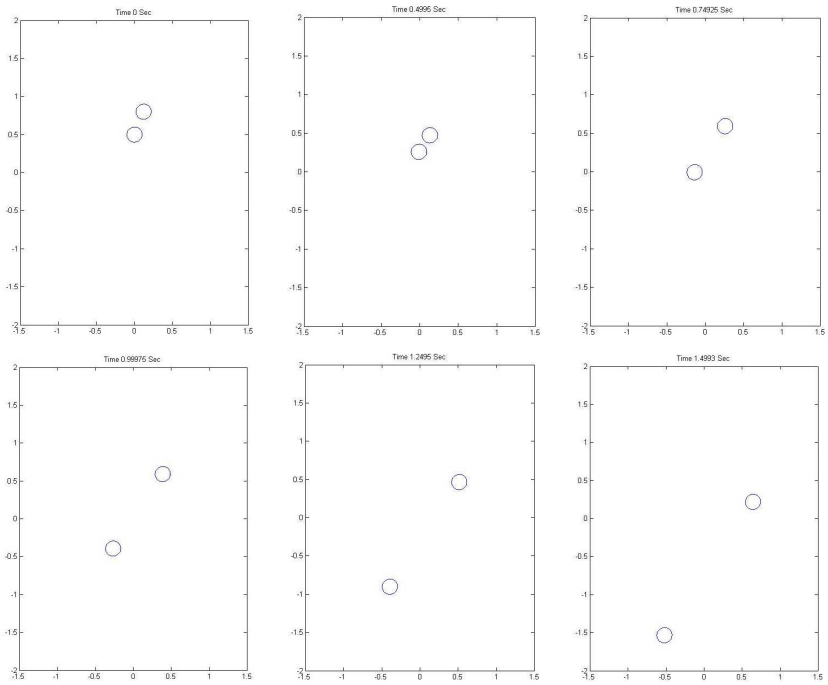

Figure 3.14: Simulation of 2 particles moving under gravity at t = 0.0, t = 0.5, t = 0.75, t = 1.0, t = 1.25 and t = 1.5

The time history of two particles falling down and colliding:

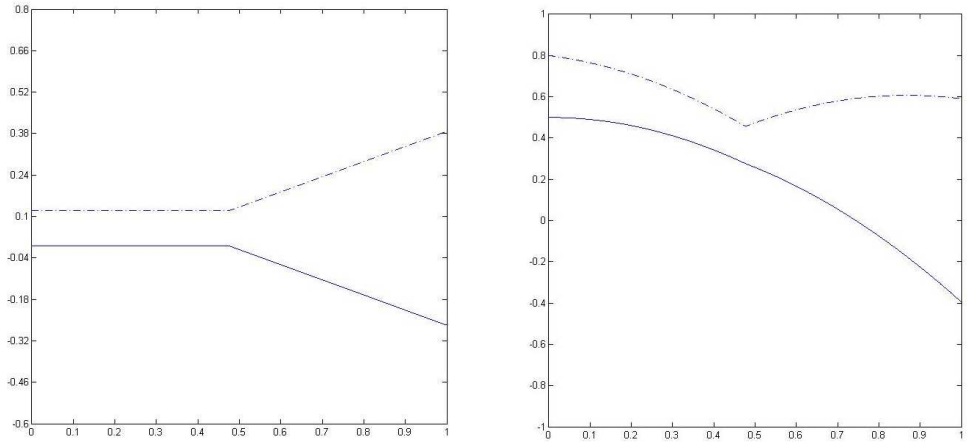

Figure 3.15: x-coordinate and y-coordinate of 2 particles w.r.t. time.

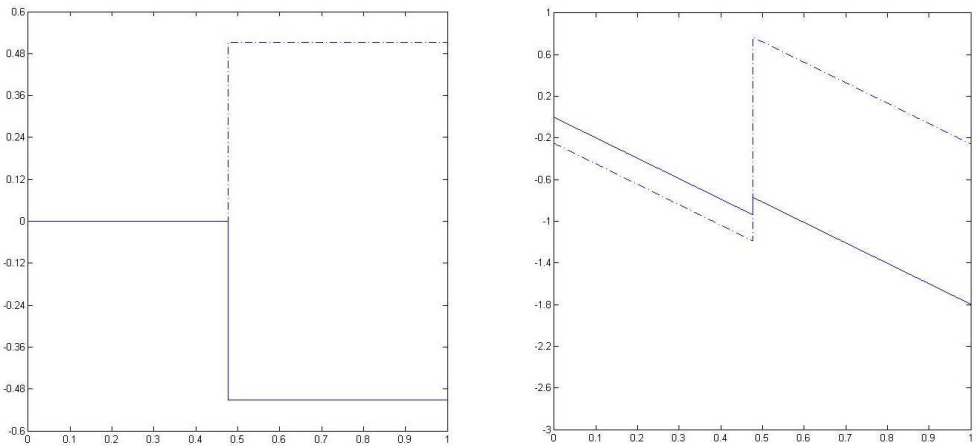

Figure 3.16: u-component and v-component of the translational velocity of 2 particles w.r.t. time.

The solid line represents the first particle and the dashed line represents the second particle. Figure 3.15 (left) shows the x-coordinate of the center of the two particles and similarly, figure 3.15 (right) shows the y-coordinate of the center of the two particles. Figure 3.16 (left) shows the u-component of velocity of the two particles and similarly, figure 3.16 (right) shows the v-component of velocity of the two particles.

The results show a big difference compared with the results of the previous collision models (model 1, model 2 and model 3). The particles are separated through a big distance during the collision process.

3.5.5. Characteristics

Some of the characteristics of this collision model are as follows:

1. In this model, we do not apply a repulsive force and instead the contact force between particles is computed.

2. By using conservation of linear momentum along the particles line of centers, the rebound velocities for both the particles can be calculated.
3. The coefficient of restitution e_{dc} controls and determines the nature of the collision and the rebound velocity.
4. The linear momentum is conserved for the system of both colliding particles along the line through the center and hence the particle velocity is not updated explicitly.
5. The collision process in this method starts when the distance between particles is less than a threshold value $d_\circ$ for smooth particles.
6. The computed linear velocities are independent of the body forces.
7. An advantage of this method is that there is no need to choose a stiffness parameter a priori.
8. Each particle is treated individually, i.e., one by one computation of the repulsive force is required for each particle in an iterative way.

3.5.6. Conclusion

An efficient approach is introduced to simulate collision between particles. Instead of applying a repulsive force between particles, as was done by the previous approaches, the contact force is calculated using conservation of linear momentum. An advantage of this method is that there is no need to choose a stiffness parameter *a priori*.

3.6. Comparison of the results

From the above 2-particle results, collision model 1, collision model 2 and collision model 3 show similar results and all the three collision models can be used for a few number of particles. When the number of particles increase and when we have to deal with the case of particle sedimentation, collision model 1 and collision model 2 can lead to particle overlaps as discussed in the individual conclusions of collision model 1 and collision model 2 due to the dependence of the collision models on the distance between the particles. Secondly, the repulsive forces in collision model 1 and collision model 2 are computed individually for every particle in an iterative way and this does not include the combined force of all the particles acting on a particle (computed globally) which can also lead to particle overlaps. Collision model 3, on the other hand, computes the new velocities of the colliding particles in a global way using a minimization procedure which guarantees to avoid particle overlaps even for large number of particles. Secondly, the ability of collision model 3 to treat particles for a large time-step also gives an advantage over the other collision models. Collision model 5 based on the conservation of linear momentum can be useful in some particular situations e.g. pure dry collisions but, later, as we have to deal with particles in the fluid, we did not find the results much convincing (the particles separate too much after collision) as compared to other collision models. Further improvements in the collision model 5 can be made such as the introduction of body forces and the hydrodynamic forces.

Overall we conclude that collision model 1 and collision model 2 which are the repulsive force collision models, can be used in the case of a few number of particles or while using smaller time-steps. Collision model 4 which is an extension of collision model 3 can be used as an agglomeration model (sticky or gluey particles). In the later results, we will neglect the collision model 5 and leave it for future research. Our favorite collision model is model 3 as it can be used for simulating many particles without overlapping and due to its ability to work even for large time-steps.

Now we give an example to show that collision model 3 can be used for large time-steps by comparing collision model 3 with collision model 2.

3.6.1. Comparison of collision model 2 and collision model 3 with larger time-step

We have compared collision model 2 and collision model 3 using a larger time-step $h = 0.01$ to show that collision model 3 works even for large time step while other collision models fail as the time-step gets too big. Collision mode 2 is used as an example for the comparison with collision model 3. The other repulsive force collision models also overlap for larger time-step. The upper particle is given an initial vertical velocity $v = -10.25$ so that the particles can collide during they fall.

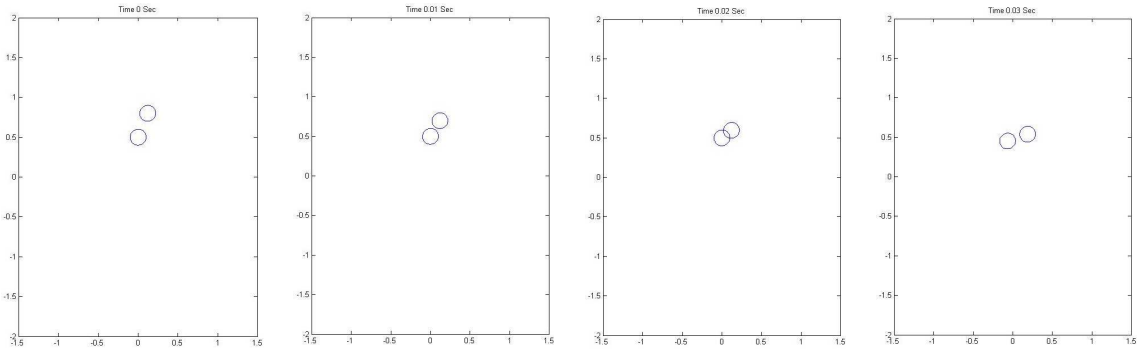

Figure 3.17: Simulation of 2 particles moving under gravity at t = 0.0, t = 0.01, t = 0.02 and t = 0.03 using collision model 2

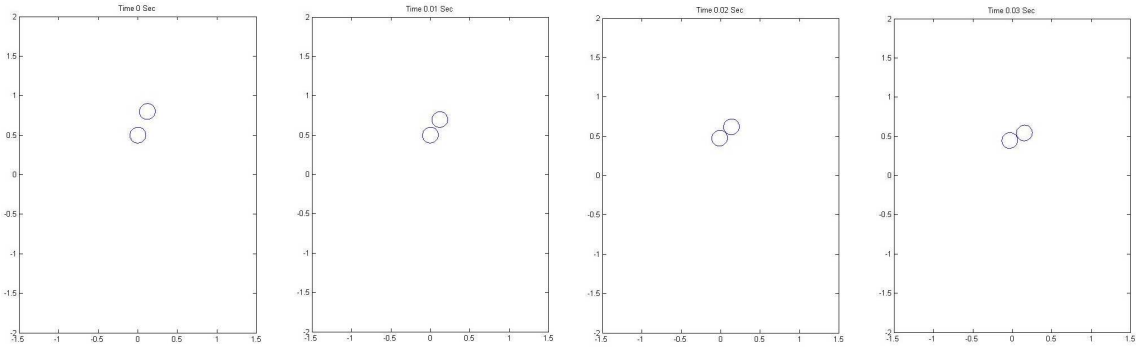

Figure 3.18: Simulation of 2 particles moving under gravity at t = 0.0, t = 0.01, t = 0.02 and t = 0.03 using collision model 3

Figure 3.17 shows that for a large time-step the particles overlaped using collision model 2 whereas the particles did not overlap using the collision model 3 (figure 3.18).

3.7. Strategy to check particle collision/overlap

In collision model 3 and collision model 4, we have used a special strategy to find whether the particles will collide/overlap or not in the next time-step instead of relying only on the exact distance between the particles to activate the collision models, i.e., we check whether,

$$D_{ij} + h(\mathbf{V}_j - \mathbf{V}_i) \cdot \mathbf{e}_{ij} \leq 0 \tag{3.7.1}$$

which implies that the particles can collide/overlap in the next time-step. Here $\mathbf{e}_{ij} = \frac{\mathbf{X}_j - \mathbf{X}_i}{|\mathbf{X}_j - \mathbf{X}_i|}$ is the unit vector along the line through the center of the particles, D_{ij} is the signed distance defined by eq. (3.3.1), h is the time-step and $\mathbf{V}_i$ and $\mathbf{X}_i$ are the velocity and position of the center of the ith particle respectively. This strategy is also applicable for the non-circular particles. In this particular case, we take $\mathbf{V}_i$ and $\mathbf{X}_i$ as the velocity and position of the surface/boundary point of the ith particle which is likely to collide with the boundary point of the jth particle.

It would be interesting to check this scheme with the repulsive force collision models (model 1 and model 2) by extending the definition of D_{ij} as

$$D_{ij} = D_{ij} + h(\mathbf{V}_j - \mathbf{V}_i) \cdot \mathbf{e}_{ij} \tag{3.7.2}$$

which may help the collision models to become less dependent on the smaller time-steps.

3.8. Many particles

It is hard to simulate a large number of particles while avoiding overlaps. We have simulated many particles using collision model 1, collision model 2 and collision model 3. In collision model 1 and 2, the stiffness parameter has to be chosen such that the resulting repulsive force should neither be too small which can cause the particles to overlap nor the repulsive force should be too much which may result in unrealistic new velocities for the particles. Additionally, the time-step has to be reduced during collisions to get a satisfactory non-overlapping result. Collision model 3 can deal very efficiently with large number of particles as it computes globally the new velocities of the particles which does not require the time-step to be reduced.

Results for 50 circular particles falling and sedimenting in a channel are presented. The acceleration of gravity is $g = 9.8$, the particle diameter is 0.2, density of the particle is 1.25 and hence mass of the particle is $m = 0.03$. Particles are released from rest in a channel with a width of 3 and height of 4.

3.8.1. Numerical results

The particles fall under the action of gravity and settle down (sediment) at the bottom of the cavity without overlapping. Collision model 1, collision model 2 and collision model 3 are used for the simulation.

We present results for the time step of 0.00075.

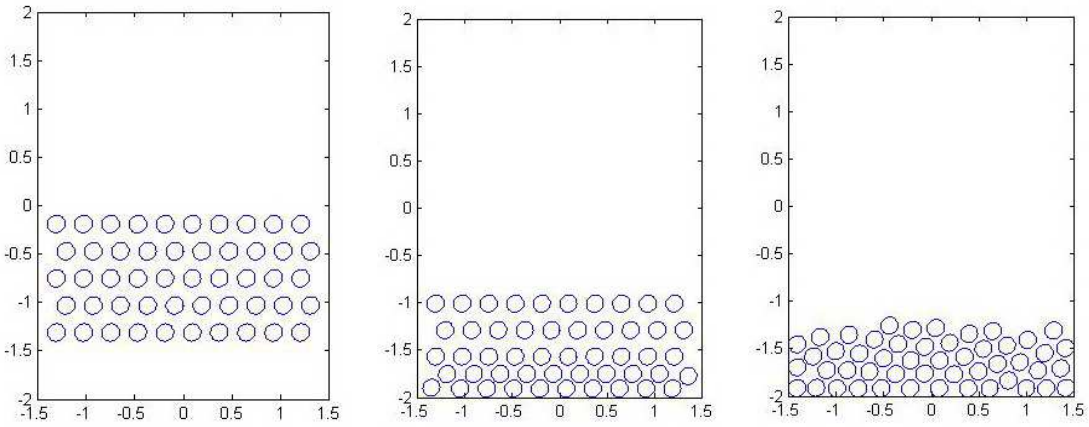

Figure 3.19: Simulation of 50 particles moving under gravity at t = 0.0, t = 0.1 and t = 0.15 with collision model 1

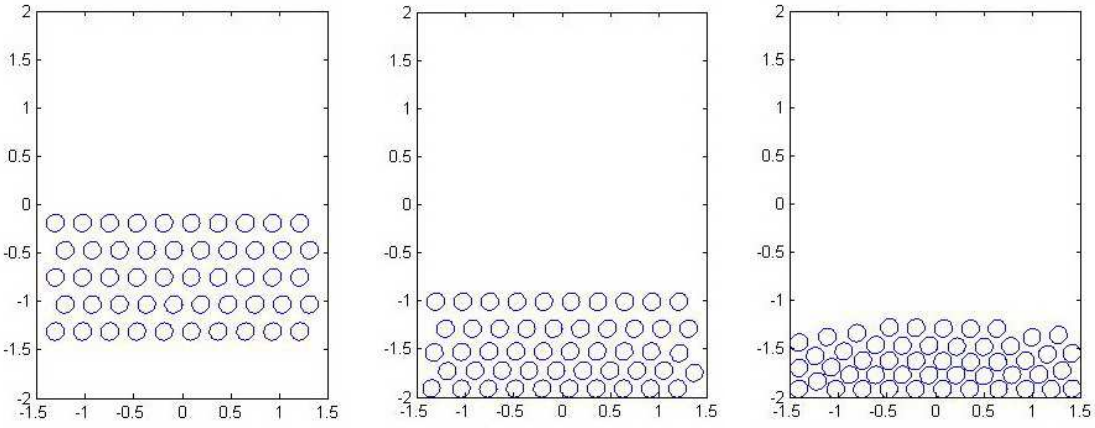

Figure 3.20: Simulation of 50 particles moving under gravity at t = 0.0, t = 0.1 and t = 0.15 with collision model 2

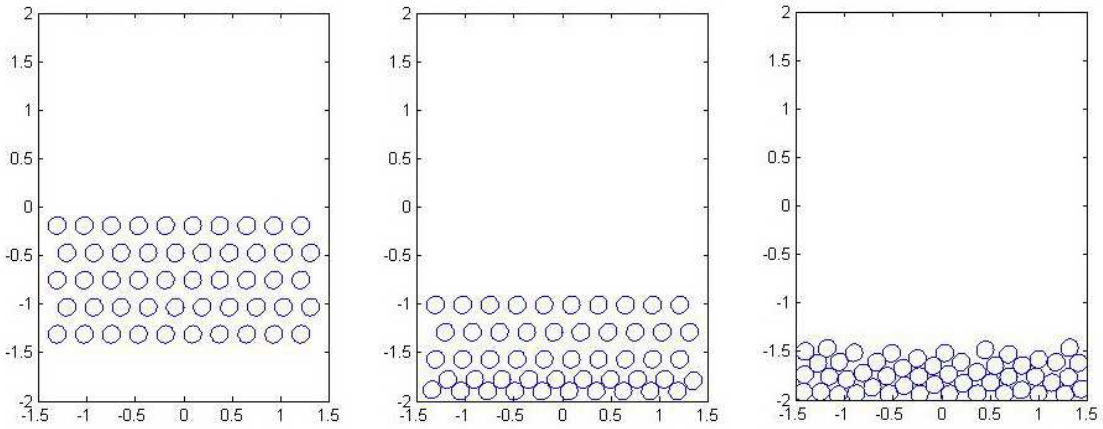

Figure 3.21: Simulation of 50 particles moving under gravity at t = 0.0, t = 0.1 and t = 0.15 with collision model 3

Remark: We can see from Fig. 3.21 (right) that collision model 3 gives much more compact distribution of particles as compared to collision model 1 and collision model 2 (Fig. 3.19 (right) and Fig. 3.20 (right)).

3.8.2. Comparison of collision model 3 and gluey particle model

As the gluey particle model uses the same strategy to calculate the new particle velocities with the exception of sticking and un-sticking as a further step, we have simulated 27 circular particles falling on an inclined plane and compared the results for collision model 3 and gluey particle model.

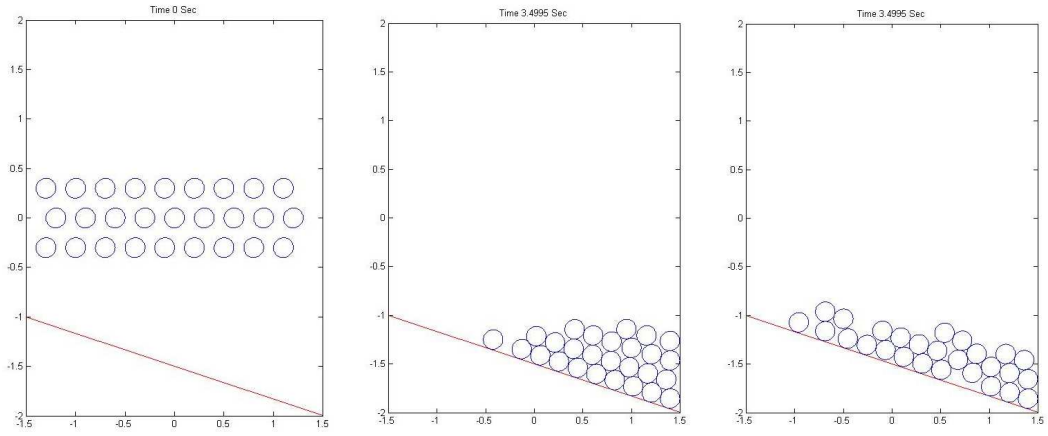

Figure 3.22: Simulation of 27 particles moving under gravity at t = 0.0 and t = 3.5 with collision model 3 and gluey particle model

The second figure 3.22 (center) shows the final positions of the particles using collision model 3 and the last figure 3.22 (right) shows the final positions of the particles using collision model 4 at time $t = 3.5$.

3.8.3. Conclusion

All the collision models work fine for the sedimentation of 50 particles. If the number of particles is increased, and if collision model 1 or collision model 2 is used, particles may overlap and behave unrealistically. Moreover, due to the tight and pack situation, the particles experience a big force from the surrounding particles and hence they can shoot out with high velocities. Collision model 3, on the other hand, can handle the situation for the case of many particles.

3.9. General shape particles

A circular body can easily be identified by its center coordinates and angle but a general shape body requires a collection of data points to identify it along with its center of mass and angle. However, for a general shape body the calculation of moment acting on the center of mass is not simple as in the case of circular bodies. Collision forces acting on the circular bodies are mostly normal to the surface for the case of many collision models but for general shape bodies the torque acting is necessary to calculate. The calculation of distance between two general shape particles is also a bit more expensive as it is not the simple direct center-to-center distance between them but rather point to point distance calculation is needed. Hence, the collision models are also required to be modified accordingly.

We treat the general shape particles as polygons consisting of n number of vertices. The area, centroid and moment of the polygon is calculated once which is further used for the calculation of particle's position and velocity. The maximum distance r_{max} from centroid to vertex of the polygon is calculated by finding the distances of all the vertices from the centroid of the polygon which can be used as the radius of the polygon.

3.9.1. Distance between particles

The distance between two particles (polygons) is calculated in two steps. Firstly, the center-to-center distance between the two polygons is found. If this distance is less than $r_{max1} + r_{max2} + d_\circ$, then in the next step, the minimum distance between the two polygons is calculated as the minimum distance between the vertices of the two polygons. Furthermore, a check for any vertex from one polygon which may be inside the second polygon can also be performed for the case if the polygons are overlapping.

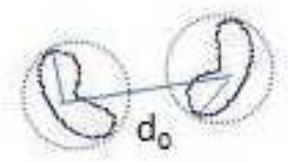

Figure 3.23: 2 particles with $d_\circ$ as the critical distance (minimum distance to activate the collision model)

3.9.2. Numerical results

Simulations are performed for 2 bean-shaped particles and later for many particles (36 particles) falling under gravitational force. The acceleration of gravity is $g = 9.8$. The width and height of the channel is 3 and 4, respectively.

In the 2 bean-shaped particles, the first particle is released from rest and the second (upper) particle is given a vertical velocity $v = -0.15$ so that the particles can collide during they fall while in the 36 bean-shaped particles, the particles are released from rest.

2 bean-shaped particles falling with time step of 0.00075.

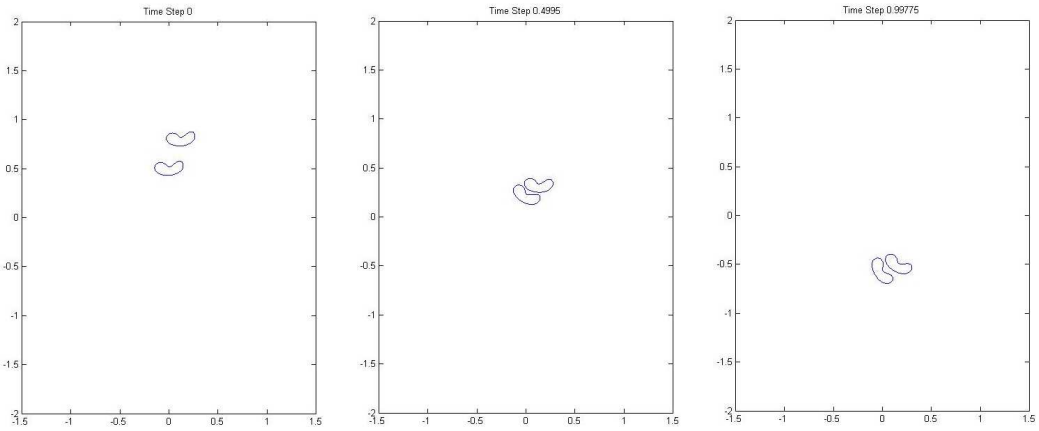

Figure 3.24: Simulation of 2 bean-shaped particles moving under gravity at $t = 0.0$, $t = 0.5$ and $t = 1.0$ using collision model 3

Sedimentation of many bean-shaped particles falling with time step of 0.00075.

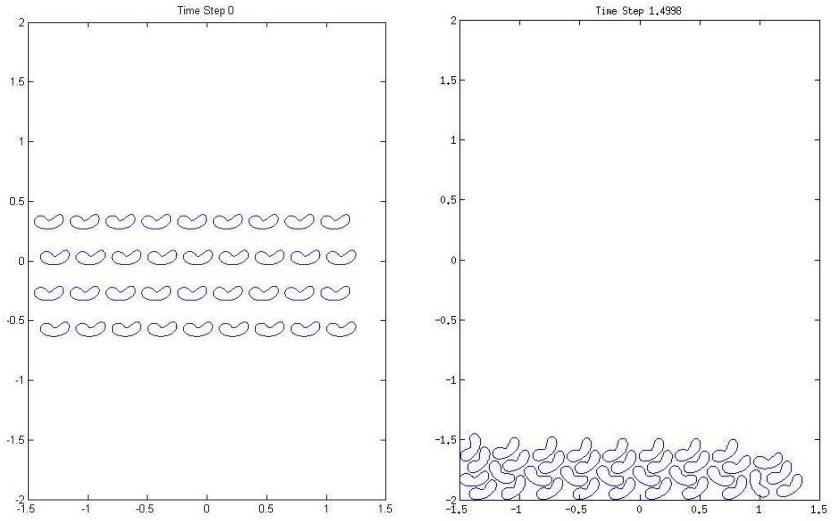

Figure 3.25: Simulation of 36 bean-shaped particles moving under gravity at $t = 0.0$ and $t = 1.5$ using collision model 3

3.9.3. Conclusion

For the case of circular particles only center-to-center distances are enough for the calculation of collision forces. But in the case of general shape particles, extra effort is required for the calculation of the exact distances of the two approaching particles. Circular particles have collision forces acting normally on them and hence no torque acting on them. For the case of general shape particles, torques are also required to be calculated for the exact motion of the particles.

4

Collision Models and CFD

After examining and analyzing different collision models, we describe here how to treat and combine the particles with the CFD part and how to use the collision models to simulate particulate flow. Many different approaches have been used for multiphase flow such as the Eulerian approach in which a fixed mesh is used which is independent of the particles (Fictitious Boundary Method FBM), the Lagrangian approach in which the mesh moves and follows the motion of the particle's boundary (Arbitrary Lagrangian Eulerian ALE). Each approach has its own advantages as in the Eulerian approach there is no need for the re-meshing of the computational grid and saves a lot of computational cost whereas the ALE method gives a higher accuracy for the numerical simulation of particulate flow.

For the direct simulation of fluid-particle mixtures, the particle collisions are found using a collision model and this collision model is coupled with the global computation of the flow. In most of the collision models, each particle in the fluid is treated individually and the Navier-Stokes equations are solved in the moving domain contained by the fluid. For the collision models Model 1 and Model 2 discussed in the previous Chapter, the repulsive force $F_i^{'}$ is calculated for each particle and hence the particle velocity is updated along with other forces acting on the particle as shown in Eq. (2.2.1). On the other hand, in the collision models Model 3 and Model 4, all the forces acting on the particles are taken into account simultaneously and the new velocities are found for each particle using a minimization procedure which finds the particle's velocity in a global way.

We will focus here on the technique of FBM (Eulerian approach) for the treatment of particles, the extra boundary conditions arising due to the moving particle boundaries, the forces and torque acting on the particle boundaries and the collision forces arising due to the particle-particle and particle-wall collisions in the fluid.

4.1. Fictitious Boundary Method

Many different approaches have been presented to deal with the particles in the fluid and the calculation of hydrodynamic forces acting on the particle. Glowinski, Joseph and coauthors [19] proposed a semi-implicit approach for the calculation of drag and lift forces and particle movement in the fluid. Similarly, Patankar, Singh, Joseph, Glowinski and Pan [38] also used an implicit approach for the particle treatment. Wan and Turek [60] described an explicit way to treat the fluid, particles inside the fluid (particle motion) and the explicit calculation of drag and lift forces acting on the particle boundaries.

The fluid domain can be extended into the whole domain Ω_T containing the fluid domain Ω_f and particle domain Ω_i by applying the boundary conditions at the interface between the particles and the fluid which can be taken as an additional constraint to the governing Navier-Stokes equations

$$\mathbf{u}(\mathbf{X}) = \mathbf{U_i} + \omega_i \times (\mathbf{X} - \mathbf{X_i}), \tag{4.1.1}$$

where $\mathbf{X} \in \overline{\Omega}_i$ and $\mathbf{U_i}$ is the ith particle velocity. To start the FBM, a coarse mesh is chosen which describes the geometrical details and a boundary parameterization with respect to the boundary conditions. The internal solid objects are introduced in the corresponding components in all matrices and vectors in the solution process as unknown degrees of freedom. Then, the extra conditions arising due to the interior objects are incorporated implicitly in all the iterative solution steps. The FBM has a considerable advantage that the computational domain does not require to be changed in time, and no re-meshing is required. More precisely, the mesh and the flow features can be handled independent of each other [55, 60].

For the description of the concepts regarding the fictitious boundary method, consider a bounded domain Ω_f with piecewise smooth boundary Γ. The incompressible Navier-Stokes equations can be written as

$$\rho_f \left(\frac{\partial \mathbf{u}}{\partial t} + \mathbf{u} \cdot \nabla \mathbf{u} \right) - \nabla \cdot \sigma = \mathbf{0}, \quad \nabla \cdot \mathbf{u} = 0 \quad \forall\, t \in (0,T) \tag{4.1.2}$$

where σ is the total stress tensor in the fluid phase defined as

$$\sigma = -p\mathbf{I} + \mu[\nabla \mathbf{u} + (\nabla \mathbf{u})^T]. \tag{4.1.3}$$

Here $\mathbf{u}$ is the fluid velocity, p the pressure, μ the dynamic viscosity coefficient and ρ_f the fluid density. Hence using the FBM, the domain of definition of the fluid velocity $\mathbf{u}$ is extended according to Eq. (4.1.1) which can be seen as an additional constraint to the Navier-Stokes equations (4.1.2), i.e. [58]

$$\begin{cases} \nabla \cdot \mathbf{u} = 0 & (a) \quad \text{for } \mathbf{X} \in \Omega_T\,, \\ \rho_f \left(\frac{\partial \mathbf{u}}{\partial t} + \mathbf{u} \cdot \nabla \mathbf{u} \right) - \nabla \cdot \sigma = \mathbf{0} & (b) \quad \text{for } \mathbf{X} \in \Omega_f\,, \\ \mathbf{u}(\mathbf{X}) = \mathbf{U_i} + \omega_i \times (\mathbf{X} - \mathbf{X_i}) & (c) \quad \text{for } \mathbf{X} \in \overline{\Omega}_i,\ i = 1,...,N. \end{cases} \tag{4.1.4}$$

4.1.1. Integrating boundary conditions with FBM

Wan and Turek [55] described an iterative filtering technique for implementing boundary conditions in iterative solution steps for the fictitious boundary conditions.

Using this technique a mesh (Eulerian mesh) is used which is independent of the internal objects. The interior objects are treated as unknown degrees of freedom which are implicitly incorporated in all the corresponding components of matrices and vectors in all the iterative solution steps. This enables the use of standard grid refinement tools in the interior regions simply and accurately. Later, using the iterative filtering technique, the "correct" boundary conditions are imposed before and after each iterative step by modifying the corresponding vector components which furthermore guarantees the smooth performance of multigrid solvers [16, 37] without any modifications [55].

Iterative filtering techniques

In [55], these filtering techniques have been illustrated in detail and three different treatments have been discussed to integrate the boundary conditions arising due to the internal objects. These boundary conditions are involved in the solution process of the matrix-vector problem after the discretization process. Fully explicit treatment, semi-implicit treatment and fully implicit treatment are the three approaches to modify the components of the matrix-vector problem due to the projection of the boundary conditions on the corresponding vector components and performing the elimination process.

Another approach known as 'fictitious boundary condition' [55] can be used in which there is no need to change the bilinear forms or the boundary conditions during the solution process. Here, specific values for the density and viscosity are used to satisfy - approximately - the corresponding boundary conditions.

Density-viscosity blocking techniques

The density or viscosity of the fluid determines the state of the fluid and for 'huge' values of density or viscosity the fluid is changed to solid state. Using this approach, high values for density or viscosity parameters are prescribed to mark a solid body inside the fluid domain [55].

This method is very easy to implement as compared to the iterative filtering technique method and only appropriate values for the density and viscosity have to be prescribed. On the other hand finite parameters chosen for the density and viscosity to approximate the 'infinite' values for the solids can cause computational errors [55].

4.1.2. Calculation of hydrodynamic forces and torque

Let $\Omega_T = \Omega_f \cup \{\Omega_i\}_{i=1}^N$ be the entire computational domain. Let $\mathbf{n}$ be the unit normal vector on the boundary Ω_i pointed outward to the flow region. The hydrodynamic forces $\mathbf{F_i}$ acting on the surface of the ith particle and the torque T_i acting about the center of mass of the ith particle can be calculated as in [60]

$$\mathbf{F_i} = (-1)\int_{\partial\Omega_i} \sigma\cdot\mathbf{n}\, d\Gamma_i, \quad T_i = (-1)\int_{\partial\Omega_i} (\mathbf{X}-\mathbf{X_i})\times(\sigma\cdot\mathbf{n})\, d\Gamma_i, \tag{4.1.5}$$

where $\partial\Omega_i$ is the boundary of the ith particle and $\mathbf{X_i}$ is the position of the mass center of the ith particle.

Wan and Turek [60] presented a volume integral approach instead of the surface integral approach for the calculation of hydrodynamic forces acting on the moving solid bodies. In [60], the surface integral is replaced with a volume integral, which is computationally less expensive, by defining a parameter α_i

$$\alpha_i(\mathbf{X}) = \begin{cases} 1 & \text{for } \mathbf{X}\in\Omega_i, \\ & \\ 0 & \text{for } \mathbf{X}\in\Omega_f, \end{cases}. \tag{4.1.6}$$

The gradient of α_i, in a weak sense, approximates the normal vector $\mathbf{n}$ pointed outward at the wall surface of the rigid bodies and is zero elsewhere [14],

$$\mathbf{n} = \nabla\alpha_i. \tag{4.1.7}$$

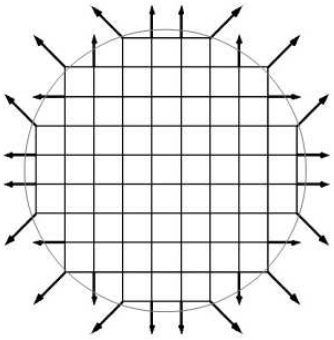

Figure 4.1: Normal vectors $\mathbf{n} = \nabla\alpha_i$ on the particle's boundary (cells where $\alpha_i = 1$).

Therefore, the forces and torque acting on the wall surface and about the center of mass of the ith particle respectively can be written as [60]

$$\mathbf{F}_i = (-1)\int_{\Omega_i} \sigma \cdot \nabla\alpha_i \, d\Omega_i, \quad T_i = (-1)\int_{\Omega_i} (\mathbf{X} - \mathbf{X_i}) \times (\sigma \cdot \nabla\alpha_i) \, d\Omega_i. \tag{4.1.8}$$

On the finite element level, this can be computed as

$$\mathbf{F}_i = -\sum_{T_{h,i} \in T} \sigma_h \cdot \nabla\alpha_{h,i}, \quad T_i = -\sum_{T_{h,i} \in T} (\mathbf{X} - \mathbf{X_i}) \times \sigma_h \cdot \nabla\alpha_{h,i}, \tag{4.1.9}$$

where $T_{h,i}$ are the elements crossed by the ith particle as shown in figure 4.1 and $\alpha_{h,i}(\mathbf{x})$ are the finite element interpolant of $\alpha_i(\mathbf{x})$.

Hence, we can use Eq. (4.1.8) to calculate the hydrodynamic forces $\mathbf{F}_i$ and torque T_i using the volume integral over the whole domain Ω_T instead of the surface integral over the wall surface of the rigid bodies. Since the volume integrals need to be computed only on the mesh cells around the rigid bodies, this makes it convenient to calculate the drag and lift forces [60].

4.1.3. Particle-particle and particle-wall collision forces and torque on a particle

After finding the drag and lift forces acting on the particle surface, the particle-particle and particle-wall forces and torque due to the particle collisions are computed using the collision models discussed in the previous Chapter. When the inter-particle or particle-wall distance is less than a particular value d_0, then the collisions are considered and a collision model is used to maintain a minimum fixed distance between particles (particle-particle) and wall-particles which avoids overlap and numerical errors due to closeness of particles. The particle's velocity and position is updated using Eq. (2.2.1) and Eq. (2.2.2) in Chapter 2.

4.2. FBM-Steps

The overall strategy for solving the coupled system of fluid and particles can be summarized as follows:

1. Assume that the particle position $\mathbf{X_i^n}$ and velocity $\mathbf{U_i^n}$ is given at time t^n $(i = 1,...,N)$.

2. Identify the fictitious boundaries by checking which mesh cells belong to the interior of the solid objects or come inside the solid boundaries.

3. The fictitious boundary conditions, given in Eq. (4.1.4) (c), are applied using the particle position $\mathbf{X_i^n}$ and velocity $\mathbf{U_i^n}$.

4. Solve the equation of fluid along with the particles i.e. Eq. (4.1.4) to find the fluid velocity $\mathbf{u^{n+1}}$ and the pressure p^{n+1} at time t^{n+1} on the whole computational domain Ω_T.

5. Find the hydrodynamic forces $\mathbf{F_i^{n+1}}$ and the torque T_i^{n+1} acting on the particle using Eq. (4.1.8).

6. Detect particle collisions between the approaching particles [49, 56] by calculating the distance between them.

7. If particle collisions are detected then calculate the collision forces $F_i^{'n+1}$ acting on the particles using an appropriate collision model.

8. Find the new translational velocities $\mathbf{U_i^{n+1}}$ and angular velocities ω_i^{n+1} of the solid particles by solving the Newton-Euler Eqs. (2.2.1) and using the collision forces $F_i^{'n+1}$ if any.

9. Update the position $\mathbf{X_i^{n+1}}$ and angle θ_i^{n+1} of the particles using Eq. (2.2.2).

10. Repeat the steps 2 - 9 for the next time step.

We illustrate the FBM steps using a flow chart diagram as follows:

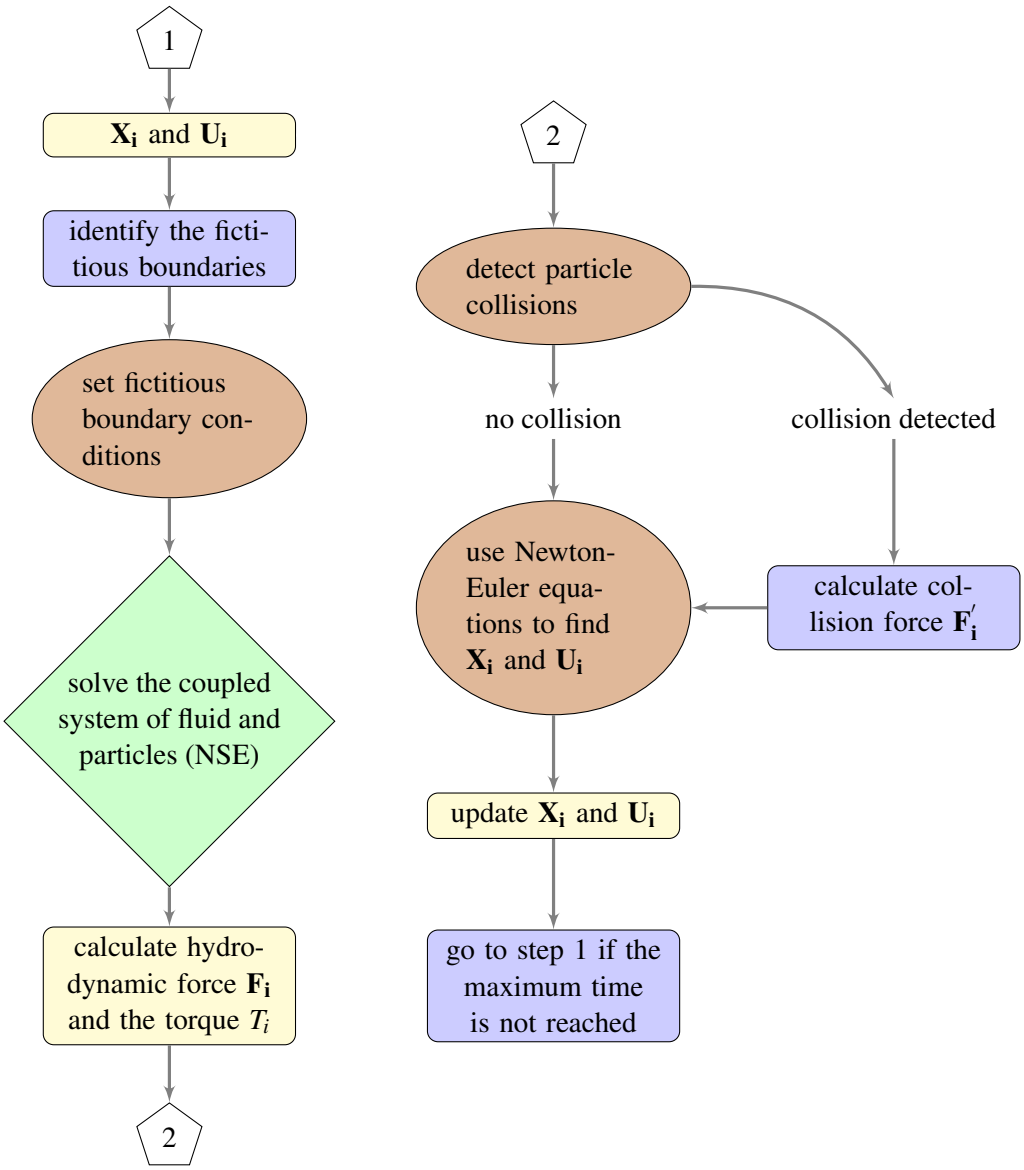

Figure 4.2: A flow-chart describing the FBM steps

5

Numerical Experiments

In this chapter, we will present the numerical results for the collision models discussed in the previous chapter 3. The results are presented by combining these collision models with the CFD part and simulating after integrating with our CFD code FEATFLOW. The methodology of combining the collision models and to treat particles in the fluid has been described in chapter 4. The results for the case of two circular particles, many circular particles and general shape particles in fluid are discussed. Later, applications for particles in annulus and particles in lid driven cavity [24] are presented.

Sedimentation of particles is discussed and the efficiency of collision models for the case of many particles is observed. Bean shaped particles are simulated after modifications in collision models as an example for general shape particles. Different type of particles (circle, square and ellipse) inside an annulus are simulated and are compared.

5.1. 2-particles

Two circular particles are allowed to fall inside a channel using collision model 1, collision model 2, collision model 3 and 'No Collision Model' (without using any collision model) and these results are compared with the reference values of collision model 3 results using a very fine mesh on level 7. The number of elements on level 1 = 259, hence the number of elements on level 7 = 1060864.

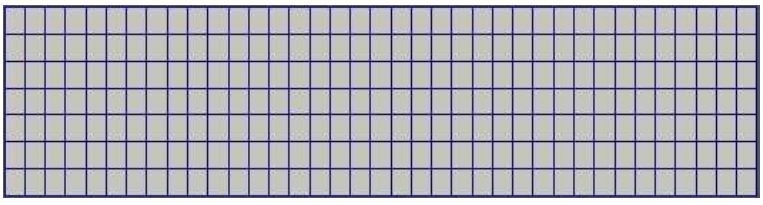

Figure 5.1: Channel mesh (Coarse mesh LEVEL 1) rotated by 90 degrees

Simulations are performed at three different mesh refinement levels, i.e., mesh level 4, mesh level 5 and mesh level 6. Collision model 3 (with mesh level 7) has been used for the reference values because this collision model has shown the best results as discussed in chapter 3.

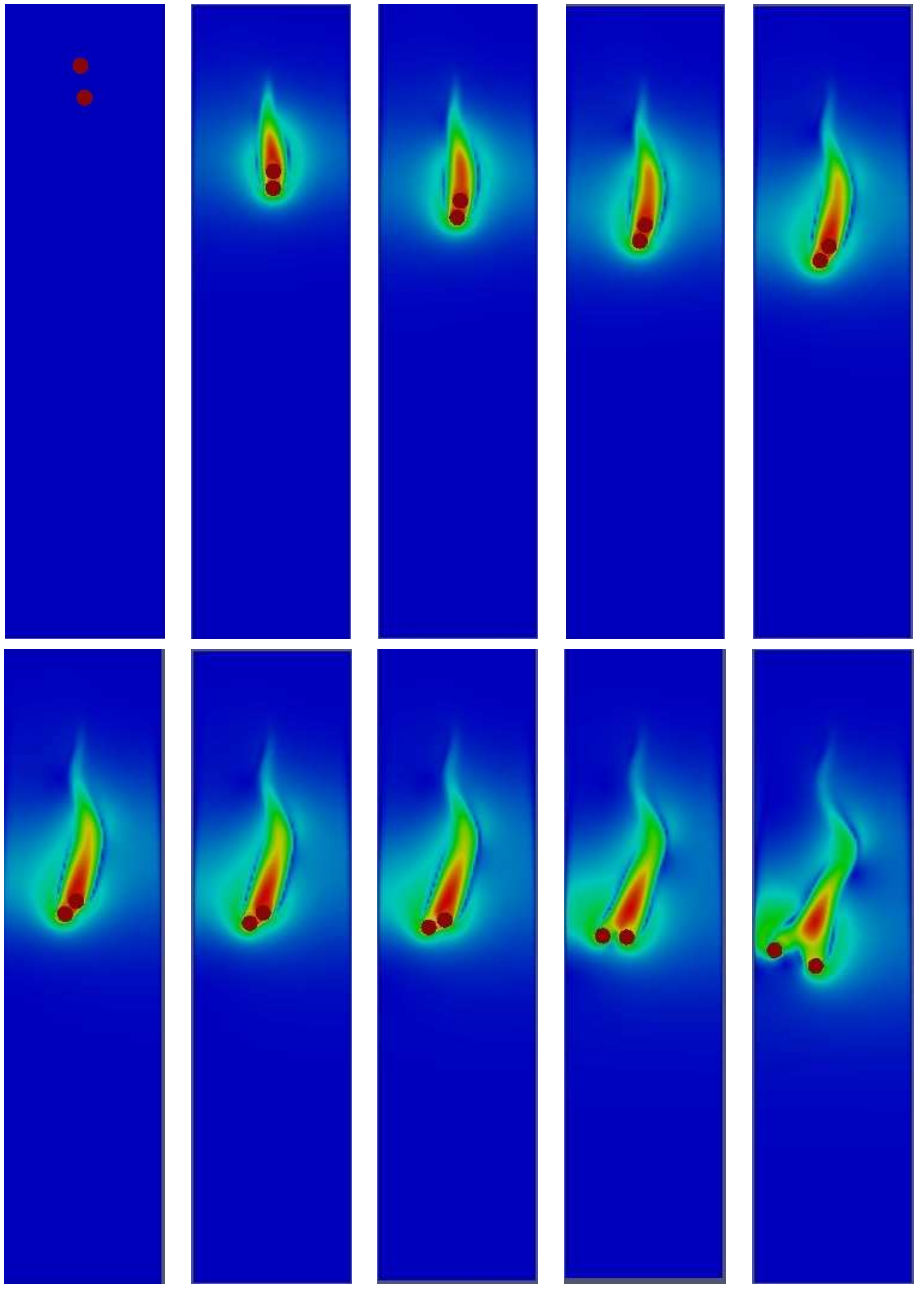

Figure 5.2: Simulation of 2 particles moving under gravity at t = 0.0, t = 0.15, t = 0.18, t = 0.20, t = 0.22, t = 0.23, t = 0.24, t = 0.25, t = 0.27 and t = 0.30

The (dimensionless) fluid density is $\rho_f = 1.0$, the acceleration due to gravity is $g = 981$, the viscosity is $\mu = 0.01$, the particle diameter is 0.2, density of the particle is $\rho_s = 1.5$ and, hence, the mass of the particle is $m_s = 0.047$ and solid-to-fluid density ratio is 1.5. Particles are released from rest in a channel with a width of 2 and height of 8. Initially, the center coordinates of the first particle are $(0.95, 7.2)$ and the center coordinates of the second particle are $(1.0, 6.8)$. The current initial position of the particles ensures that they will have collision during their fall and will undergo the well known phenomena of drafting, kissing and tumbling [15, 23, 26]. The same configuration is used for all the tests for two circular particles.

5.1.1. Collision Model 3 with mesh level 7 (Reference values)

The positions and velocities of the two falling particles obtained for the time-steps 0.001, 0.0003 and 0.0001 are observed together with mesh level 7 as reference values to be compared later with the results of the different collision models.

Level 7:

The time history of two particles falling down and colliding with time-step 0.0001.

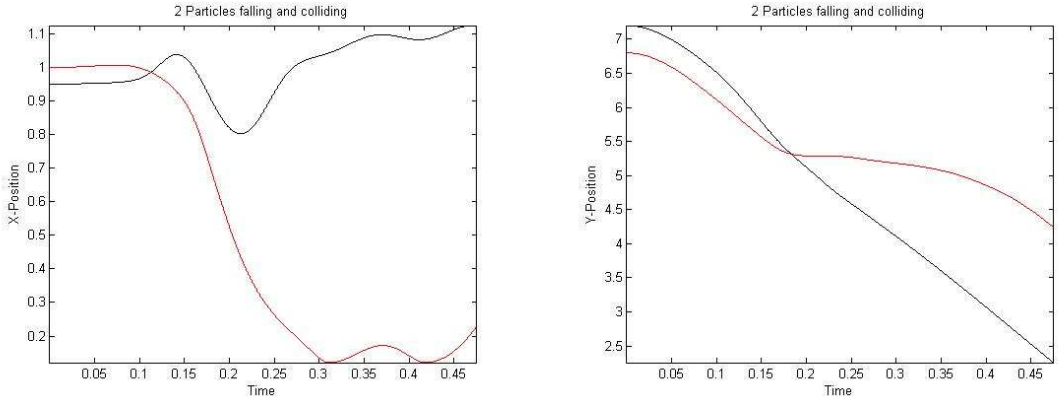

Figure 5.3: x-coordinate and y-coordinate of 2 particles w.r.t. time.

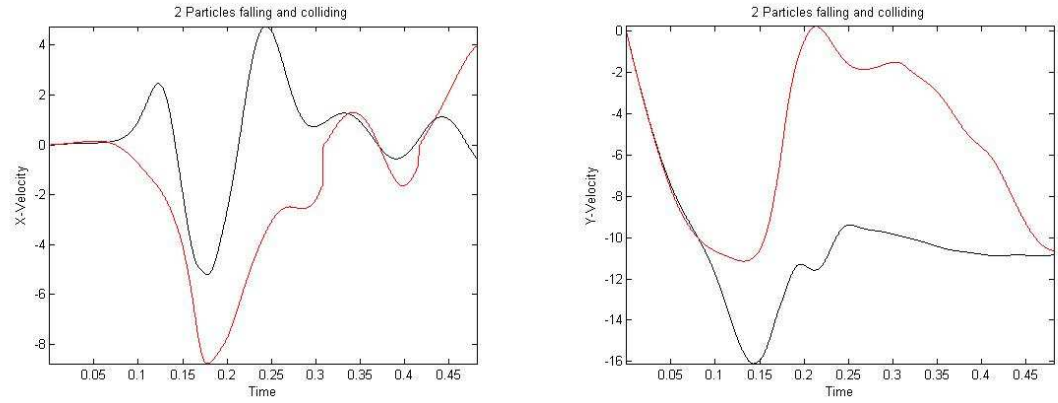

Figure 5.4: u-component and v-component of the translational velocity of 2 particles w.r.t. time.

The red line represents the first particle and the black line represents the second particle. Figure 5.3 (left) shows the x-coordinate of the center of the two particles and similarly, figure 5.3 (right) shows the y-coordinate of the center of the two particles. Figure 5.4 (left) shows the u-component of the velocity of the two particles and similarly, figure 5.4 (right) shows the v-component of the velocity of the two particles.

Our main focus in the graphs will be at the time interval between $t = 0.1$ and $t = 0.3$ because during this time interval the particles undergo the process of drafting, kissing and tumbling along with the collision of particles.

Now we present tables for the position and velocity of the 2 particles using time-steps 0.001, 0.0003 and 0.0001.

Table 5.1: Position, Minimum distance and Terminal speed of 2 particles (Level 7)

	same x-pos.		same y-pos.		Terminal Vel.				min Dist.	
					Particle1		Particle2		between particles	
$tstep$	at t	p_x	at t	p_y	at t	v_t	at t	v_t	at t	d_{min}
0.001	0.114	0.986	0.204	5.182	0.450	-11.090	0.450	-11.030	0.195	0.219
0.0003	0.113	0.985	0.184	5.306	0.450	-10.910	0.450	-10.420	0.174	0.208
0.0001	0.113	0.985	0.183	5.315	0.450	-10.850	0.450	-9.314	0.158	0.229

Table 5.1 compares the time t when the 2 particles have the same x-position and similarly when the 2 particles have the same y-position by using three different time-steps. Moreover, the time t at which each particle attains the terminal speed during their downward motion is presented.

Initially the particles have different x-coordinate and y-coordinate positions but as they fall and undergo the phenomena of drafting, kissing and tumbling as well as experience the collision forces, their positions take the same x-value and similarly the same y-value at some instant. The instant at which the 2 particles have the same x-position or the same y-position may vary with the change in mesh level, time-step and collision model and is used to compare the collision models. Furthermore, the minimum distance between the particles is also helpful to check if the particles overlap or how close these particles are during the collision process.

Table 5.2: Min/Max velocity of 2 particles (Level 7)

	Min/Max x-vel.				Min/Max y-vel.			
	Particle1		Particle2		Particle1		Particle2	
$tstep$	at t	v_{x1}	at t	v_{x2}	at t	v_{y1}	at t	v_{y2}
0.001	0.195	-7.267	0.198	-8.694	0.144	-15.262	0.222	-0.713
0.0003	0.177	-5.263	0.180	-8.6708	0.143	-16.055	0.213	-0.075
0.0001	0.177	-5.195	0.178	-8.769	0.143	-16.104	0.213	-0.227

Table 5.2 compares the time t when each particle's x-velocity and similarly y-velocity has an extreme value (maximum/minimum value) using three different time-steps. Figure 5.4 shows that at different values of time t the particles attain minimum/maximum x-velocity and y-velocity.

Again, the extreme values of the velocity of the 2 particles may vary due to the collision process and are used as a criteria to compare the collision models.

From Table 5.1 and 5.2 we can see that the particles have the same x-position $p_x \approx 0.99$ at time $t \approx 0.11$, same y-position $p_y \approx 5.31$ at time $t \approx 0.18$. The minimum distance between the particles is $d_{min} \approx 0.22$ at time $t \approx 0.16$. Here $d_{min} > 0.2$ which shows that the particles do not overlap because the radius of each particle is 0.1. The extreme values for the x-velocity of the first particle is $v_{x1} \approx -5.20$ at time $t \approx 0.18$, y-velocity of the first particle is $v_{y1} \approx -16.10$ at time $t \approx 0.14$, x-velocity of the second particle is $v_{x2} \approx -8.77$ at time $t \approx 0.18$ and y-velocity of the second particle is $v_{y2} \approx -0.22$ at time $t \approx 0.21$. The first particle attains the terminal velocity $v_{t1} \approx -10.90$ at time $t \approx 0.45$ and the second particle attains the terminal velocity $v_{t2} \approx -9.31$ at time $t \approx 0.45$. We will use these values to compare the results of the collision models.

5.1.2. No Collision Model (Model 0)

The positions and velocities of the two falling particles for the time steps 0.001, 0.0003 and 0.0001 are observed on mesh level 4, 5 and 6.

Level 4:

The time history of two particles falling down and colliding with time-step 0.0001.

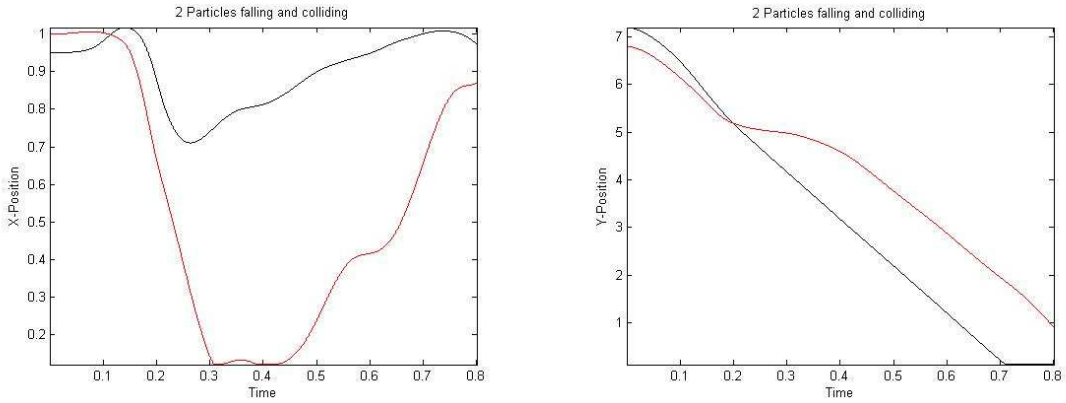

Figure 5.5: x-coordinate and y-coordinate of 2 particles w.r.t. time.

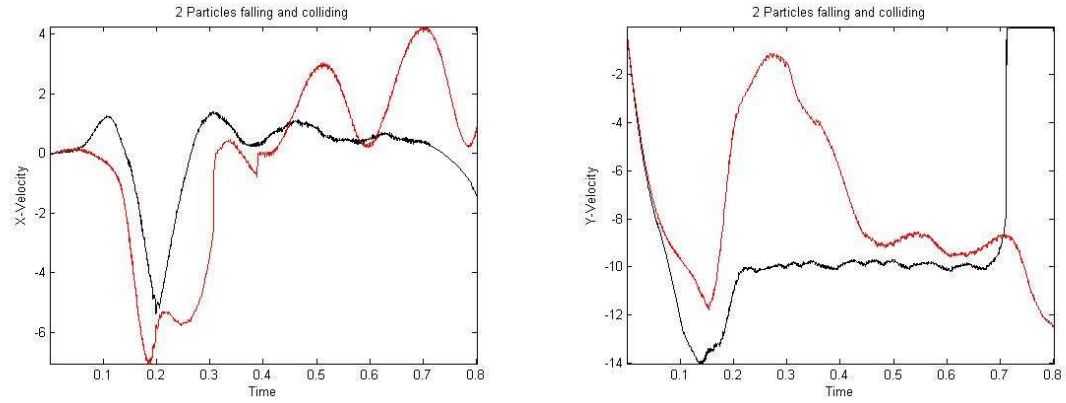

Figure 5.6: u-component and v-component of the translational velocity of 2 particles w.r.t. time.

The red line represents the first particle and the black line represents the second particle. Figure 5.5 (left) shows the x-coordinate of the center of the two particles and similarly, figure 5.5 (right) shows the y-coordinate of the center of the two particles. Figure 5.6 (left) shows the u-component of the velocity of the two particles and similarly, figure 5.6 (right) shows the v-component of the velocity of the two particles.

Tables for position and velocity of the 2 particles using time-steps 0.001, 0.0003 and 0.0001 are presented below.

Table 5.3: Position, Minimum distance and Terminal speed of 2 particles (Level 4)

	same x-pos.		same y-pos.		Terminal Vel.				min Dist.	
					Particle1		Particle2		between particles	
$tstep$	at t	p_x	at t	p_y	at t	v_t	at t	v_t	at t	d_{min}
0.001	0.138	1.028	0.234	4.643	0.450	-9.493	0.450	-9.079	0.189	0.162
0.0003	0.141	1.021	0.261	4.259	0.513	-10.130	0.513	-7.288	0.218	0.180
0.0001	0.115	0.999	0.199	5.195	0.471	-9.791	0.471	-9.105	0.164	0.196
Reference Values										
0.0001	0.113	0.985	0.183	5.315	0.450	-10.850	0.450	-9.314	0.158	0.229

Table 5.3 compares the time t when the 2 particles have the same x-position and similarly when the 2 particles have the same y-position by using three different time-steps. Moreover, the time t at which each particle attains the terminal speed during their downward motion is presented.

Table 5.4: Min/Max velocity of 2 particles (Level 4)

	Min/Max x-vel.				Min/Max y-vel.			
	Particle1		Particle2		Particle1		Particle2	
$tstep$	at t	v_{x1}	at t	v_{x2}	at t	v_{y1}	at t	v_{y2}
0.001	0.225	-3.430	0.225	-7.369	0.135	-14.452	0.294	-2.225
0.0003	0.255	-3.761	0.243	-6.772	0.148	-14.585	0.331	-1.303
0.0001	0.199	-5.377	0.185	-7.039	0.140	-14.014	0.271	-1.140
Reference Values								
0.0001	0.177	-5.195	0.178	-8.769	0.143	-16.104	0.213	-0.227

Table 5.4 compares the time t when each particle's x-velocity and similarly y-velocity has an extreme value (maximum/minimum value) using three different time-steps. Figure 5.6 shows that at different values of time t the particles attain minimum/maximum x-velocity and y-velocity.

In the 'No Collision Model' we have simulated the 2 particles in the absence of collision model/forces and from Table 5.3 we can see that the minimum distance between the particles d_{min} is less than 0.2. Hence in the absence of collision forces the particles overlapped.

Level 5:

The time history of two particles falling down and colliding with time-step 0.0001.

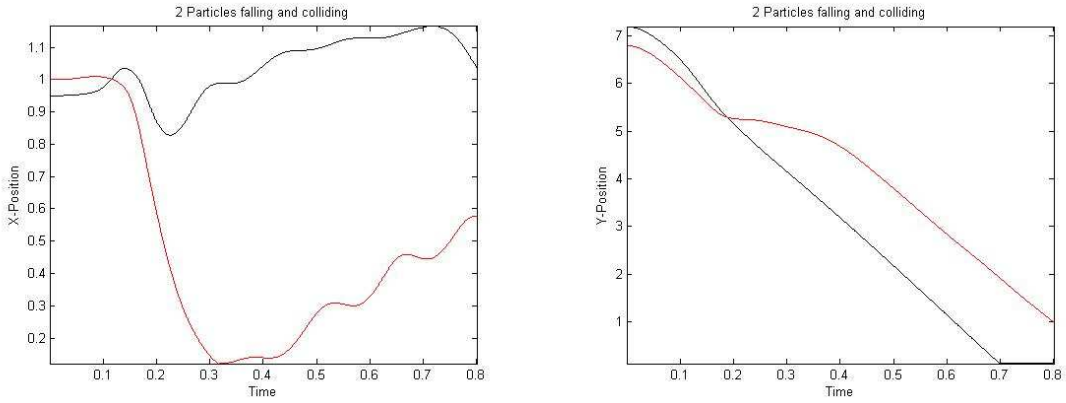

Figure 5.7: x-coordinate and y-coordinate of 2 particles w.r.t. time.

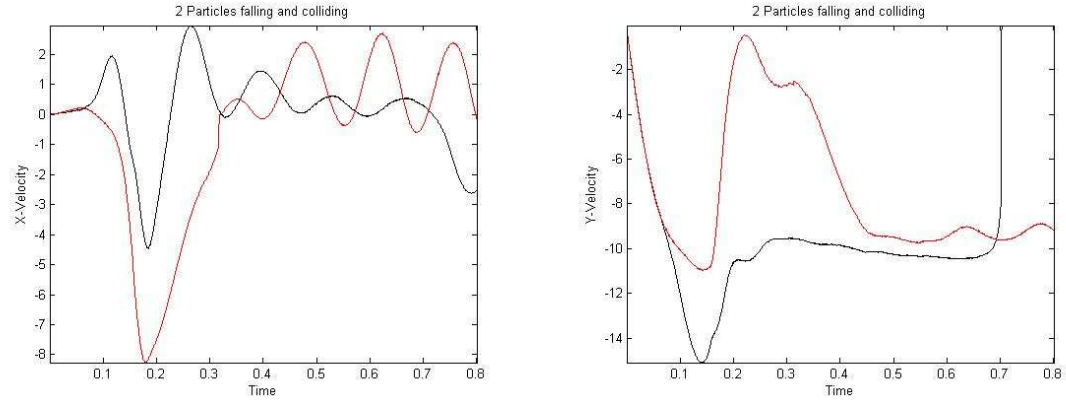

Figure 5.8: u-component and v-component of the translational velocity of 2 particles w.r.t. time.

The red line represents the first particle and the black line represents the second particle. Figure 5.7 (left) shows the x-coordinate of the center of the two particles and similarly, figure 5.7 (right) shows the y-coordinate of the center of the two particles. Figure 5.8 (left) shows the u-component of the velocity of the two particles and similarly, figure 5.8 (right) shows the v-component of the velocity of the two particles.

Tables for position and velocity of the 2 particles using time-steps 0.001, 0.0003 and 0.0001 are presented below.

Table 5.5: Position, Minimum distance and Terminal speed of 2 particles (Level 5)

	same x-pos.		same y-pos.		Terminal Vel.				min Dist.	
					Particle1		Particle2		between particles	
$tstep$	at t	p_x	at t	p_y	at t	v_t	at t	v_t	at t	d_{min}
0.001	0.111	1.002	0.189	5.274	0.528	-10.470	0.528	-9.545	0.165	0.190
0.0003	0.113	1.000	0.189	5.271	0.518	-10.460	0.518	-9.952	0.163	0.195
0.0001	0.116	1.002	0.188	5.298	0.525	-10.280	0.525	-9.638	0.163	0.199
Reference Values										
0.0001	0.113	0.985	0.183	5.315	0.450	-10.850	0.450	-9.314	0.158	0.229

Table 5.5 compares the time t when the 2 particles have the same x-position and similarly when the 2 particles have the same y-position by using three different time-steps. Moreover, the time t at which each particle attains the terminal speed during their downward motion is presented.

Table 5.6: Min/Max velocity of 2 particles (Level 5)

	Min/Max x-vel.				Min/Max y-vel.			
	Particle1		Particle2		Particle1		Particle2	
$tstep$	at t	v_{x1}	at t	v_{x2}	at t	v_{y1}	at t	v_{y2}
0.001	0.183	-4.698	0.183	-8.734	0.138	-15.154	0.219	-0.900
0.0003	0.183	-4.597	0.180	-8.415	0.142	-15.277	0.224	-0.690
0.0001	0.184	-4.465	0.180	-8.263	0.137	-15.081	0.224	-0.466
Reference Values								
0.0001	0.177	-5.195	0.178	-8.769	0.143	-16.104	0.213	-0.227

Table 5.6 compares the time t when each particle's x-velocity and similarly y-velocity has an extreme value (maximum/minimum value) using three different time-steps. Figure 5.8 shows that at different values of time t the particles attain minimum/maximum x-velocity and y-velocity.

Again Table 5.5 shows that the particles overlap ($d_{min} < 0.2$) using the mesh level 5.

Level 6:

The time history of two particles falling down and colliding with time-step 0.0001.

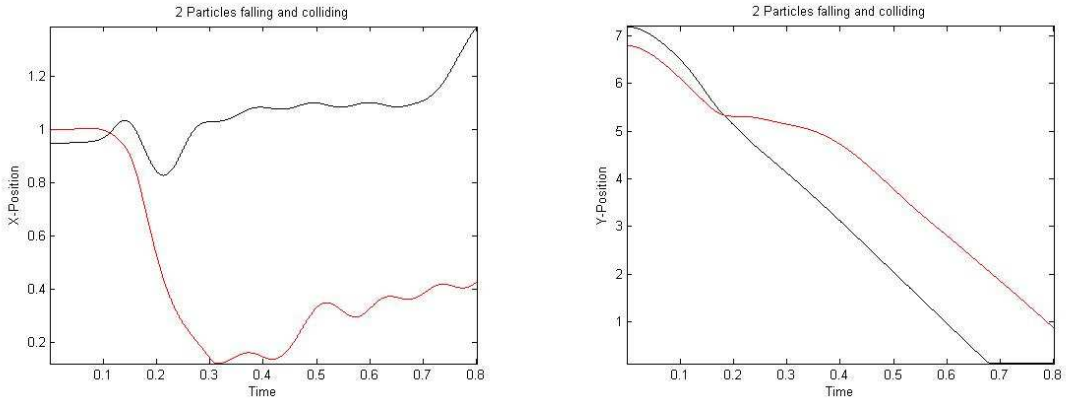

Figure 5.9: x-coordinate and y-coordinate of 2 particles w.r.t. time.

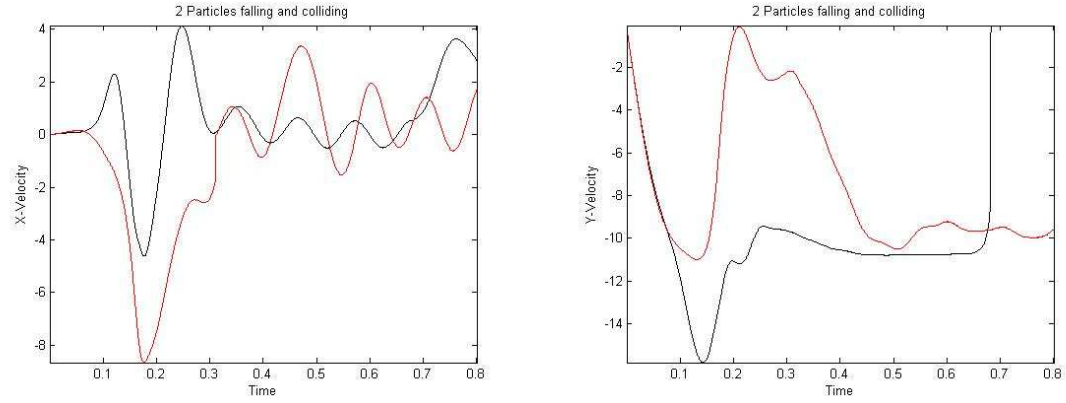

Figure 5.10: u-component and v-component of the translational velocity of 2 particles w.r.t. time.

The red line represents the first particle and the black line represents the second particle. Figure 5.9 (left) shows the x-coordinate of the center of the two particles and similarly, figure 5.9 (right) shows the y-coordinate of the center of the two particles. Figure 5.10 (left) shows the u-component of the velocity of the two particles and similarly, figure 5.10 (right) shows the v-component of the velocity of the two particles.

Tables for position and velocity of the 2 particles using time-steps 0.001, 0.0003 and 0.0001 are presented below.

Table 5.7: Position, Minimum distance and Terminal speed of 2 particles (Level 6)

	same x-pos.		same y-pos.		Terminal Vel.				min Dist.	
					Particle1		Particle2		between particles	
$tstep$	at t	p_x	at t	p_y	at t	v_t	at t	v_t	at t	d_{min}
0.001	0.111	0.990	0.189	5.307	0.525	-10.750	0.525	-9.802	0.177	0.212
0.0003	0.112	0.988	0.182	5.335	0.517	-10.870	0.517	-10.590	0.169	0.206
0.0001	0.113	0.989	0.182	5.342	0.502	-10.770	0.502	-10.490	0.169	0.207
Reference Values										
0.0001	0.113	0.985	0.183	5.315	0.450	-10.850	0.450	-9.314	0.158	0.229

Table 5.7 compares the time t when the 2 particles have the same x-position and similarly when the 2 particles have the same y-position by using three different time-steps. Moreover, the time t at which each particle attains the terminal speed during their downward motion is presented.

Table 5.8: Min/Max velocity of 2 particles (Level 6)

	Min/Max x-vel.				Min/Max y-vel.			
	Particle1		Particle2		Particle1		Particle2	
$tstep$	at t	v_{x1}	at t	v_{x2}	at t	v_{y1}	at t	v_{y2}
0.001	0.186	-6.454	0.183	-8.872	0.138	-15.295	0.216	0.069
0.0003	0.178	-4.992	0.177	-8.790	0.141	-15.837	0.211	-0.063
0.0001	0.177	-4.619	0.177	-8.662	0.142	-15.836	0.211	-0.077
Reference Values								
0.0001	0.177	-5.195	0.178	-8.769	0.143	-16.104	0.213	-0.227

Table 5.8 compares the time t when each particle's x-velocity and similarly y-velocity has an extreme value (maximum/minimum value) using three different time-steps. Figure 5.10 shows that at different values of time t the particles attain minimum/maximum x-velocity and y-velocity.

Here, from Table 5.7, we find an interesting result that the particles did not overlap in the absence of any collision model/forces which shows that by using a higher mesh level we can avoid the collision/overlapping of the particles.

Now we present the results on all the levels together for the direct comparison of Model 0 on different levels.

Table 5.9: Position, Minimum distance and Terminal speed of 2 particles

	same x-pos.		same y-pos.		Terminal Vel.				min Dist.	
					Particle1		Particle2		between particles	
$tstep$	at t	p_x	at t	p_y	at t	v_t	at t	v_t	at t	d_{min}
Level 4										
0.001	0.138	1.028	0.234	4.643	0.450	-9.493	0.450	-9.079	0.189	0.162
0.0003	0.141	1.021	0.261	4.259	0.513	-10.130	0.513	-7.288	0.218	0.180
0.0001	0.115	0.999	0.199	5.195	0.471	-9.791	0.471	-9.105	0.164	0.196
Level 5										
0.001	0.111	1.002	0.189	5.274	0.528	-10.470	0.528	-9.545	0.165	0.190
0.0003	0.113	1.000	0.189	5.271	0.518	-10.460	0.518	-9.952	0.163	0.195
0.0001	0.116	1.002	0.188	5.298	0.525	-10.280	0.525	-9.638	0.163	0.199
Level 6										
0.001	0.111	0.990	0.189	5.307	0.525	-10.750	0.525	-9.802	0.177	0.212
0.0003	0.112	0.988	0.182	5.335	0.517	-10.870	0.517	-10.590	0.169	0.206
0.0001	0.113	0.989	0.182	5.342	0.502	-10.770	0.502	-10.490	0.169	0.207
Reference Values										
0.0001	0.113	0.985	0.183	5.315	0.450	-10.850	0.450	-9.314	0.158	0.229

Table 5.10: Min/Max velocity of 2 particles

	Min/Max x-vel.				Min/Max y-vel.			
	Particle1		Particle2		Particle1		Particle2	
$tstep$	at t	v_{x1}	at t	v_{x2}	at t	v_{y1}	at t	v_{y2}
Level 4								
0.001	0.225	-3.430	0.225	-7.369	0.135	-14.452	0.294	-2.225
0.0003	0.255	-3.761	0.243	-6.772	0.148	-14.585	0.331	-1.303
0.0001	0.199	-5.377	0.185	-7.039	0.140	-14.014	0.271	-1.140
Level 5								
0.001	0.183	-4.698	0.183	-8.734	0.138	-15.154	0.219	-0.900
0.0003	0.183	-4.597	0.180	-8.415	0.142	-15.277	0.224	-0.690
0.0001	0.184	-4.465	0.180	-8.263	0.137	-15.081	0.224	-0.466
Level 6								
0.001	0.186	-6.454	0.183	-8.872	0.138	-15.295	0.216	0.069
0.0003	0.178	-4.992	0.177	-8.790	0.141	-15.837	0.211	-0.063
0.0001	0.177	-4.619	0.177	-8.662	0.142	-15.836	0.211	-0.077
Reference Values								
0.0001	0.177	-5.195	0.178	-8.769	0.143	-16.104	0.213	-0.227

Summary

The results of the 'No Collision Model' show that a higher mesh level (with small time steps) can avoid the particle's overlapping. Using the mesh level 4 and the mesh level 5, the particles overlapped but as we increased the level of the mesh to 6, the particles did not overlap. But in most of the simulations we have to consider the computational cost which is increased by increasing the mesh level. Also we have to decrease the time-step. For the case of many particles when there are more particles interacting with each other at the same time, it is harder to avoid the particle's

overlapping by increasing the mesh level and reducing the time-step. Hence a good collision model is necessary to keep the particles at a 'safer' distance.

5.1.3. Repulsive Force Collision Model (Model 1)

The positions and velocities of the two falling particles for the time-steps 0.001, 0.0003 and 0.0001 are observed on mesh level 4, 5 and 6.

Level 4:

The time history of two particles falling down and colliding with time-step 0.0001.

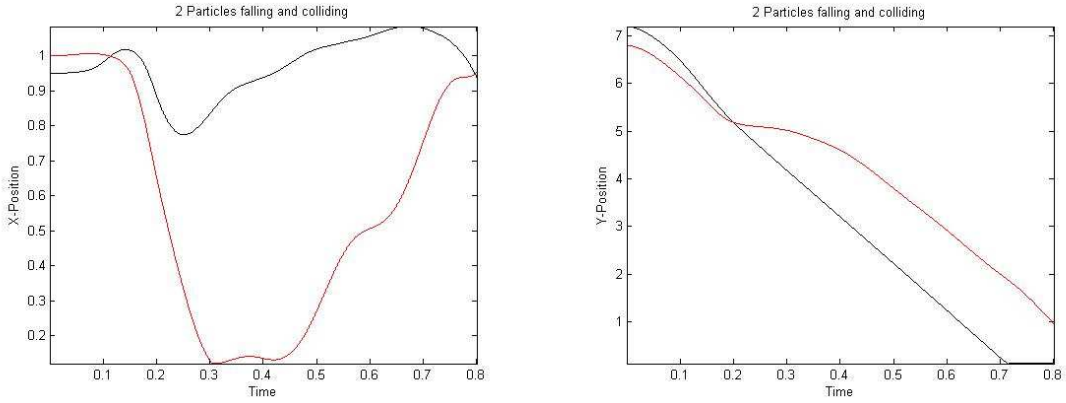

Figure 5.11: x-coordinate and y-coordinate of 2 particles w.r.t. time.

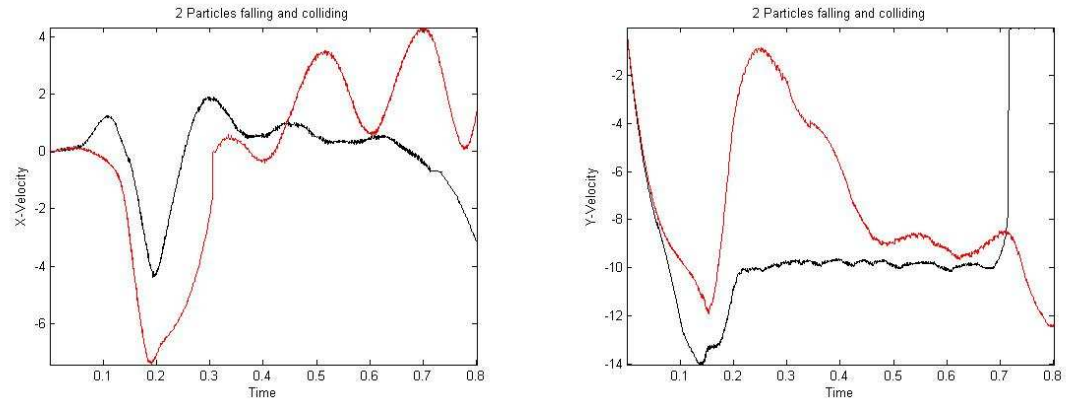

Figure 5.12: u-component and v-component of the translational velocity of 2 particles w.r.t. time.

The red line represents the first particle and the black line represents the second particle. Figure 5.11 (left) shows the x-coordinate of the center of the two particles and similarly, figure 5.11 (right) shows the y-coordinate of the center of the two particles. Figure 5.12 (left) shows the u-component of the velocity of the two particles and similarly, figure 5.12 (right) shows the v-component of the velocity of the two particles.

Tables for position and velocity of the 2 particles using time-steps 0.001, 0.0003 and 0.0001 are presented below.

Table 5.11: Position, Minimum distance and Terminal speed of 2 particles (Level 4)

	same x-pos.		same y-pos.		Terminal Vel.				min Dist.	
					Particle1		Particle2		between particles	
$tstep$	at t	p_x	at t	p_y	at t	v_t	at t	v_t	at t	d_{min}
0.001	0.138	1.028	0.255	4.394	0.600	-9.640	0.600	-8.960	0.144	0.198
0.0003	0.141	1.021	0.266	4.204	0.540	-9.890	0.540	-8.130	0.1508	0.199
0.0001	0.115	0.999	0.200	5.190	0.315	-9.728	0.592	-9.135	0.164	0.201
Reference Values										
0.0001	0.113	0.985	0.183	5.315	0.450	-10.850	0.450	-9.314	0.158	0.229

Table 5.11 compares the time t when the 2 particles have the same x-position and similarly when the 2 particles have the same y-position by using three different time-steps. Moreover, the time t at which each particle attains the terminal speed during their downward motion is presented.

Table 5.12: Min/Max velocity of 2 particles (Level 4)

	Min/Max x-vel.				Min/Max y-vel.			
	Particle1		Particle2		Particle1		Particle2	
$tstep$	at t	v_{x1}	at t	v_{x2}	at t	v_{y1}	at t	v_{y2}
0.001	0.240	-3.8226	0.246	-7.814	0.135	-14.456	0.297	-3.463
0.0003	0.255	-3.467	0.253	-7.585	0.145	-14.573	0.315	-1.760
0.0001	0.193	-4.381	0.191	-7.448	0.140	-14.013	0.251	-0.878
Reference Values								
0.0001	0.177	-5.195	0.178	-8.769	0.143	-16.104	0.213	-0.227

Table 5.12 compares the time t when each particle's x-velocity and similarly y-velocity has an extreme value (maximum/minimum value) using three different time-steps. Figure 5.12 shows that at different values of time t the particles attain minimum/maximum x-velocity and y-velocity.

We can see from Table 5.11 that the particles overlapped ($d_{min} < 0.2$) instead of using the collision model 1 with mesh level 4. This shows that collision model 1 may not be reliable to stop the overlapping of the particles. To avoid the overlapping of the particles, one way is to increase the magnitude of the collision forces by adjusting the stiffness parameters in the collision model 1.

Level 5:

The time history of two particles falling down and colliding with time-step 0.0001.

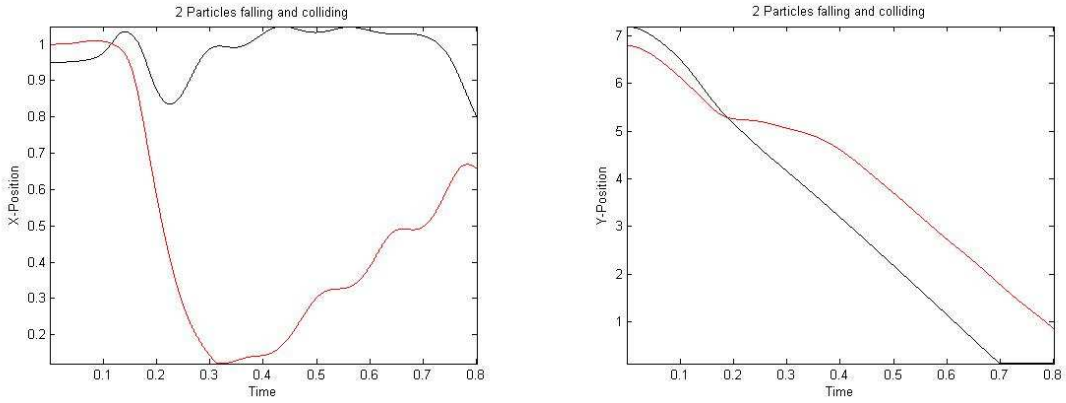

Figure 5.13: x-coordinate and y-coordinate of 2 particles w.r.t. time.

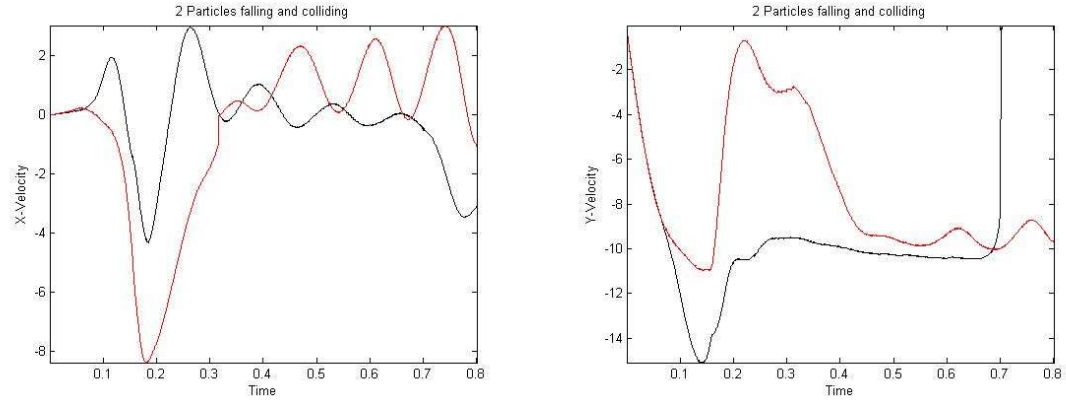

Figure 5.14: u-component and v-component of the translational velocity of 2 particles w.r.t. time.

The red line represents the first particle and the black line represents the second particle. Figure 5.13 (left) shows the x-coordinate of the center of the two particles and similarly, figure 5.13 (right) shows the y-coordinate of the center of the two particles. Figure 5.14 (left) shows the u-component of the velocity of the two particles and similarly, figure 5.14 (right) shows the v-component of the velocity of the two particles.

Tables for position and velocity of the 2 particles using time-steps 0.001, 0.0003 and 0.0001 are presented below.

Table 5.13: Position, Minimum distance and Terminal speed of 2 particles (Level 5)

	same x-pos.		same y-pos.		Terminal Vel.				min Dist.	
					Particle1		Particle2		between particles	
$tstep$	at t	p_x	at t	p_y	at t	v_t	at t	v_t	at t	d_{min}
0.001	0.111	1.002	0.189	5.279	0.525	-10.400	0.525	-9.230	0.156	0.200
0.0003	0.113	1.000	0.189	5.264	0.517	-10.400	0.517	-9.700	0.160	0.200
0.0001	0.116	1.002	0.188	5.293	0.592	-10.410	0.592	-10.410	0.160	0.201
Reference Values										
0.0001	0.113	0.985	0.183	5.315	0.450	-10.850	0.450	-9.314	0.158	0.229

Table 5.13 compares the time t when the 2 particles have the same x-position and similarly when the 2 particles have the same y-position by using three different time-steps. Moreover, the time t at which each particle attains the terminal speed during their downward motion is presented.

Table 5.14: Min/Max velocity of 2 particles (Level 5)

	Min/Max x-vel.				Min/Max y-vel.			
	Particle1		Particle2		Particle1		Particle2	
$tstep$	at t	v_{x1}	at t	v_{x2}	at t	v_{y1}	at t	v_{y2}
0.001	0.186	-4.844	0.186	-8.907	0.138	-15.155	0.216	-1.257
0.0003	0.183	-4.496	0.183	-8.581	0.141	-15.277	0.222	-1.020
0.0001	0.184	-4.320	0.181	-8.395	0.137	-15.081	0.219	-0.680
Reference Values								
0.0001	0.177	-5.195	0.178	-8.769	0.143	-16.104	0.213	-0.227

Table 5.14 compares the time t when each particle's x-velocity and similarly y-velocity has an extreme value (maximum/minimum value) using three different time-steps. Figure 5.14 shows that at different values of time t the particles attain minimum/maximum x-velocity and y-velocity.

With an increase in the mesh level to level 5, the collision model 1 showed better results as compared to the level 4 results. The particles did not overlap as shown by the results in Table 5.13 ($d_{min} \geq 0.20$). If we compare it with our reference results, where $d_{min} \approx 0.22$ then the collision forces are not enough to maintain that minimum distance.

Level 6:

The time history of two particles falling down and colliding with time-step 0.0001.

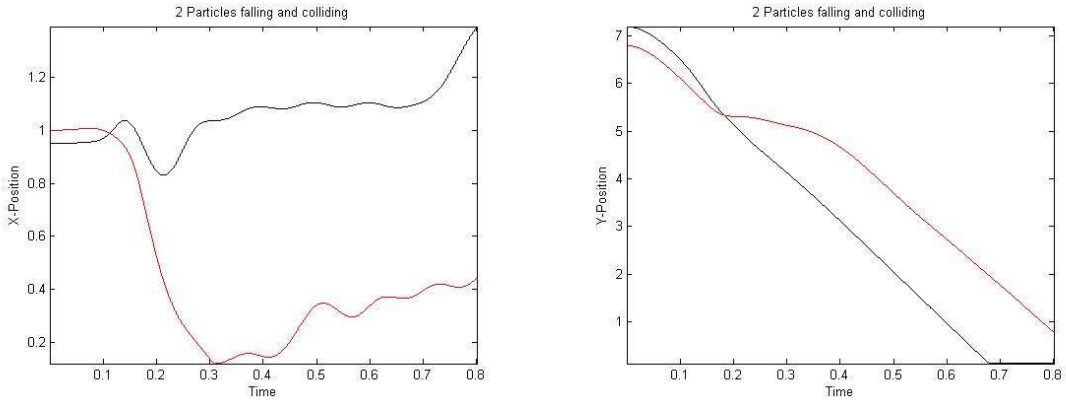

Figure 5.15: x-coordinate and y-coordinate of 2 particles w.r.t. time.

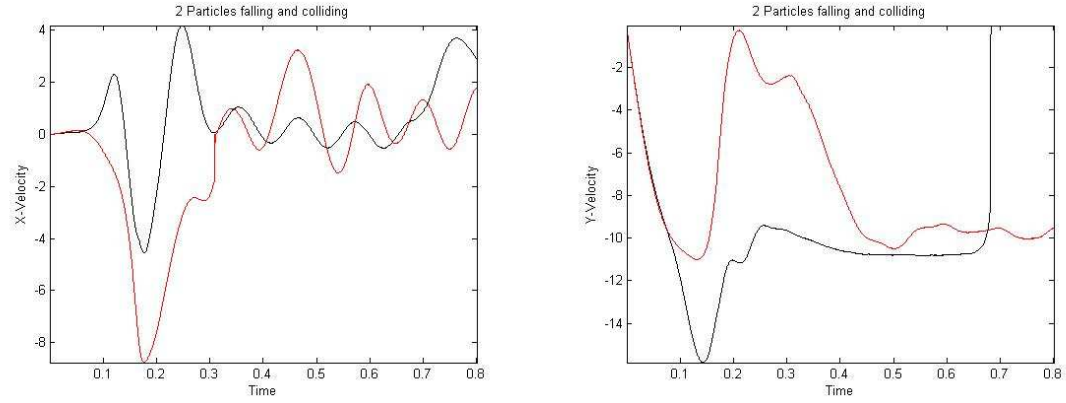

Figure 5.16: u-component and v-component of the translational velocity of 2 particles w.r.t. time.

The red line represents the first particle and the black line represents the second particle. Figure 5.15 (left) shows the x-coordinate of the center of the two particles and similarly, figure 5.15 (right) shows the y-coordinate of the center of the two particles. Figure 5.16 (left) shows the u-component of the velocity of the two particles and similarly, figure 5.16 (right) shows the v-component of the velocity of the two particles.

Tables for position and velocity of the 2 particles using time-steps 0.001, 0.0003 and 0.0001 are presented below.

Table 5.15: Position, Minimum distance and Terminal speed of 2 particles (Level 6)

	same x-pos.		same y-pos.		Terminal Vel.				min Dist.	
					Particle1		Particle2		between particles	
$tstep$	at t	p_x	at t	p_y	at t	v_t	at t	v_t	at t	d_{min}
0.001	0.111	0.990	0.189	5.308	0.510	-10.700	0.510	-9.870	0.177	0.213
0.0003	0.113	0.989	0.182	5.336	0.585	-10.800	0.585	-9.420	0.168	0.207
0.0001	0.113	0.989	0.182	5.339	0.555	-10.810	0.555	-9.510	0.167	0.208
Reference Values										
0.0001	0.113	0.985	0.183	5.315	0.450	-10.850	0.450	-9.314	0.158	0.229

Table 5.15 compares the time t when the 2 particles have the same x-position and similarly when the 2 particles have the same y-position by using three different time-steps. Moreover, the time t at which each particle attains the terminal speed during their downward motion is presented.

Table 5.16: Min/Max velocity of 2 particles (Level 6)

	Min/Max x-vel.				Min/Max y-vel.			
	Particle1		Particle2		Particle1		Particle2	
$tstep$	at t	v_{x1}	at t	v_{x2}	at t	v_{y1}	at t	v_{y2}
0.001	0.186	-6.437	0.183	-8.924	0.138	-15.296	0.216	0.055
0.0003	0.178	-4.946	0.178	-8.903	0.141	-15.838	0.211	-0.254
0.0001	0.177	-4.557	0.177	-8.772	0.142	-15.837	0.210	-0.253
Reference Values								
0.0001	0.177	-5.195	0.178	-8.769	0.143	-16.104	0.213	-0.227

Table 5.16 compares the time t when each particle's x-velocity and similarly y-velocity has an extreme value (maximum/minimum value) using three different time-steps. Figure 5.16 shows that at different values of time t the particles attain minimum/maximum x-velocity and y-velocity.

We have seen in the results of the 'No Collision Model' with mesh level 6, the particles did not overlap in the absence of the collision model. By comparing the results of Table 5.15 with the results of the 'No Collision Model' (Table 5.7 comparison of d_{min}), it is clear that with the addition of the collision forces the results have improved.

Now we present the results on all the levels together for the direct comparison of Model 1 on different levels.

Table 5.17: Position, Minimum distance and Terminal speed of 2 particles

	same x-pos.		same y-pos.		Terminal Vel.				min Dist.	
					Particle1		Particle2		between particles	
$tstep$	at t	p_x	at t	p_y	at t	v_t	at t	v_t	at t	d_{min}
Level 4										
0.001	0.138	1.028	0.255	4.394	0.600	-9.640	0.600	-8.960	0.144	0.198
0.0003	0.141	1.021	0.266	4.204	0.540	-9.890	0.540	-8.130	0.1508	0.199
0.0001	0.115	0.999	0.200	5.190	0.315	-9.728	0.592	-9.135	0.164	0.201
Level 5										
0.001	0.111	1.002	0.189	5.279	0.525	-10.400	0.525	-9.230	0.156	0.200
0.0003	0.113	1.000	0.189	5.264	0.517	-10.400	0.517	-9.700	0.160	0.200
0.0001	0.116	1.002	0.188	5.293	0.592	-10.410	0.592	-10.410	0.160	0.201
Level 6										
0.001	0.111	0.990	0.189	5.308	0.510	-10.700	0.510	-9.870	0.177	0.213
0.0003	0.113	0.989	0.182	5.336	0.585	-10.800	0.585	-9.420	0.168	0.207
0.0001	0.113	0.989	0.182	5.339	0.555	-10.810	0.555	-9.510	0.167	0.208
Reference Values										
0.0001	0.113	0.985	0.183	5.315	0.450	-10.850	0.450	-9.314	0.158	0.229

Table 5.18: Min/Max velocity of 2 particles

	Min/Max x-vel.				Min/Max y-vel.			
	Particle1		Particle2		Particle1		Particle2	
$tstep$	at t	v_{x1}	at t	v_{x2}	at t	v_{y1}	at t	v_{y2}
Level 4								
0.001	0.240	-3.8226	0.246	-7.814	0.135	-14.456	0.297	-3.463
0.0003	0.255	-3.467	0.253	-7.585	0.145	-14.573	0.315	-1.760
0.0001	0.193	-4.381	0.191	-7.448	0.140	-14.013	0.251	-0.878
Level 5								
0.001	0.186	-4.844	0.186	-8.907	0.138	-15.155	0.216	-1.257
0.0003	0.183	-4.496	0.183	-8.581	0.141	-15.277	0.222	-1.020
0.0001	0.184	-4.320	0.181	-8.395	0.137	-15.081	0.219	-0.680
Level 6								
0.001	0.186	-6.437	0.183	-8.924	0.138	-15.296	0.216	0.055
0.0003	0.178	-4.946	0.178	-8.903	0.141	-15.838	0.211	-0.254
0.0001	0.177	-4.557	0.177	-8.772	0.142	-15.837	0.210	-0.253
Reference Values								
0.0001	0.177	-5.195	0.178	-8.769	0.143	-16.104	0.213	-0.227

Summary

The results of the collision model 1 shows that by using the mesh level 4 and mesh level 5, the repulsive forces were not enough to avoid overlapping. Mesh level 6 when used with the collision model 1, shows better results comparing with the results of the 'No Collision Model (Level 6)' and the results of the reference values.

5.1.4. Repulsive Force Collision Model (Model 2)

The positions and velocities of the two falling particles for the time-steps 0.001, 0.0003 and 0.0001 are observed on mesh level 4, 5 and 6.

Level 4:

The time history of two particles falling down and colliding with time-step 0.0001.

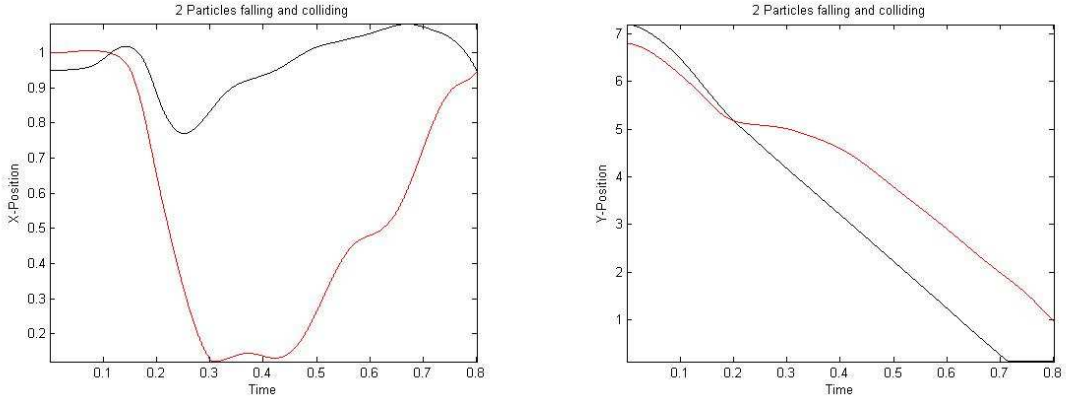

Figure 5.17: x-coordinate and y-coordinate of 2 particles w.r.t. time.

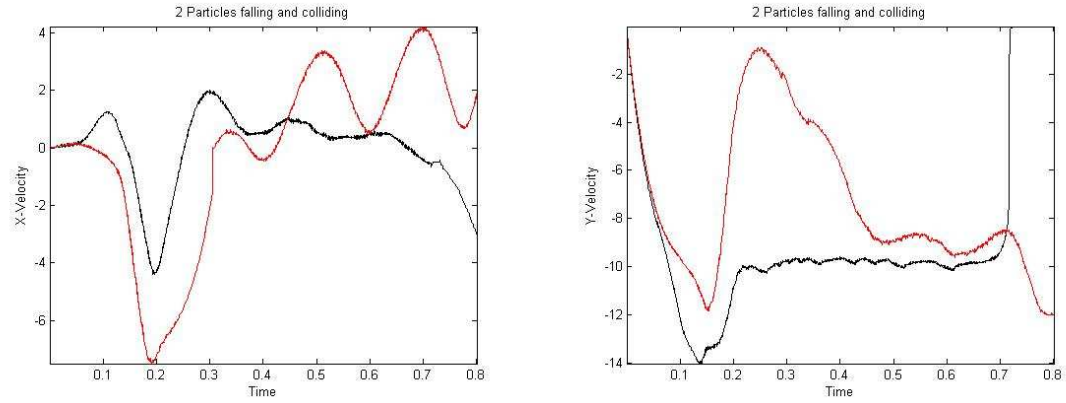

Figure 5.18: u-component and v-component of the translational velocity of 2 particles w.r.t. time.

The red line represents the first particle and the black line represents the second particle. Figure 5.17 (left) shows the x-coordinate of the center of the two particles and similarly, figure 5.17 (right) shows the y-coordinate of the center of the two particles. Figure 5.18 (left) shows the u-component of the velocity of the two particles and similarly, figure 5.18 (right) shows the v-component of the velocity of the two particles.

Tables for position and velocity of the 2 particles using time-steps 0.001, 0.0003 and 0.0001 are presented below.

Table 5.19: Position, Minimum distance and Terminal speed of 2 particles (Level 4)

	same x-pos.		same y-pos.		Terminal Vel.				min Dist.	
					Particle1		Particle2		between particles	
$tstep$	at t	p_x	at t	p_y	at t	v_t	at t	v_t	at t	d_{min}
0.001	0.138	1.028	0.264	4.278	0.510	-9.710	0.510	-9.080	0.171	0.200
0.0003	0.141	1.021	0.272	4.129	0.549	-10.000	0.549	-8.318	0.198	0.200
0.0001	0.115	0.999	0.201	5.181	0.315	-9.728	0.592	-9.135	0.166	0.201
Reference Values										
0.0001	0.113	0.985	0.183	5.315	0.450	-10.850	0.450	-9.314	0.158	0.229

Table 5.19 compares the time t when the 2 particles have the same x-position and similarly when the 2 particles have the same y-position by using three different time-steps. Moreover, the time t at which each particle attains the terminal speed during their downward motion is presented.

Table 5.20: Min/Max velocity of 2 particles (Level 4)

	Min/Max x-vel.				Min/Max y-vel.			
	Particle1		Particle2		Particle1		Particle2	
$tstep$	at t	v_{x1}	at t	v_{x2}	at t	v_{y1}	at t	v_{y2}
0.001	0.246	-4.3006	0.252	-7.902	0.135	-14.452	0.306	-3.508
0.0003	0.262	-4.054	0.261	-7.827	0.144	-14.534	0.338	-1.431
0.0001	0.196	-4.410	0.191	-7.498	0.140	-14.014	0.252	-0.930
Reference Values								
0.0001	0.177	-5.195	0.178	-8.769	0.143	-16.104	0.213	-0.227

Table 5.20 compares the time t when each particle's x-velocity and similarly y-velocity has an extreme value (maximum/minimum value) using three different time-steps. Figure 5.18 shows that at different values of time t the particles attain minimum/maximum x-velocity and y-velocity.

We can see from Table 5.19 that the particles did not overlap using the mesh level 4 as compared with the results of Table 5.11 of collision model 1 using mesh level 4 where the particles overlapped. If we compare the results shown in Table 5.19 with the results of the reference values then the collision forces are not enough to maintain the minimum distance $d_{min} \approx 0.22$.

Level 5:

The time history of two particles falling down and colliding with time-step 0.0001.

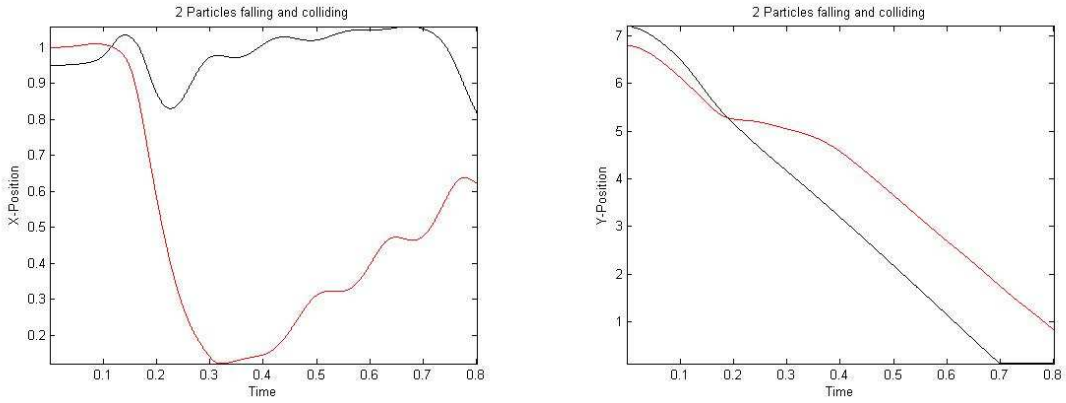

Figure 5.19: x-coordinate and y-coordinate of 2 particles w.r.t. time.

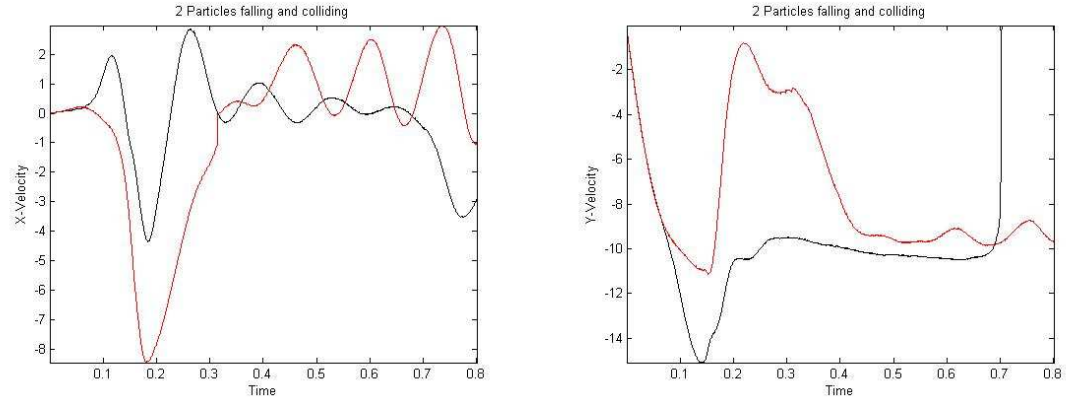

Figure 5.20: u-component and v-component of the translational velocity of 2 particles w.r.t. time.

The red line represents the first particle and the black line represents the second particle. Figure 5.19 (left) shows the x-coordinate of the center of the two particles and similarly, figure 5.19 (right) shows the y-coordinate of the center of the two particles. Figure 5.20 (left) shows the u-component of the velocity of the two particles and similarly, figure 5.20 (right) shows the v-component of the velocity of the two particles.

Tables for position and velocity of the 2 particles using time-steps 0.001, 0.0003 and 0.0001 are presented below.

Table 5.21: Position, Minimum distance and Terminal speed of 2 particles (Level 5)

	same x-pos.		same y-pos.		Terminal Vel.				min Dist.	
					Particle1		Particle2		between particles	
$tstep$	at t	p_x	at t	p_y	at t	v_t	at t	v_t	at t	d_{min}
0.001	0.111	1.002	0.192	5.247	0.510	-10.300	0.510	-9.190	0.162	0.203
0.0003	0.113	1.000	0.190	5.255	0.513	-10.400	0.513	-9.580	0.163	0.203
0.0001	0.116	1.002	0.189	5.284	0.592	-10.410	0.592	-10.410	0.164	0.204
Reference Values										
0.0001	0.113	0.985	0.183	5.315	0.450	-10.850	0.450	-9.314	0.158	0.229

Table 5.21 compares the time t when the 2 particles have the same x-position and similarly when the 2 particles have the same y-position by using three different time-steps. Moreover, the time t at which each particle attains the terminal speed during their downward motion is presented.

Table 5.22: Min/Max velocity of 2 particles (Level 5)

	Min/Max x-vel.				Min/Max y-vel.			
	Particle1		Particle2		Particle1		Particle2	
$tstep$	at t	v_{x1}	at t	v_{x2}	at t	v_{y1}	at t	v_{y2}
0.001	0.186	-5.008	0.183	-8.870	0.138	-15.154	0.219	-1.385
0.0003	0.183	-4.584	0.184	-8.601	0.142	-15.277	0.219	-1.115
0.0001	0.185	-4.368	0.182	-8.453	0.137	-15.081	0.219	-0.814
Reference Values								
0.0001	0.177	-5.195	0.178	-8.769	0.143	-16.104	0.213	-0.227

Table 5.22 compares the time t when each particle's x-velocity and similarly y-velocity has an extreme value (maximum/minimum value) using three different time-steps. Figure 5.20 shows that at different values of time t the particles attain minimum/maximum x-velocity and y-velocity.

Again, if we compare the results of Table 5.21 with our reference results then the collision forces are not enough to maintain the minimum distance $d_{min} \approx 0.22$.

Level 6:

The time history of two particles falling down and colliding with time-step 0.0001.

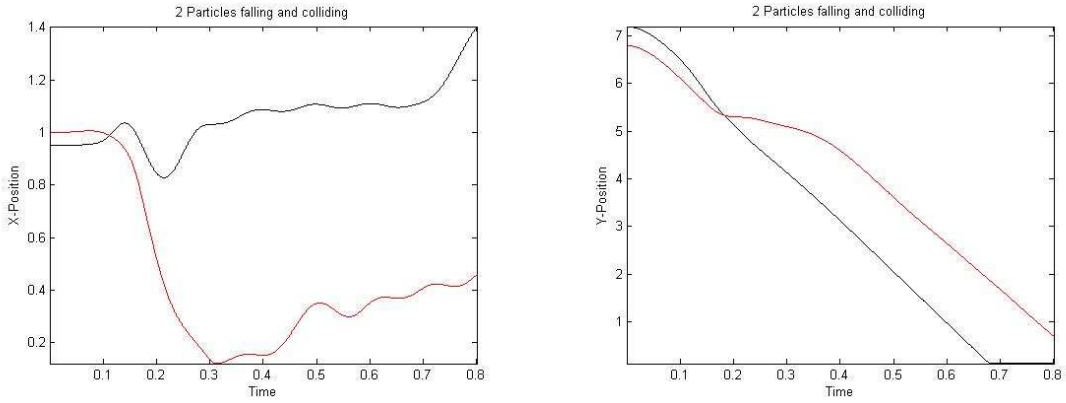

Figure 5.21: x-coordinate and y-coordinate of 2 particles w.r.t. time.

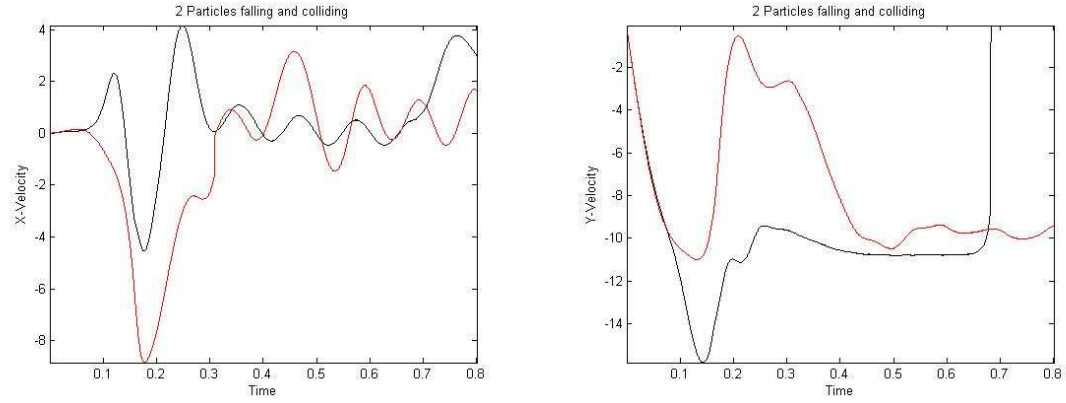

Figure 5.22: u-component and v-component of the translational velocity of 2 particles w.r.t. time.

The red line represents the first particle and the black line represents the second particle. Figure 5.21 (left) shows the x-coordinate of the center of the two particles and similarly, figure 5.21 (right) shows the y-coordinate of the center of the two particles. Figure 5.22 (left) shows the u-component of the velocity of the two particles and similarly, figure 5.22 (right) shows the v-component of the velocity of the two particles.

Tables for position and velocity of the 2 particles using time-steps 0.001, 0.0003 and 0.0001 are presented below.

Table 5.23: Position, Minimum distance and Terminal speed of 2 particles (Level 6)

	same x-pos.		same y-pos.		Terminal Vel.				min Dist.	
					Particle1		Particle2		between particles	
$tstep$	at t	p_x	at t	p_y	at t	v_t	at t	v_t	at t	d_{min}
0.001	0.111	0.990	0.189	5.309	0.480	-10.700	0.480	-9.517	0.177	0.214
0.0003	0.112	0.988	0.183	5.328	0.549	-10.800	0.549	-9.580	0.168	0.210
0.0001	0.113	0.989	0.183	5.337	0.555	-10.810	0.555	-9.510	0.167	0.210
Reference Values										
0.0001	0.113	0.985	0.183	5.315	0.450	-10.850	0.450	-9.314	0.158	0.229

Table 5.23 compares the time t when the 2-particles have the same x-position and similarly when the 2-particles have the same y-position by using three different time-steps. Moreover, the time t at which each particle attains the terminal speed during their downward motion is presented.

Table 5.24: Min/Max velocity of 2 particles (Level 6)

	Min/Max x-vel.				Min/Max y-vel.			
	Particle1		Particle2		Particle1		Particle2	
$tstep$	at t	v_{x1}	at t	v_{x2}	at t	v_{y1}	at t	v_{y2}
0.001	0.186	-6.437	0.183	-8.950	0.138	-15.295	0.213	-0.111
0.0003	0.177	-4.937	0.178	-8.964	0.141	-15.837	0.209	-0.508
0.0001	0.177	-4.550	0.178	-8.851	0.142	-15.836	0.209	-0.511
Reference Values								
0.0001	0.177	-5.195	0.178	-8.769	0.143	-16.104	0.213	-0.227

Table 5.24 compares the time t when each particle's x-velocity and similarly y-velocity has an extreme value (maximum/minimum value) using three different time-steps. Figure 5.22 shows that at different values of time t the particles attain minimum/maximum x-velocity and y-velocity.

From the comparison of the results in Table 5.23 and 5.24 with the reference results, it is clear that the results of collision model 2 with mesh level 6 have improved.

Now we present the results on all the levels together for the direct comparison of Model 2 on different levels.

Table 5.25: Position, Minimum distance and Terminal speed of 2 particles

	same x-pos.		same y-pos.		Terminal Vel.				min Dist.	
					Particle1		Particle2		between particles	
$tstep$	at t	p_x	at t	p_y	at t	v_t	at t	v_t	at t	d_{min}
Level 4										
.001	0.138	1.028	0.264	4.278	0.510	-9.710	0.510	-9.080	0.171	0.200
0.0003	0.141	1.021	0.272	4.129	0.549	-10.000	0.549	-8.318	0.198	0.200
0.0001	0.115	0.999	0.201	5.181	0.315	-9.728	0.592	-9.135	0.166	0.201
Level 5										
0.001	0.111	1.002	0.192	5.247	0.510	-10.300	0.510	-9.190	0.162	0.203
0.0003	0.113	1.000	0.190	5.255	0.513	-10.400	0.513	-9.580	0.163	0.203
0.0001	0.116	1.002	0.189	5.284	0.592	-10.410	0.592	-10.410	0.164	0.204
Level 6										
0.001	0.111	0.990	0.189	5.309	0.480	-10.700	0.480	-9.517	0.177	0.214
0.0003	0.112	0.988	0.183	5.328	0.549	-10.800	0.549	-9.580	0.168	0.210
0.0001	0.113	0.989	0.183	5.337	0.555	-10.810	0.555	-9.510	0.167	0.210
Reference Values										
0.0001	0.113	0.985	0.183	5.315	0.450	-10.850	0.450	-9.314	0.158	0.229

Table 5.26: Min/Max velocity of 2 particles

	Min/Max x-vel.				Min/Max y-vel.			
	Particle1		Particle2		Particle1		Particle2	
$tstep$	at t	v_{x1}	at t	v_{x2}	at t	v_{y1}	at t	v_{y2}
Level 4								
0.001	0.246	-4.3006	0.252	-7.902	0.135	-14.452	0.306	-3.508
0.0003	0.262	-4.054	0.261	-7.827	0.144	-14.534	0.338	-1.431
0.0001	0.196	-4.410	0.191	-7.498	0.140	-14.014	0.252	-0.930
Level 5								
0.001	0.186	-5.008	0.183	-8.870	0.138	-15.154	0.219	-1.385
0.0003	0.183	-4.584	0.184	-8.601	0.142	-15.277	0.219	-1.115
0.0001	0.185	-4.368	0.182	-8.453	0.137	-15.081	0.219	-0.814
Level 6								
0.001	0.186	-6.437	0.183	-8.950	0.138	-15.295	0.213	-0.111
0.0003	0.177	-4.937	0.178	-8.964	0.141	-15.837	0.209	-0.508
0.0001	0.177	-4.550	0.178	-8.851	0.142	-15.836	0.209	-0.511
Reference Values								
0.0001	0.177	-5.195	0.178	-8.769	0.143	-16.104	0.213	-0.227

Summary

Collision model 2 using mesh level 6 shows better results as compared to the results of collision model 2 using mesh level 4 and mesh level 5. Collision model 2 results with mesh level 6 can also be considered better by comparing with the results of the 'No Collision Model (Level 6)' and the results of the reference values.

5.1.5. Collision Model Based on a Minimization Procedure (Model 3)

The positions and velocities of the two falling particles for the time-steps 0.001, 0.0003 and 0.0001 are observed on mesh level 4, 5 and 6.

Level 4:

The time history of two particles falling down and colliding with time-step 0.0001.

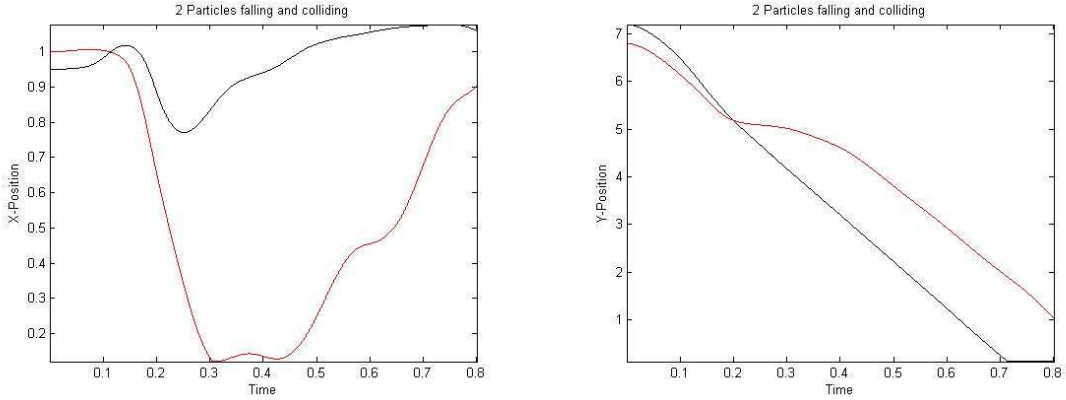

Figure 5.23: x-coordinate and y-coordinate of 2 particles w.r.t. time.

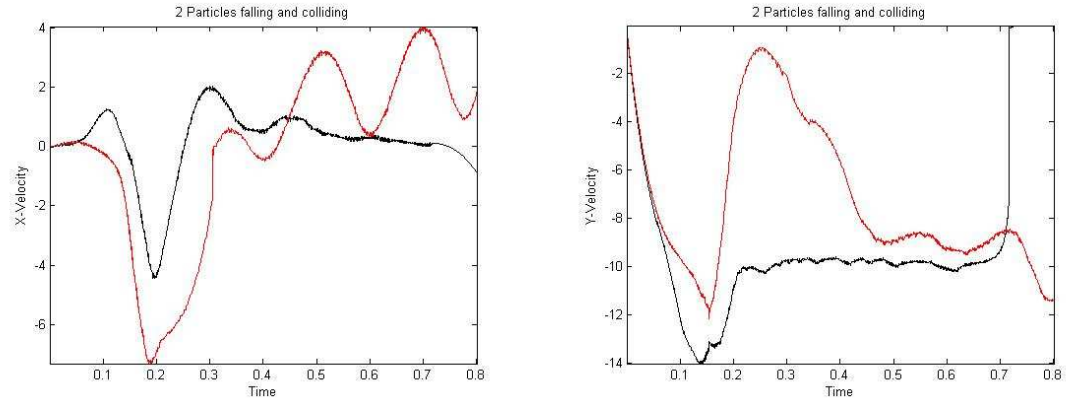

Figure 5.24: u-component and v-component of the translational velocity of 2 particles w.r.t. time.

The red line represents the first particle and the black line represents the second particle. Figure 5.23 (left) shows the x-coordinate of the center of the two particles and similarly, figure 5.23 (right) shows the y-coordinate of the center of the two particles. Figure 5.24 (left) shows the u-component of the velocity of the two particles and similarly, figure 5.24 (right) shows the v-component of the velocity of the two particles.

Tables for position and velocity of the 2 particles using time-steps 0.001, 0.0003 and 0.0001 are presented below.

Table 5.27: Position, Minimum distance and Terminal speed of 2 particles (Level 4)

	same x-pos.		same y-pos.		Terminal Vel.				min Dist.	
					Particle1		Particle2		between particles	
$tstep$	at t	p_x	at t	p_y	at t	v_t	at t	v_t	at t	d_{min}
0.001	0.138	1.028	0.255	4.390	0.450	-9.152	0.450	-9.152	0.204	0.200
0.0003	0.141	1.021	0.266	4.205	0.378	-9.792	0.696	-9.134	0.175	0.200
0.0001	0.115	0.999	0.200	5.189	0.313	-9.715	0.645	-9.298	0.156	0.200
Reference Values										
0.0001	0.113	0.985	0.183	5.315	0.450	-10.850	0.450	-9.314	0.158	0.229

Table 5.27 compares the time t when the 2 particles have the same x-position and similarly when the 2 particles have the same y-position by using three different time-steps. Moreover, the time t at which each particle attains the terminal speed during their downward motion is presented.

Table 5.28: Min/Max velocity of 2 particles (Level 4)

	Min/Max x-vel.				Min/Max y-vel.			
	Particle1		Particle2		Particle1		Particle2	
$tstep$	at t	v_{x1}	at t	v_{x2}	at t	v_{y1}	at t	v_{y2}
0.001	0.240	-3.797	0.252	-7.830	0.135	-14.452	0.288	-3.491
0.0003	0.256	-3.516	0.259	-7.539	0.148	-14.585	0.322	-1.724
0.0001	0.193	-4.458	0.190	-7.315	0.140	-14.014	0.255	-0.910
Reference Values								
0.0001	0.177	-5.195	0.178	-8.769	0.143	-16.104	0.213	-0.227

Table 5.28 compares the time t when each particle's x-velocity and similarly y-velocity has an extreme value (maximum/minimum value) using three different time-steps. Figure 5.24 shows that at different values of time t the particles attain minimum/maximum x-velocity and y-velocity.

If we compare the results shown in Table 5.27 with the results of Model 0, Model 1 and Model 2 on level 4, we find that the particles did not overlap using Model 3 as well as using Model 2. By comparing the results in Table 5.27 with the reference values, it can be seen that the collision forces are not enough to maintain the minimum distance $d_{min} \approx 0.22$.

Level 5:

The time history of two particles falling down and colliding with time-step 0.0001.

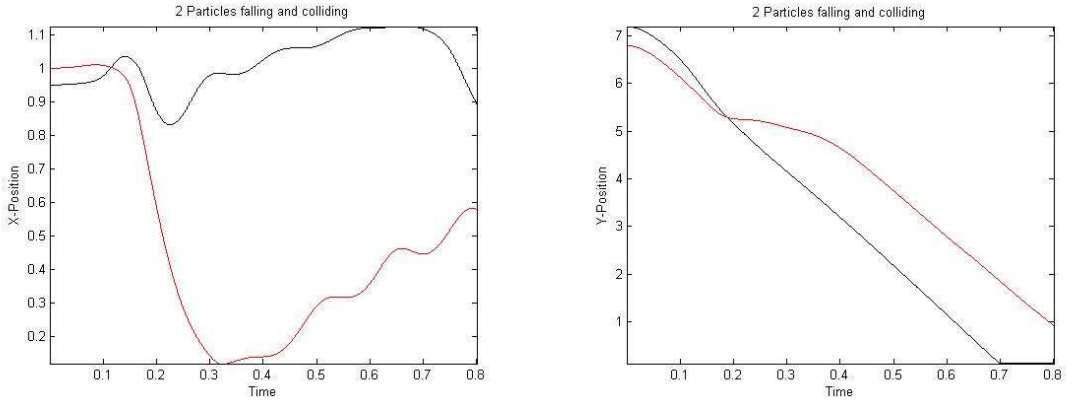

Figure 5.25: x-coordinate and y-coordinate of 2 particles w.r.t. time.

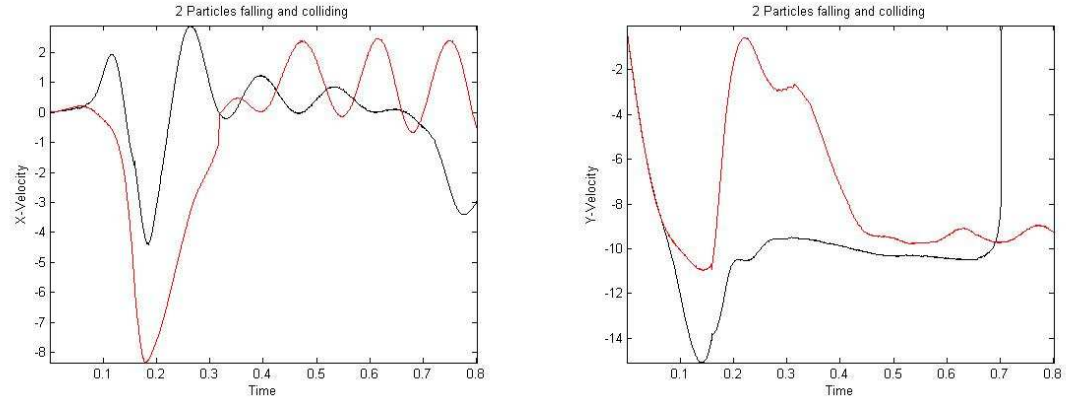

Figure 5.26: u-component and v-component of the translational velocity of 2 particles w.r.t. time.

The red line represents the first particle and the black line represents the second particle. Figure 5.25 (left) shows the x-coordinate of the center of the two particles and similarly, figure 5.25 (right) shows the y-coordinate of the center of the two particles. Figure 5.26 (left) shows the u-component of the velocity of the two particles and similarly, figure 5.26 (right) shows the v-component of the velocity of the two particles.

Tables for position and velocity of the 2 particles using time-steps 0.001, 0.0003 and 0.0001 are presented below.

Table 5.29: Position, Minimum distance and Terminal speed of 2 particles (Level 5)

	same x-pos.		same y-pos.		Terminal Vel.				min Dist.	
					Particle1		Particle2		between particles	
$tstep$	at t	p_x	at t	p_y	at t	v_t	at t	v_t	at t	d_{min}
0.001	0.111	1.002	0.192	5.248	0.450	-10.300	0.450	-9.060	0.159	0.200
0.0003	0.113	1.000	0.189	5.264	0.495	-10.400	0.495	-9.767	0.158	0.200
0.0001	0.116	1.002	0.188	5.295	0.540	-10.290	0.540	-9.742	0.162	0.200
Reference Values										
0.0001	0.113	0.985	0.183	5.315	0.450	-10.850	0.450	-9.314	0.158	0.229

Table 5.29 compares the time t when the 2 particles have the same x-position and similarly when the 2 particles have the same y-position by using three different time-steps. Moreover, the time t at which each particle attains the terminal speed during their downward motion is presented.

Table 5.30: Min/Max velocity of 2 particles (Level 5)

	Min/Max x-vel.				Min/Max y-vel.			
	Particle1		Particle2		Particle1		Particle2	
$tstep$	at t	v_{x1}	at t	v_{x2}	at t	v_{y1}	at t	v_{y2}
0.001	0.186	-4.893	0.183	-8.874	0.138	-15.154	0.216	-1.437
0.0003	0.183	-4.506	0.182	-8.590	0.142	-15.277	0.222	-1.032
0.0001	0.184	-4.399	0.179	-8.339	0.137	-15.081	0.223	-0.565
Reference Values								
0.0001	0.177	-5.195	0.178	-8.769	0.143	-16.104	0.213	-0.227

Table 5.30 compares the time t when each particle's x-velocity and similarly y-velocity has an extreme value (maximum/minimum value) using three different time-steps. Figure 5.26 shows that at different values of time t the particles attain minimum/maximum x-velocity and y-velocity.

The results shown in Table 5.29 have improved on level 5 when compared with the results of the reference values and these results show that Model 3 with level 5 can be used for the simulation of 2 particles.

Level 6:

The time history of two particles falling down and colliding with time-step 0.0001.

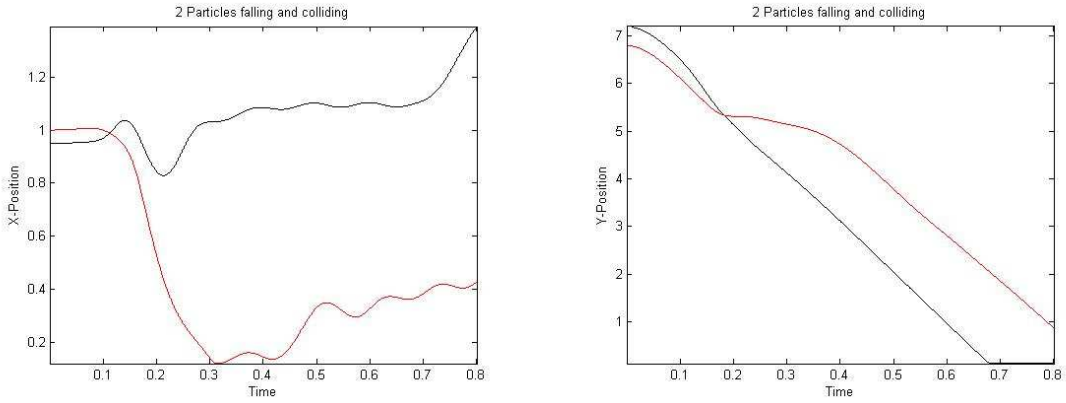

Figure 5.27: x-coordinate and y-coordinate of 2 particles w.r.t. time.

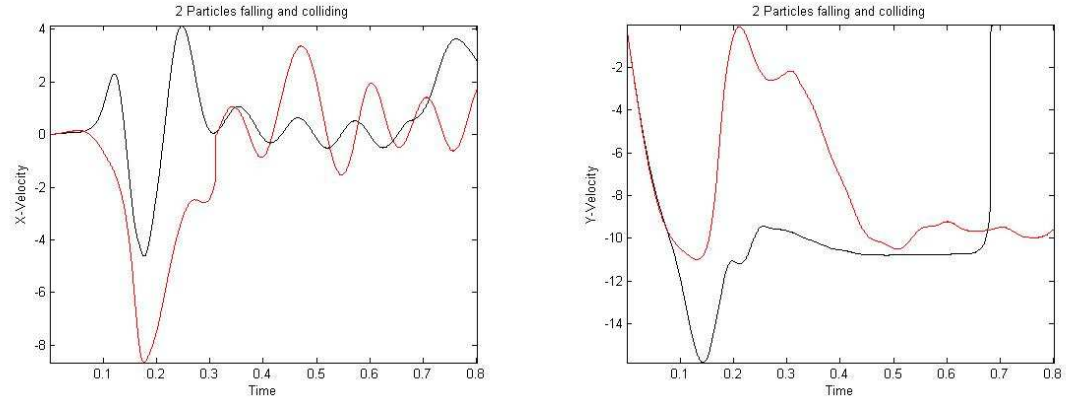

Figure 5.28: u-component and v-component of the translational velocity of 2 particles w.r.t. time.

The red line represents the first particle and the black line represents the second particle. Figure 5.27 (left) shows the x-coordinate of the center of the two particles and similarly, figure 5.27 (right) shows the y-coordinate of the center of the two particles. Figure 5.28 (left) shows the u-component of the velocity of the two particles and similarly, figure 5.28 (right) shows the v-component of the velocity of the two particles.

Tables for position and velocity of the 2 particles using time-steps 0.001, 0.0003 and 0.0001 are presented below.

Table 5.31: Position, Minimum distance and Terminal speed of 2 particles (Level 6)

	same x-pos.		same y-pos.		Terminal Vel.				min Dist.	
					Particle1		Particle2		between particles	
$tstep$	at t	p_x	at t	p_y	at t	v_t	at t	v_t	at t	d_{min}
0.001	0.111	0.990	0.189	5.307	0.480	-10.760	0.480	-9.629	0.177	0.212
0.0003	0.111	0.988	0.182	5.335	0.540	-10.870	0.540	-9.954	0.169	0.206
0.0001	0.113	0.989	0.182	5.342	0.570	-10.760	0.570	-9.452	0.169	0.207
Reference Values										
0.0001	0.113	0.985	0.183	5.315	0.450	-10.850	0.450	-9.314	0.158	0.229

Table 5.31 compares the time t when the 2 particles have the same x-position and similarly when the 2 particles have the same y-position by using three different time-steps. Moreover, the time t at which each particle attains the terminal speed during their downward motion is presented.

Table 5.32: Min/Max velocity of 2 particles (Level 6)

	Min/Max x-vel.				Min/Max y-vel.			
	Particle1		Particle2		Particle1		Particle2	
$tstep$	at t	v_{x1}	at t	v_{x2}	at t	v_{y1}	at t	v_{y2}
0.001	0.186	-6.454	0.183	-8.872	0.138	-15.295	0.216	0.069
0.0003	0.178	-4.992	0.177	-8.790	0.141	-15.837	0.211	-0.063
0.0001	0.177	-4.619	0.177	-8.662	0.142	-15.836	0.211	-0.077
Reference Values								
0.0001	0.177	-5.195	0.178	-8.769	0.143	-16.104	0.213	-0.227

Table 5.32 compares the time t when each particle's x-velocity and similarly y-velocity has an extreme value (maximum/minimum value) using three different time-steps. Figure 5.28 shows that at different values of time t the particles attain minimum/maximum x-velocity and y-velocity.

From the comparison of the results in Table 5.31 and 5.32 with the reference results, it is clear that the results of collision model 3 with mesh level 6 are very close to the reference results. Moreover, we can see that for all the mesh levels (level 4, level 5 and level 6), collision model 3 did not allow the particles to overlap.

Now we present the results on all the levels together for the direct comparison of Model 3 on different levels.

Table 5.33: Position, Minimum distance and Terminal speed of 2 particles

	same x-pos.		same y-pos.		Terminal Vel.				min Dist.	
					Particle1		Particle2		between particles	
$tstep$	at t	p_x	at t	p_y	at t	v_t	at t	v_t	at t	d_{min}
Level 4										
0.001	0.138	1.028	0.255	4.390	0.450	-9.152	0.450	-9.152	0.204	0.200
0.0003	0.141	1.021	0.266	4.205	0.378	-9.792	0.696	-9.134	0.175	0.200
0.0001	0.115	0.999	0.200	5.189	0.313	-9.715	0.645	-9.298	0.156	0.200
Level 5										
0.001	0.111	1.002	0.192	5.248	0.450	-10.300	0.450	-9.060	0.159	0.200
0.0003	0.113	1.000	0.189	5.264	0.495	-10.400	0.495	-9.767	0.158	0.200
0.0001	0.116	1.002	0.188	5.295	0.540	-10.290	0.540	-9.742	0.162	0.200
Level 6										
0.001	0.111	0.990	0.189	5.307	0.480	-10.760	0.480	-9.629	0.177	0.212
0.0003	0.111	0.988	0.182	5.335	0.540	-10.870	0.540	-9.954	0.169	0.206
0.0001	0.113	0.989	0.182	5.342	0.570	-10.760	0.570	-9.452	0.169	0.207
Reference Values										
0.0001	0.113	0.985	0.183	5.315	0.450	-10.850	0.450	-9.314	0.158	0.229

Table 5.34: Min/Max velocity of 2 particles

	Min/Max x-vel.				Min/Max y-vel.			
	Particle1		Particle2		Particle1		Particle2	
$tstep$	at t	v_{x1}	at t	v_{x2}	at t	v_{y1}	at t	v_{y2}
Level 4								
0.001	0.240	-3.797	0.252	-7.830	0.135	-14.452	0.288	-3.491
0.0003	0.256	-3.516	0.259	-7.539	0.148	-14.585	0.322	-1.724
0.0001	0.193	-4.458	0.190	-7.315	0.140	-14.014	0.255	-0.910
Level 5								
0.001	0.186	-4.893	0.183	-8.874	0.138	-15.154	0.216	-1.437
0.0003	0.183	-4.506	0.182	-8.590	0.142	-15.277	0.222	-1.032
0.0001	0.184	-4.399	0.179	-8.339	0.137	-15.081	0.223	-0.565
Level 6								
0.001	0.186	-6.454	0.183	-8.872	0.138	-15.295	0.216	0.069
0.0003	0.178	-4.992	0.177	-8.790	0.141	-15.837	0.211	-0.063
0.0001	0.177	-4.619	0.177	-8.662	0.142	-15.836	0.211	-0.077
Reference Values								
0.0001	0.177	-5.195	0.178	-8.769	0.143	-16.104	0.213	-0.227

Summary

Collision model 3 using mesh level 6 shows better results as compared to the results of collision model 3 using mesh level 4 and mesh level 5. Collision model 3 results with mesh level 6 can also be considered good when compared with the results of the other collision models with Level 6 which are very nearly the same.

Now we present the results of all the collision models combined together on each level for the direct comparison between the models.

Table 5.35: Position, Minimum distance and Terminal speed of 2 particles (**Level 4**)

	same x-pos.		same y-pos.		Terminal Vel.				min Dist.	
					Particle1		Particle2		between particles	
$tstep$	at t	p_x	at t	p_y	at t	v_t	at t	v_t	at t	d_{min}
Model 0										
0.001	0.138	1.028	0.234	4.643	0.450	-9.493	0.450	-9.079	0.189	0.162
0.0003	0.141	1.021	0.261	4.259	0.513	-10.130	0.513	-7.288	0.218	0.180
0.0001	0.115	0.999	0.199	5.195	0.471	-9.791	0.471	-9.105	0.164	0.196
Model 1										
0.001	0.138	1.028	0.255	4.394	0.600	-9.640	0.600	-8.960	0.144	0.198
0.0003	0.141	1.021	0.266	4.204	0.540	-9.890	0.540	-8.130	0.1508	0.199
0.0001	0.115	0.999	0.200	5.190	0.315	-9.728	0.592	-9.135	0.164	0.201
Model 2										
0.001	0.138	1.028	0.264	4.278	0.510	-9.710	0.510	-9.080	0.171	0.200
0.0003	0.141	1.021	0.272	4.129	0.549	-10.000	0.549	-8.318	0.198	0.200
0.0001	0.115	0.999	0.201	5.181	0.315	-9.728	0.592	-9.135	0.166	0.201
Model 3										
0.001	0.138	1.028	0.255	4.390	0.450	-9.152	0.450	-9.152	0.204	0.200
0.0003	0.141	1.021	0.266	4.205	0.378	-9.792	0.696	-9.134	0.175	0.200
0.0001	0.115	0.999	0.200	5.189	0.313	-9.715	0.645	-9.298	0.156	0.200
Reference Values										
0.0001	0.113	0.985	0.183	5.315	0.450	-10.850	0.450	-9.314	0.158	0.229

Table 5.36: Min/Max velocity of 2 particles (**Level 4**)

	Min/Max x-vel.				Min/Max y-vel.			
	Particle1		Particle2		Particle1		Particle2	
$tstep$	at t	v_{x1}	at t	v_{x2}	at t	v_{y1}	at t	v_{y2}
Model 0								
0.001	0.225	-3.430	0.225	-7.369	0.135	-14.452	0.294	-2.225
0.0003	0.255	-3.761	0.243	-6.772	0.148	-14.585	0.331	-1.303
0.0001	0.199	-5.377	0.185	-7.039	0.140	-14.014	0.271	-1.140
Model 1								
0.001	0.240	-3.8226	0.246	-7.814	0.135	-14.456	0.297	-3.463
0.0003	0.255	-3.467	0.253	-7.585	0.145	-14.573	0.315	-1.760
0.0001	0.193	-4.381	0.191	-7.448	0.140	-14.013	0.251	-0.878
Model 2								
0.001	0.246	-4.3006	0.252	-7.902	0.135	-14.452	0.306	-3.508
0.0003	0.262	-4.054	0.261	-7.827	0.144	-14.534	0.338	-1.431
0.0001	0.196	-4.410	0.191	-7.498	0.140	-14.014	0.252	-0.930
Model 3								
0.001	0.240	-3.797	0.252	-7.830	0.135	-14.452	0.288	-3.491
0.0003	0.256	-3.516	0.259	-7.539	0.148	-14.585	0.322	-1.724
0.0001	0.193	-4.458	0.190	-7.315	0.140	-14.014	0.255	-0.910
Reference Values								
0.0001	0.177	-5.195	0.178	-8.769	0.143	-16.104	0.213	-0.227

Table 5.37: Position, Minimum distance and Terminal speed of 2 particles (**Level 5**)

	same x-pos.		same y-pos.		Terminal Vel.				min Dist.	
					Particle1		Particle2		between particles	
tstep	at t	p_x	at t	p_y	at t	v_t	at t	v_t	at t	d_{min}
Model 0										
0.001	0.111	1.002	0.189	5.274	0.528	-10.470	0.528	-9.545	0.165	0.190
0.0003	0.113	1.000	0.189	5.271	0.518	-10.460	0.518	-9.952	0.163	0.195
0.0001	0.116	1.002	0.188	5.298	0.525	-10.280	0.525	-9.638	0.163	0.199
Model 1										
0.001	0.111	1.002	0.189	5.279	0.525	-10.400	0.525	-9.230	0.156	0.200
0.0003	0.113	1.000	0.189	5.264	0.517	-10.400	0.517	-9.700	0.160	0.200
0.0001	0.116	1.002	0.188	5.293	0.592	-10.410	0.592	-10.410	0.160	0.201
Model 2										
0.001	0.111	1.002	0.192	5.247	0.510	-10.300	0.510	-9.190	0.162	0.203
0.0003	0.113	1.000	0.190	5.255	0.513	-10.400	0.513	-9.580	0.163	0.203
0.0001	0.116	1.002	0.189	5.284	0.592	-10.410	0.592	-10.410	0.164	0.204
Model 3										
0.001	0.111	1.002	0.192	5.248	0.450	-10.300	0.450	-9.060	0.159	0.200
0.0003	0.113	1.000	0.189	5.264	0.495	-10.400	0.495	-9.767	0.158	0.200
0.0001	0.116	1.002	0.188	5.295	0.540	-10.290	0.540	-9.742	0.162	0.200
Reference Values										
0.0001	0.113	0.985	0.183	5.315	0.450	-10.850	0.450	-9.314	0.158	0.229

Table 5.38: Min/Max velocity of 2 particles (**Level 5**)

	Min/Max x-vel.				Min/Max y-vel.			
	Particle1		Particle2		Particle1		Particle2	
tstep	at t	v_{x1}	at t	v_{x2}	at t	v_{y1}	at t	v_{y2}
Model 0								
0.001	0.183	-4.698	0.183	-8.734	0.138	-15.154	0.219	-0.900
0.0003	0.183	-4.597	0.180	-8.415	0.142	-15.277	0.224	-0.690
0.0001	0.184	-4.465	0.180	-8.263	0.137	-15.081	0.224	-0.466
Model 1								
0.001	0.186	-4.844	0.186	-8.907	0.138	-15.155	0.216	-1.257
0.0003	0.183	-4.496	0.183	-8.581	0.141	-15.277	0.222	-1.020
0.0001	0.184	-4.320	0.181	-8.395	0.137	-15.081	0.219	-0.680
Model 2								
0.001	0.186	-5.008	0.183	-8.870	0.138	-15.154	0.219	-1.385
0.0003	0.183	-4.584	0.184	-8.601	0.142	-15.277	0.219	-1.115
0.0001	0.185	-4.368	0.182	-8.453	0.137	-15.081	0.219	-0.814
Model 3								
0.001	0.186	-4.893	0.183	-8.874	0.138	-15.154	0.216	-1.437
0.0003	0.183	-4.506	0.182	-8.590	0.142	-15.277	0.222	-1.032
0.0001	0.184	-4.399	0.179	-8.339	0.137	-15.081	0.223	-0.565
Reference Values								
0.0001	0.177	-5.195	0.178	-8.769	0.143	-16.104	0.213	-0.227

Table 5.39: Position, Minimum distance and Terminal speed of 2 particles (**Level 6**)

	same x-pos.		same y-pos.		Terminal Vel.				min Dist.	
					Particle1		Particle2		between particles	
$tstep$	at t	p_x	at t	p_y	at t	v_t	at t	v_t	at t	d_{min}
Model 0										
0.001	0.111	0.990	0.189	5.307	0.525	-10.750	0.525	-9.802	0.177	0.212
0.0003	0.112	0.988	0.182	5.335	0.517	-10.870	0.517	-10.590	0.169	0.206
0.0001	0.113	0.989	0.182	5.342	0.502	-10.770	0.502	-10.490	0.169	0.207
Model 1										
0.001	0.111	0.990	0.189	5.308	0.510	-10.700	0.510	-9.870	0.177	0.213
0.0003	0.113	0.989	0.182	5.336	0.585	-10.800	0.585	-9.420	0.168	0.207
0.0001	0.113	0.989	0.182	5.339	0.555	-10.810	0.555	-9.510	0.167	0.208
Model 2										
0.001	0.111	0.990	0.189	5.309	0.480	-10.700	0.480	-9.517	0.177	0.214
0.0003	0.112	0.988	0.183	5.328	0.549	-10.800	0.549	-9.580	0.168	0.210
0.0001	0.113	0.989	0.183	5.337	0.555	-10.810	0.555	-9.510	0.167	0.210
Model 3										
0.001	0.111	0.990	0.189	5.307	0.480	-10.760	0.480	-9.629	0.177	0.212
0.0003	0.111	0.988	0.182	5.335	0.540	-10.870	0.540	-9.954	0.169	0.206
0.0001	0.113	0.989	0.182	5.342	0.570	-10.760	0.570	-9.452	0.169	0.207
Reference Values										
0.0001	0.113	0.985	0.183	5.315	0.450	-10.850	0.450	-9.314	0.158	0.229

Table 5.40: Min/Max velocity of 2 particles (**Level 6**)

	Min/Max x-vel.				Min/Max y-vel.			
	Particle1		Particle2		Particle1		Particle2	
$tstep$	at t	v_{x1}	at t	v_{x2}	at t	v_{y1}	at t	v_{y2}
Model 0								
0.001	0.186	-6.454	0.183	-8.872	0.138	-15.295	0.216	0.069
0.0003	0.178	-4.992	0.177	-8.790	0.141	-15.837	0.211	-0.063
0.0001	0.177	-4.619	0.177	-8.662	0.142	-15.836	0.211	-0.077
Model 1								
0.001	0.186	-6.437	0.183	-8.924	0.138	-15.296	0.216	0.055
0.0003	0.178	-4.946	0.178	-8.903	0.141	-15.838	0.211	-0.254
0.0001	0.177	-4.557	0.177	-8.772	0.142	-15.837	0.210	-0.253
Model 2								
0.001	0.186	-6.437	0.183	-8.950	0.138	-15.295	0.213	-0.111
0.0003	0.177	-4.937	0.178	-8.964	0.141	-15.837	0.209	-0.508
0.0001	0.177	-4.550	0.178	-8.851	0.142	-15.836	0.209	-0.511
Model 3								
0.001	0.186	-6.454	0.183	-8.872	0.138	-15.295	0.216	0.069
0.0003	0.178	-4.992	0.177	-8.790	0.141	-15.837	0.211	-0.063
0.0001	0.177	-4.619	0.177	-8.662	0.142	-15.836	0.211	-0.077
Reference Values								
0.0001	0.177	-5.195	0.178	-8.769	0.143	-16.104	0.213	-0.227

5.1.6. Conclusion

Collision model 1, collision model 2, collision model 3 and 'No Collision Model' are compared at different time steps and levels during the fall of 2 particles under the action of gravity and fluid forces. Without using any collision model (No Collision Model), the particles experience a slight overlap during the collision process. Collision model 2 and collision model 3 produced good results during collision and the particles undergo the phenomena of drafting, kissing and tumbling without overlapping. Collision model 1 with mesh level 4 showed a slight overlap of particles which was removed when mesh level 5 and mesh level 6 was used. If the mesh level is increased such that we use a very fine mesh, then the need of collision models may be avoided but on the other hand it requires a lot of computational cost. In 'No Collision Model' and keeping mesh level 6, the particles did not overlap, but the simulation costs increase significantly. Hence, the collision models are beneficial in both ways i.e. the particle overlapping can be avoided and at the same time we can work with a lower mesh level when there is no need for a finer mesh. The tables described above at different mesh levels show the behavior of the collision models during the collision process. We have also obtained the level 7 results (using collision model 3) which can be taken as reference values for the comparison of different collision models. For the case of two particles, all the collision models produced good results using mesh level 6.

5.2. Many particles

Many circular particles are allowed to fall under the action of hydrodynamic forces and the gravitational force. Their sedimentation is simulated using collision model 3 as it guarantees no particle overlap.

120 circular particles are allowed to fall inside a channel of width 4 and height 6. The diameter of each particle is 0.24. The fluid density is $\rho_f = 1.0$, the acceleration due to gravity is $g = 981$, the viscosity is $\mu = 0.01$, density of the particle is $\rho_s = 1.1$ and, hence, the solid-to-fluid density ratio is 1.1.

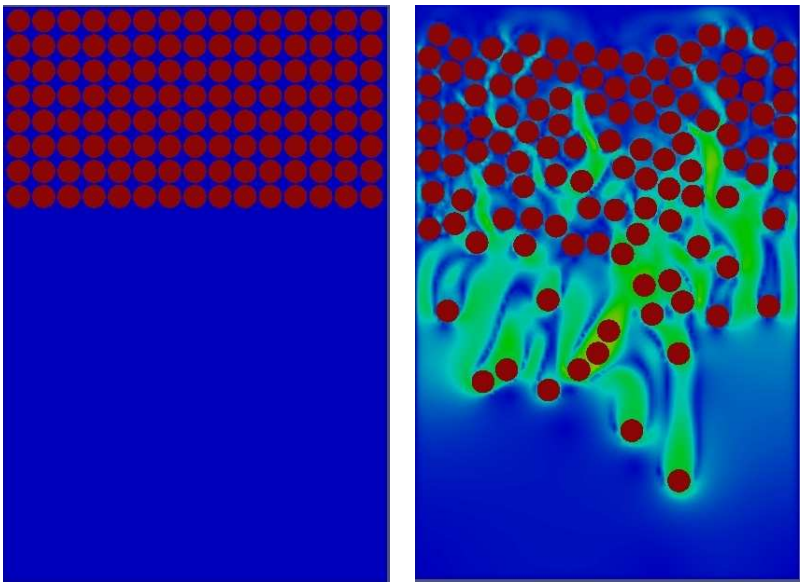

Figure 5.29: Simulation of 120 particles arranged in a block pattern at t = 0.0 and t = 1.0

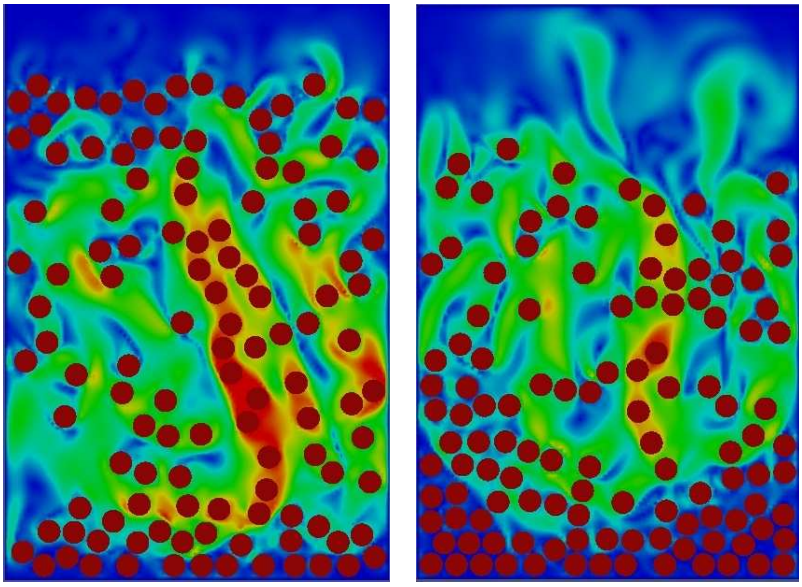

Figure 5.30: Simulation of 120 particles at t = 2.0 and t = 2.5

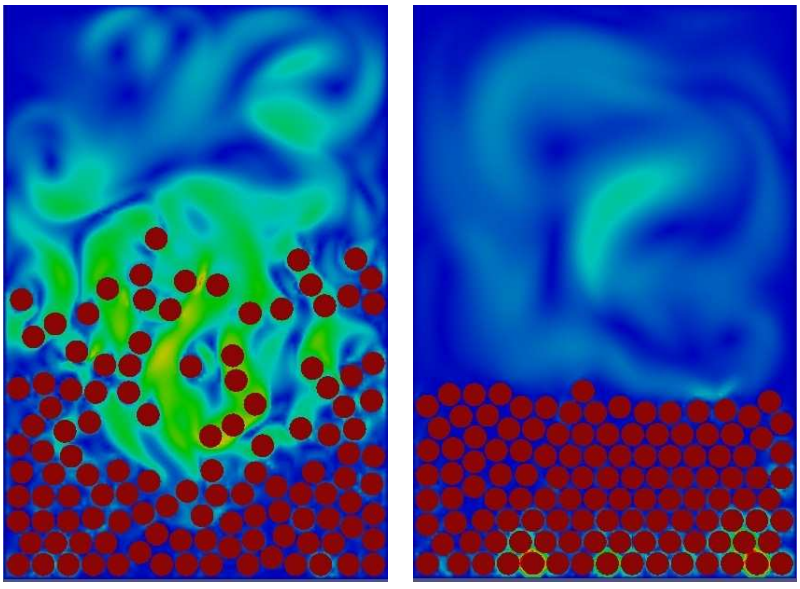

Figure 5.31: Simulation of 120 particles at t = 3.0 and t = 5.0

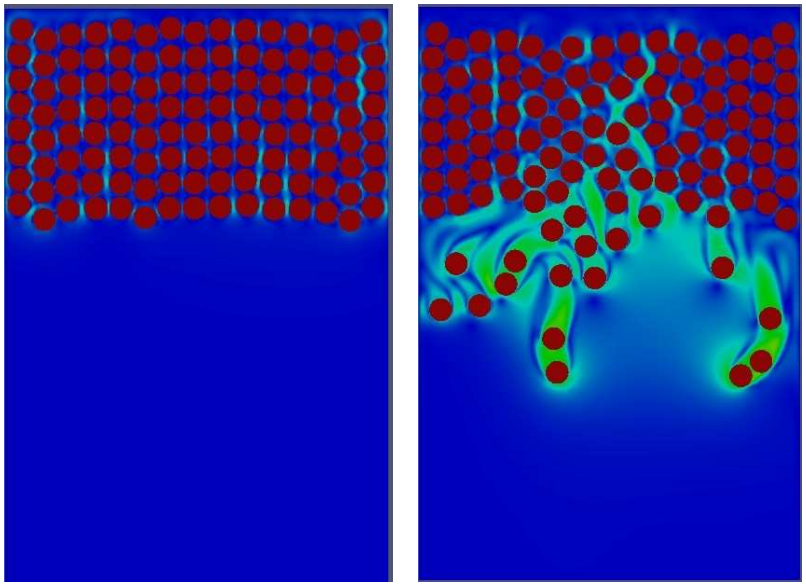

Figure 5.32: Simulation of 120 particles at t = 0.5 and t = 1.0

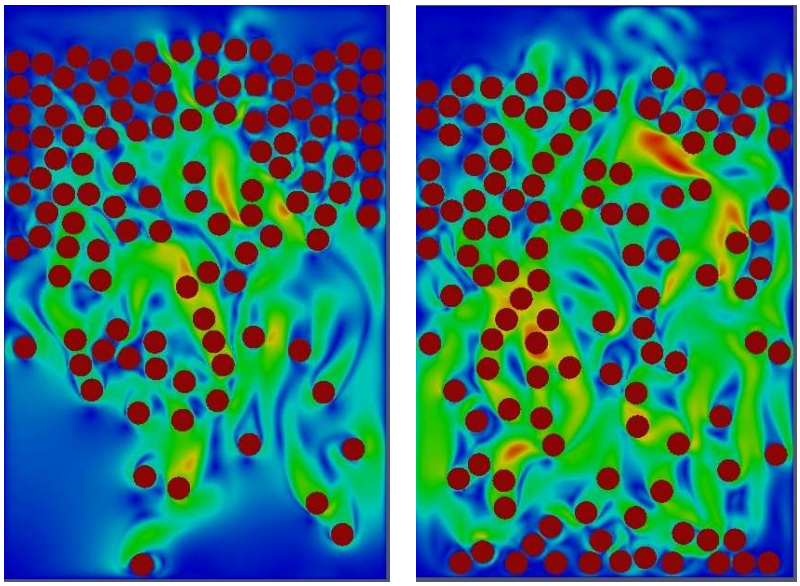

Figure 5.33: Simulation of 120 particles at t = 1.5 and t = 2.0

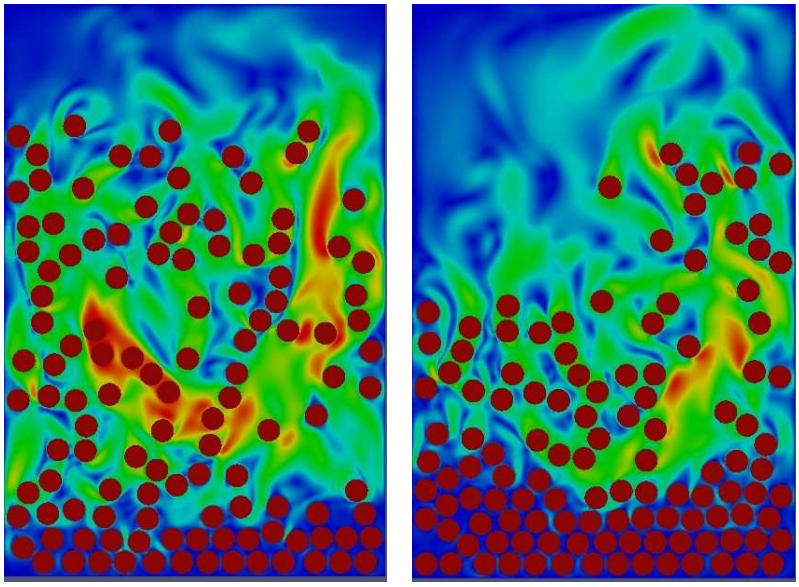

Figure 5.34: Simulation of 120 particles at t = 2.5 and t = 3.0

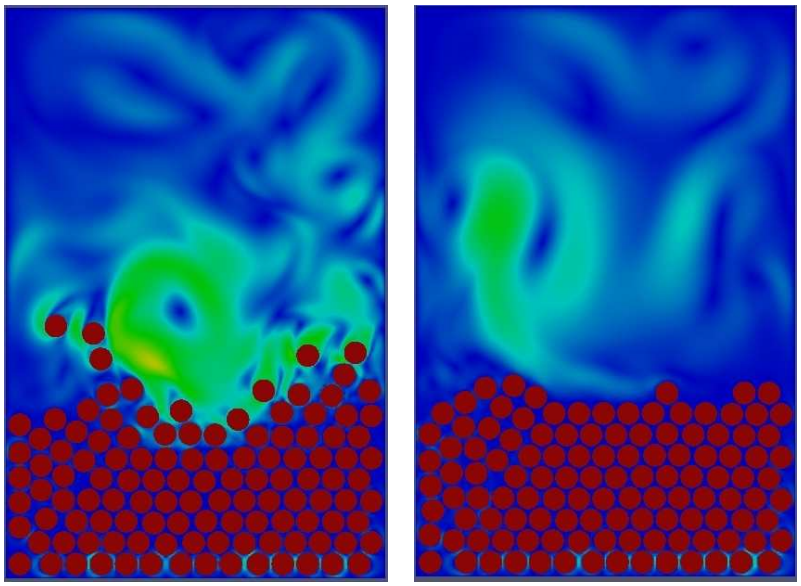

Figure 5.35: Simulation of 120 particles at t = 4.0 and t = 5.0

5.2.1. Conclusion

We have simulated many particles in fluid successfully using collision model 3. Collision model 1 and 2 can also be used to simulate a large number of particles but they additionally require the tuning of some parameters such as the time-step, which has to be reduced sufficiently and the stiffness parameters, which have to be adjusted such that the repulsive forces are neither too much nor too small to avoid overlapping.

5.3. General shape particles

The collision models are extended for general shape particles which require the calculation of the distance between approaching particles and the calculation of torque acting on the particle. The distance between the particles is calculated as the point-to-point distance between them rather than the center-to-center distance between particles. Simulations are performed for the case of two bean shaped particles falling under the action of hydrodynamic forces and the gravitational force in a channel. The number of elements on level 1 = 196.

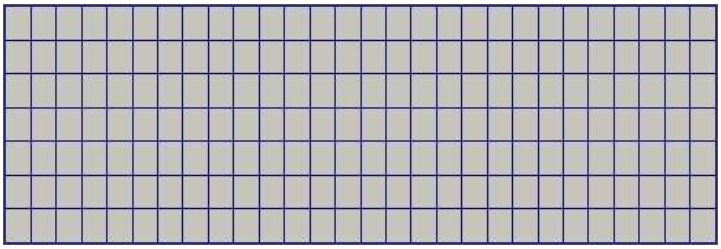

Figure 5.36: Channel mesh (Coarse mesh LEVEL 1) rotated by 90 degrees

5.3.1. Numerical results

The results for the collisions of 2 bean shaped particles are presented. The fluid density is $\rho_f = 1$, the acceleration of gravity is $g = 981$, the viscosity is $\mu = 0.01$, density of the particle is $\rho_s = 1.5$ and, hence, the solid-to-fluid density ratio is 1.5. Particles are released from rest in a channel with a width of 2 and height of 6. Initially, the center coordinates of the first particle are $(1.05, 5.0)$ and the center coordinates of the second particle are $(0.99, 4.75)$.

We present results for the collision of 2 bean shaped particles using the time step of 0.0001.

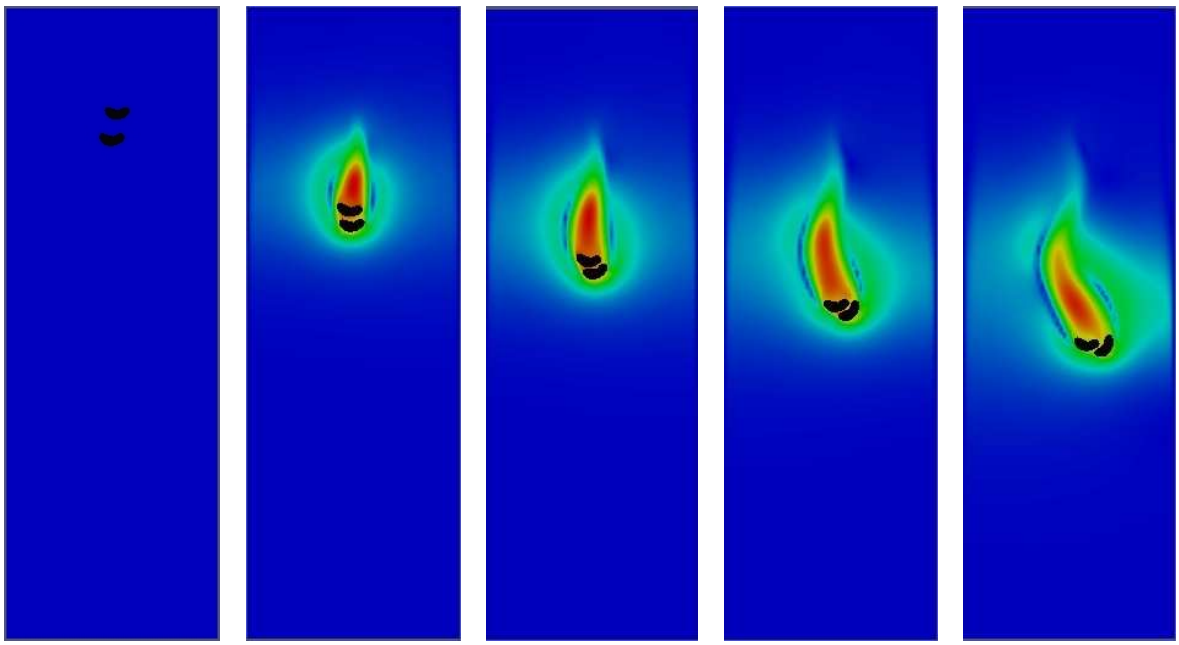

Figure 5.37: Simulation of 2 general shaped particles moving under gravity at t = 0.0, t = 0.15, t = 0.20, t = 0.25 and t = 0.30

Level 4:

The time history of two bean shaped particles falling down and colliding with time-step 0.0001.

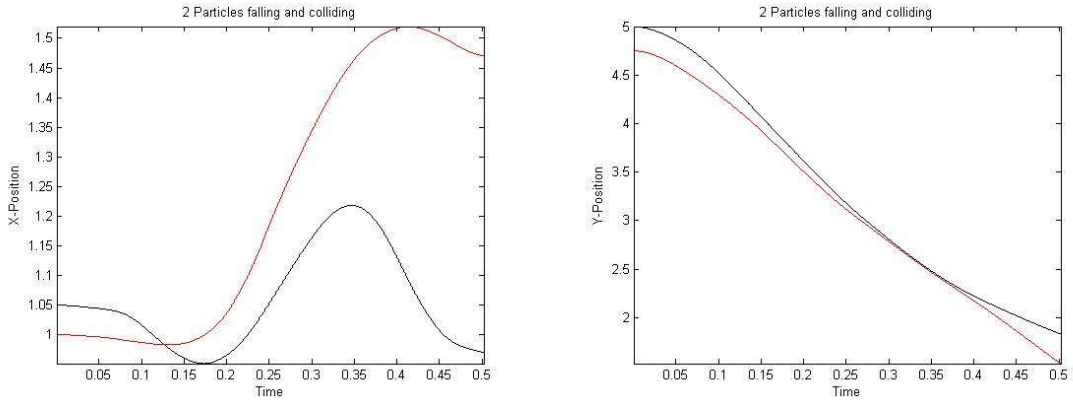

Figure 5.38: x-coordinate and y-coordinate of 2 non-circular particles w.r.t. time.

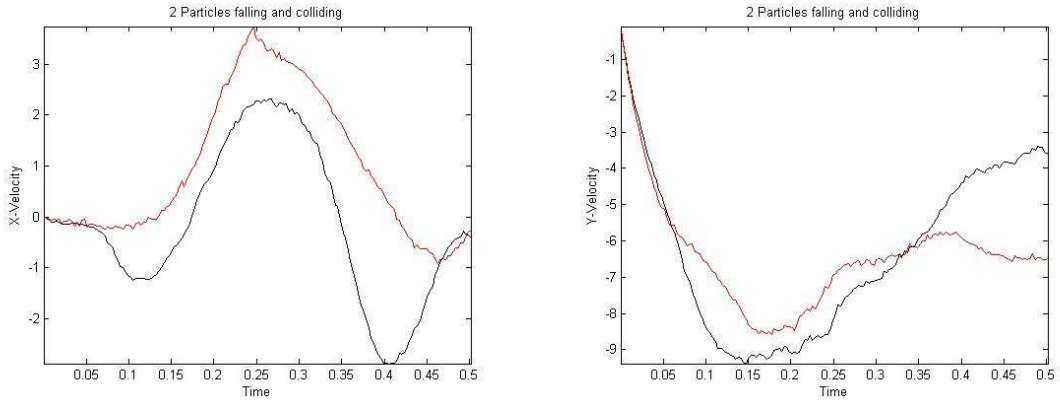

Figure 5.39: u-component and v-component of the translational velocity of 2 non-circular particles w.r.t. time.

The red line represents the first particle and the black line represents the second particle. Figure 5.38 (left) shows the x-coordinate of the center of the two particles and similarly, figure 5.38 (right) shows the y-coordinate of the center of the two particles. Figure 5.39 (left) shows the u-component of the velocity of the two particles and similarly, figure 5.39 (right) shows the v-component of the velocity of the two particles.

Level 5:

The time history of two bean shaped particles falling down and colliding with time-step 0.0001.

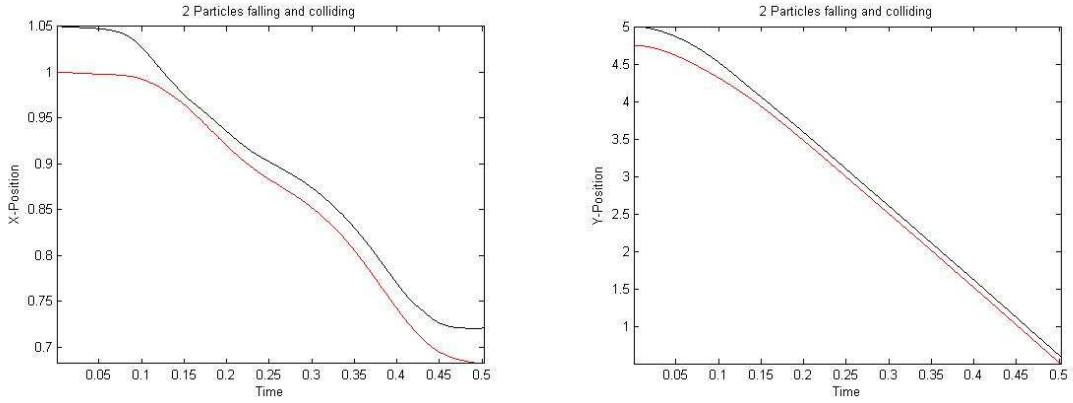

Figure 5.40: x-coordinate and y-coordinate of 2 non-circular particles w.r.t. time.

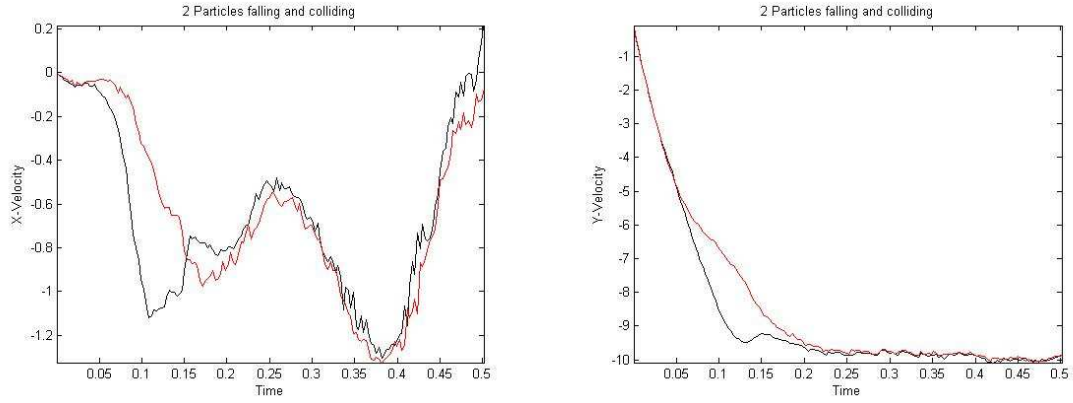

Figure 5.41: u-component and v-component of the translational velocity of 2 non-circular particles w.r.t. time.

The red line represents the first particle and the black line represents the second particle. Figure 5.40 (left) shows the x-coordinate of the center of the two particles and similarly, figure 5.40 (right) shows the y-coordinate of the center of the two particles. Figure 5.41 (left) shows the u-component of the velocity of the two particles and similarly, figure 5.41 (right) shows the v-component of the velocity of the two particles.

5.3.2. Conclusion

The bean shaped particles undergo the collision process as well as the drafting, kissing and tumbling phenomena is also observed during they fall down and their collisions are resolved using collision model 3 without overlapping. Collision model 1 and 2 can also be used for the case of general shape particles using a suitable mesh level and time-step as discussed before in the 2-particles (circular) case.

5.4. Applications

We have investigated two applications for particles in a fluid, namely 'particles in an Annulus' and 'particles in a lid driven cavity'.

5.4.1. Particles in Annulus

Circular Couette flow in an Annulus has a wide range of practical applications such as the flow of drilling mud between the rotating drill string, well drilling, filtration devices, chemical reactors and journal bearings, etc.

The behavior of the particles and their motion in an Annulus is examined. We will present results for one circular particle and general shape particles (circular, square and ellipse) in an Annulus. Two different shape particles are also simulated simultaneously and their motion is analyzed.

One circular particle in an Annulus

These tests have been carried out to find the values of the initial positions of the particle which allow the particle to move away toward the outer boundary and those initial positions which allow the particle to move toward the inner boundary when the outer boundary of the Annulus is moving and the inner boundary is fixed. Different particle radii are used to see the effect of particle size onto the initial positions of the particle. Later we will show that these results can be used for the particles in a particle separator.

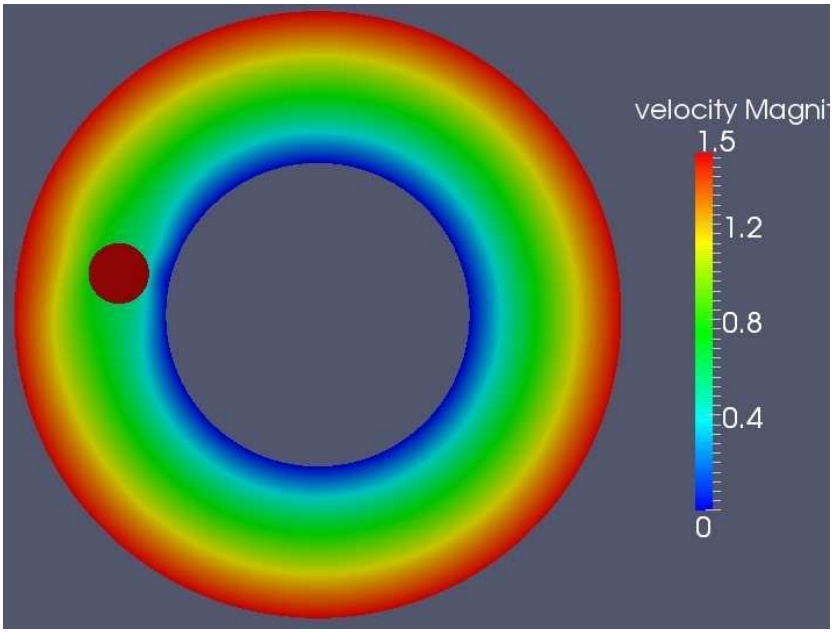

Figure 5.42: 1 circular particle moving in an Annulus

The outer boundary of the Annulus is moved with a constant (tangential) speed of $v = 1.5$ and the inner boundary is kept fixed. The radius of the inner boundary and the outer boundary of the Annulus is 0.25 and 0.5 respectively. Initial positions of the particle are changed gradually from the inner boundary toward the outer boundary and for each initial position, the particle's final position (w.r.t. radius) is analyzed when the flow reaches the steady state.

We have used different values of the Reynolds number *RE* for this procedure i.e. we have used $RE = 60, 70, 80, 90$ and 100. At each value of *RE* the particle is allowed to move freely with the fluid flow. The particle is tested for 10 different starting positions (slightly going from near the inner boundary toward the outer boundary) against each value of the radius of the particle. Eight different sizes/radii of the particle are used. The graphs for the distance of the center of the particle from the inner boundary w.r.t. the number of loops the particle has revolved inside the Annulus have been shown (1 loop = 1 complete revolution of the particle inside the Annulus).

RE = 60 :

Results for 10 different starting positions of the particle using 4 different radii of the particle are presented. The values for the radius of the particle used are $r_1 = 0.035$, $r_2 = 0.040$, $r_3 = 0.045$ and $r_4 = 0.050$.

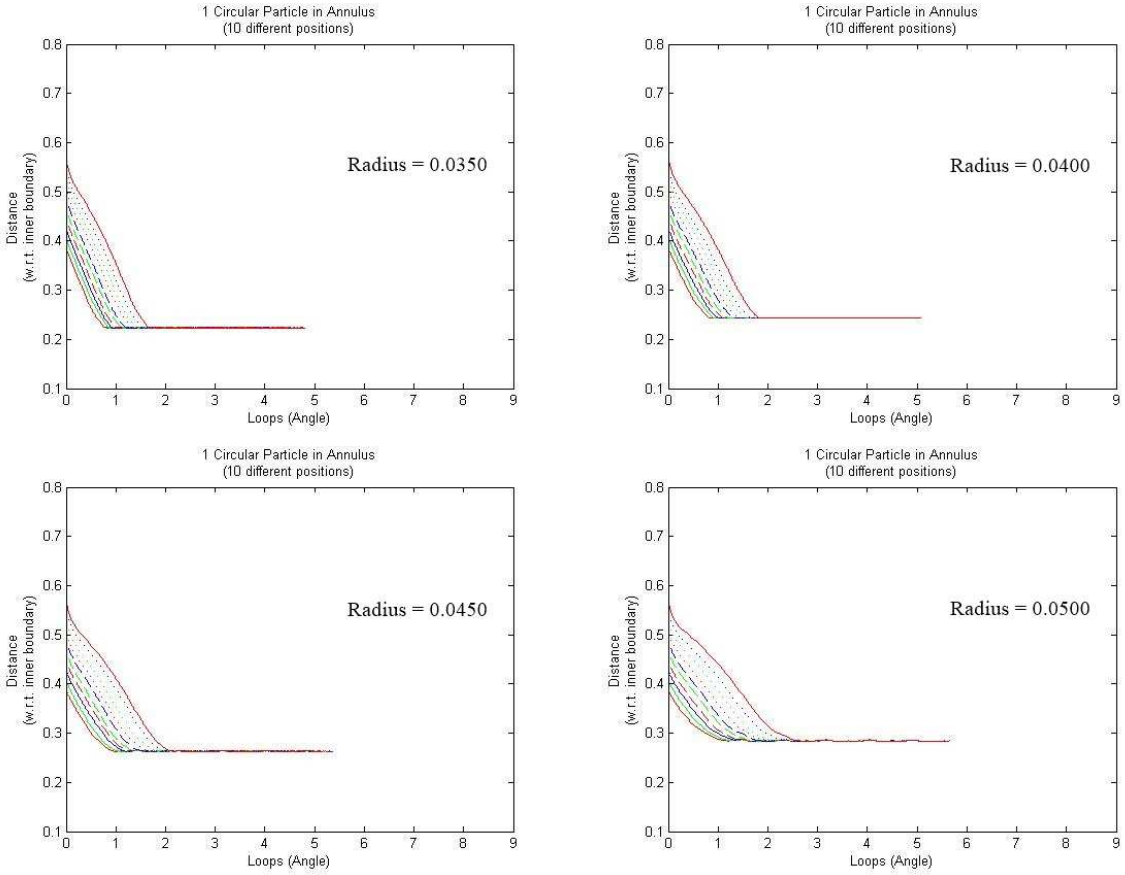

Figure 5.43: 1 circular particle moving in an Annulus

10 different lines (colored/dashed) show 10 different starting positions of the particle. The graphs show distance of the center of the particle from the inner boundary of the Annulus w.r.t. the number of loops the particle has revolved inside the Annulus.

Now we present a table using 10 different starting positions against 8 different radii of the particle. The following table shows a value of '0' if for a given radius and starting position of the particle, the particle keeps moving close to the inner boundary (non-rotating boundary) of the Annulus. Similarly, a value of '1' shows that the particle has moved away from the inner boundary toward the outer boundary (rotating boundary) of the Annulus.

The starting positions of the particle are varied inside the Annulus in the x-direction keeping the initial y-position of the particle fixed at $Y = 0$. Therefore, the starting x-positions of the particle are $p_1 = -0.345$, $p_2 = -0.350$, $p_3 = -0.355$, $p_4 = -0.360$, $p_5 = -0.365$, $p_6 = -0.370$, $p_7 = -0.375$, $p_8 = -0.380$, $p_9 = -0.385$ and $p_{10} = -0.390$. The values for the radii of the particle are $r_1 = 0.0325$, $r_2 = 0.035$, $r_3 = 0.0375$, $r_4 = 0.040$, $r_5 = 0.0425$, $r_6 = 0.045$, $r_7 = 0.0475$ and $r_8 = 0.050$.

Table 5.41: 1 circular particle moving in an Annulus ($RE = 60$)

Radius	Starting position of the particle									
	p_1	p_2	p_3	p_4	p_5	p_6	p_7	p_8	p_9	p_{10}
r_1	0	0	0	0	0	0	0	0	0	0
r_2	0	0	0	0	0	0	0	0	0	0
r_3	0	0	0	0	0	0	0	0	0	0
r_4	0	0	0	0	0	0	0	0	0	0
r_5	0	0	0	0	0	0	0	0	0	0
r_6	0	0	0	0	0	0	0	0	0	0
r_7	0	0	0	0	0	0	0	0	0	0
r_8	0	0	0	0	0	0	0	0	0	0

Table 5.41 shows the movement of the particle (toward the inner/outer boundary of the Annulus) when it reaches a uniform velocity while moving freely with the fluid flow. A value of '0' shows the movement of the particle toward the inner boundary and a value of '1' shows the movement of the particle toward the outer boundary of the Annulus.

We can see from the Table 5.41 that the particle moved toward the inner boundary of the Annulus for all the values of the radius and the starting positions of the particle using $RE = 60$.

RE = 70 :

Results for 10 different starting positions of the particle using 4 different radii of the particle are presented. The values for the radius of the particle used are $r_1 = 0.035$, $r_2 = 0.040$, $r_3 = 0.045$ and $r_4 = 0.050$.

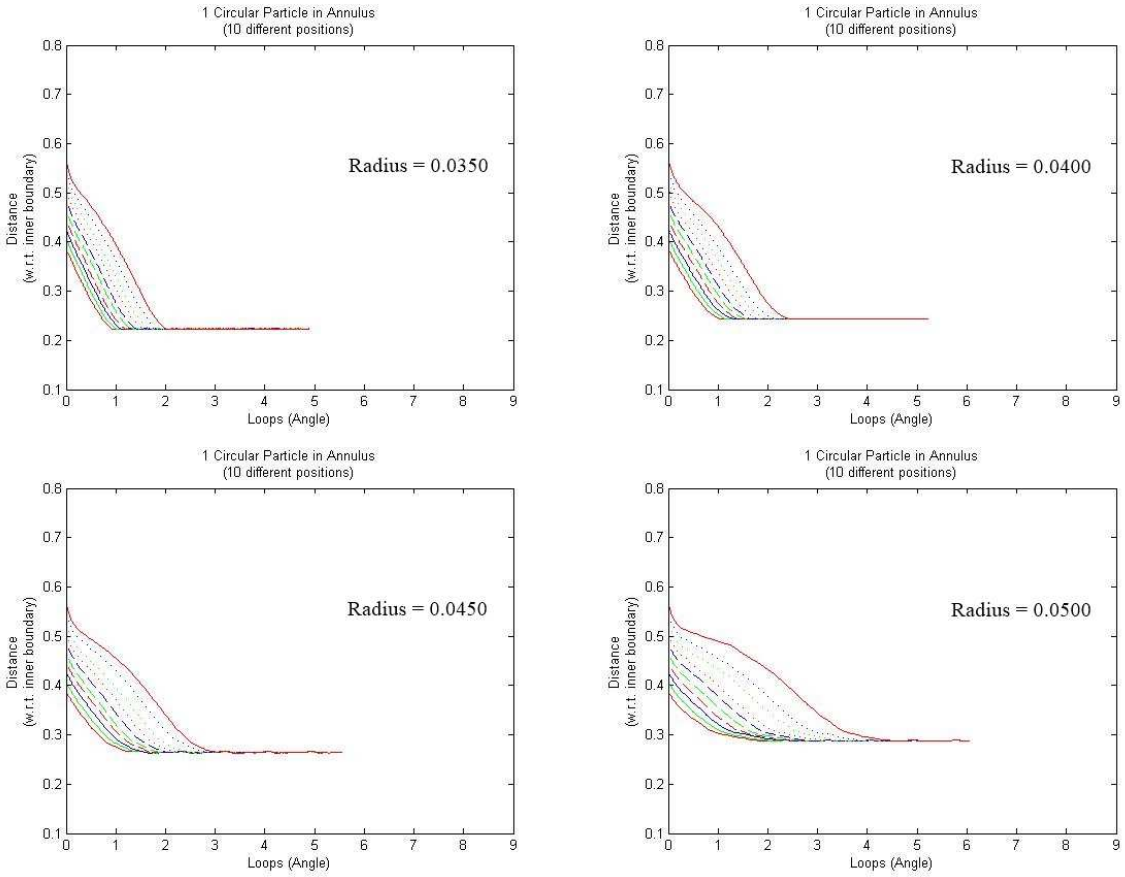

Figure 5.44: 1 circular particle moving in an Annulus

10 different lines (colored/dashed) show 10 different starting positions of the particle. The graphs show distance of the center of the particle from the inner boundary of the Annulus w.r.t. the number of loops the particle has revolved inside the Annulus.

Now we again present a table using 10 different starting positions against 8 different radii of the particle. The starting positions of the particle are varied inside the Annulus in the x-direction keeping the initial y-position of the particle fixed at $Y = 0$. Therefore, the starting x-positions of the particle are $p_1 = -0.345$, $p_2 = -0.350$, $p_3 = -0.355$, $p_4 = -0.360$, $p_5 = -0.365$, $p_6 = -0.370$, $p_7 = -0.375$, $p_8 = -0.380$, $p_9 = -0.385$ and $p_{10} = -0.390$. The values for the radii of the particle are $r_1 = 0.0325$, $r_2 = 0.035$, $r_3 = 0.0375$, $r_4 = 0.040$, $r_5 = 0.0425$, $r_6 = 0.045$, $r_7 = 0.0475$ and $r_8 = 0.050$.

Table 5.42: 1 circular particle moving in an Annulus ($RE = 70$)

	Starting position of the particle									
Radius	p_1	p_2	p_3	p_4	p_5	p_6	p_7	p_8	p_9	p_{10}
r_1	0	0	0	0	0	0	0	0	0	0
r_2	0	0	0	0	0	0	0	0	0	0
r_3	0	0	0	0	0	0	0	0	0	0
r_4	0	0	0	0	0	0	0	0	0	0
r_5	0	0	0	0	0	0	0	0	0	0
r_6	0	0	0	0	0	0	0	0	0	0
r_7	0	0	0	0	0	0	0	0	0	0
r_8	0	0	0	0	0	0	0	0	0	0

Table 5.42 shows the movement of the particle (toward the inner/outer boundary of the Annulus) when it reaches a uniform velocity while moving freely with the fluid flow. A value of '0' shows the movement of the particle toward the inner boundary and a value of '1' shows the movement of the particle toward the outer boundary of the Annulus.

Again, we can see from Table 5.42 that the particle moved toward the inner boundary of the Annulus for all the values of the radius and the starting positions of the particle using $RE = 70$.

RE = 80 :

Results for 10 different starting positions of the particle using 6 different radii of the particle are presented. The values for the radius of the particle used are $r_1 = 0.035$, $r_2 = 0.040$, $r_3 = 0.0425$, $r_4 = 0.045$, $r_5 = 0.0475$ and $r_6 = 0.050$.

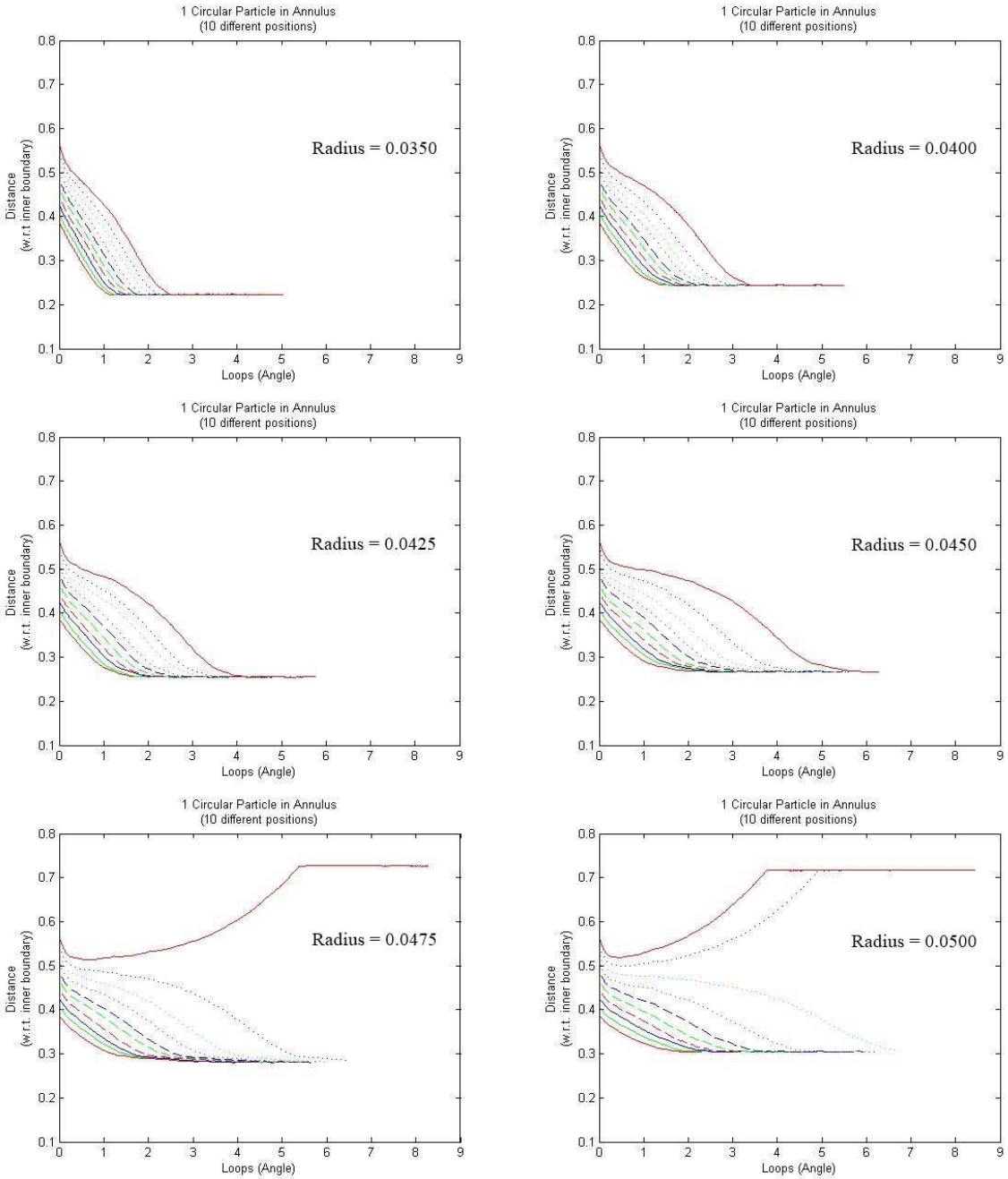

Figure 5.45: 1 circular particle moving in an Annulus

10 different lines (colored/dashed) show 10 different starting positions of the particle. The graphs show distance of the center of the particle from the inner boundary of the Annulus w.r.t. the number of loops the particle has revolved inside the Annulus.

We present a table using 10 different starting positions against 8 different radii of the particle. The starting positions of the particle are varied inside the Annulus in the x-direction keeping the initial y-position of the particle fixed at $Y = 0$. Therefore, the starting x-positions of the particle are $p_1 = -0.345$, $p_2 = -0.350$, $p_3 = -0.355$, $p_4 = -0.360$, $p_5 = -0.365$, $p_6 = -0.370$, $p_7 = -0.375$, $p_8 = -0.380$, $p_9 = -0.385$ and $p_{10} = -0.390$. The values for the radii of the particle are $r_1 = 0.0325$, $r_2 = 0.035$, $r_3 = 0.0375$, $r_4 = 0.040$, $r_5 = 0.0425$, $r_6 = 0.045$, $r_7 = 0.0475$ and $r_8 = 0.050$.

Table 5.43: 1 circular particle moving in an Annulus ($RE = 80$)

	Starting position of the particle									
Radius	p_1	p_2	p_3	p_4	p_5	p_6	p_7	p_8	p_9	p_{10}
r_1	0	0	0	0	0	0	0	0	0	0
r_2	0	0	0	0	0	0	0	0	0	0
r_3	0	0	0	0	0	0	0	0	0	0
r_4	0	0	0	0	0	0	0	0	0	0
r_5	0	0	0	0	0	0	0	0	0	0
r_6	0	0	0	0	0	0	0	0	0	0
r_7	0	0	0	0	0	0	0	0	0	1
r_8	0	0	0	0	0	0	0	0	1	1

Table 5.43 shows the movement of the particle (toward the inner/outer boundary of the Annulus) when it reaches a uniform velocity while moving freely with the fluid flow. A value of '0' shows the movement of the particle toward the inner boundary and a value of '1' shows the movement of the particle toward the outer boundary of the Annulus.

We can see from Table 5.43 that when the radius of the particle is increased and is started away from the inner boundary, the particle moves toward the outer boundary (rotating boundary) of the Annulus as it reaches the uniform velocity. For smaller radii and the starting positions near the inner boundary the particle moves toward the inner boundary of the Annulus using $RE = 80$.

RE $= 90$:

Results for 10 different starting positions of the particle using 8 different radii of the particle are presented. The values for the radius of the particle used are $r_1 = 0.0325$, $r_2 = 0.035$, $r_3 = 0.0375$, $r_4 = 0.040$, $r_5 = 0.0425$, $r_6 = 0.045$, $r_7 = 0.0475$ and $r_8 = 0.050$.

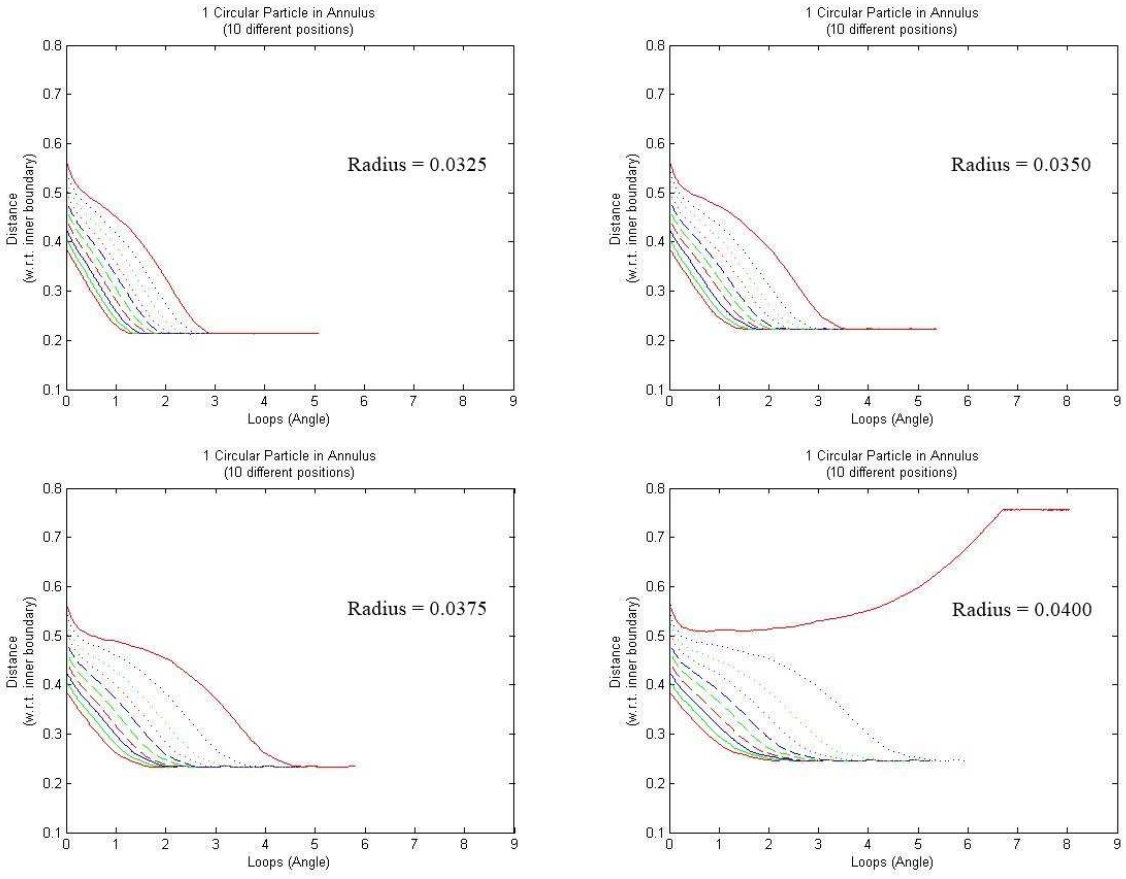

Figure 5.46: 1 circular particle moving in an Annulus

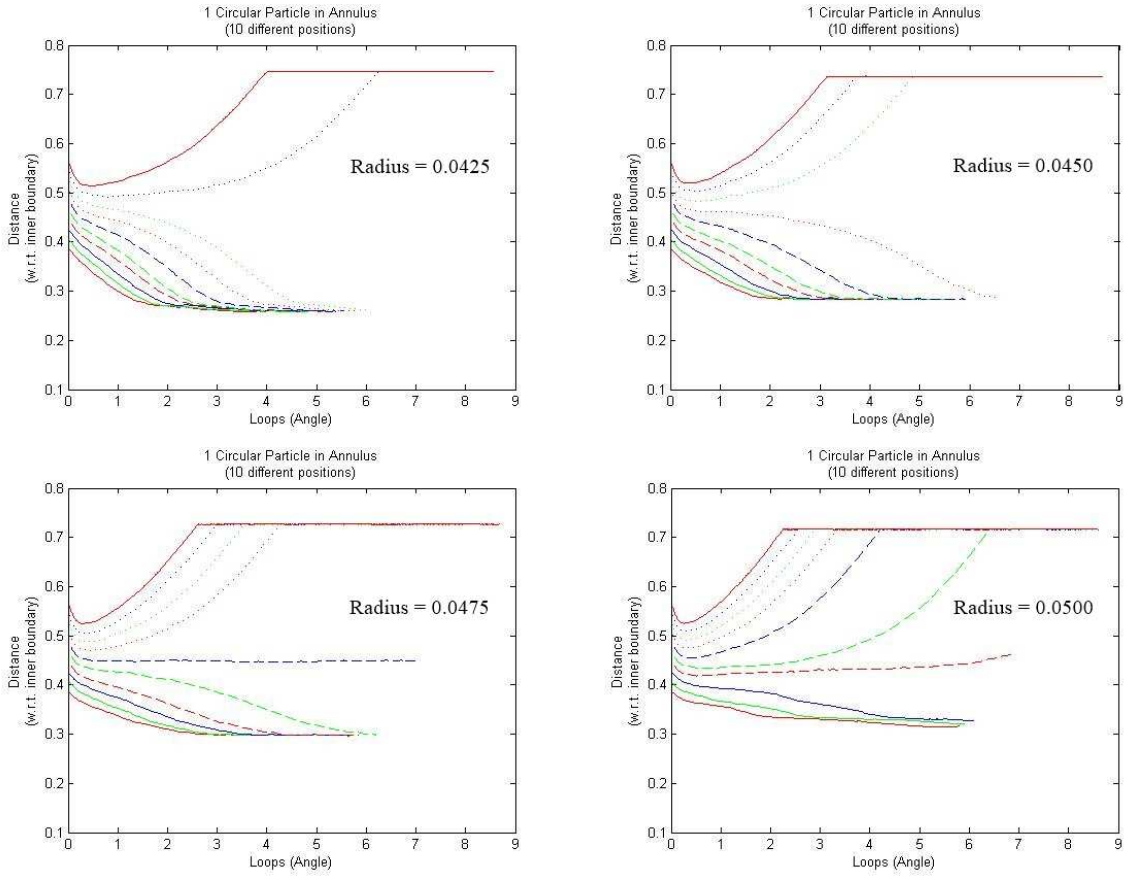

Figure 5.47: 1 circular particle moving in an Annulus

10 different lines (colored/dashed) show 10 different starting positions of the particle. The graphs show distance of the center of the particle from the inner boundary of the Annulus w.r.t. the number of loops the particle has revolved inside the Annulus.

Now we present a table using 10 different starting positions against 8 different radii of the particle. The starting positions of the particle are varied inside the Annulus in the x-direction keeping the initial y-position of the particle fixed at $Y = 0$. Therefore, the starting x-positions of the particle are $p_1 = -0.345$, $p_2 = -0.350$, $p_3 = -0.355$, $p_4 = -0.360$, $p_5 = -0.365$, $p_6 = -0.370$, $p_7 = -0.375$, $p_8 = -0.380$, $p_9 = -0.385$ and $p_{10} = -0.390$. The values for the radii of the particle are $r_1 = 0.0325$, $r_2 = 0.035$, $r_3 = 0.0375$, $r_4 = 0.040$, $r_5 = 0.0425$, $r_6 = 0.045$, $r_7 = 0.0475$ and $r_8 = 0.050$.

Table 5.44: 1 circular particle moving in an Annulus ($RE = 90$)

Radius	Starting position of the particle									
	p_1	p_2	p_3	p_4	p_5	p_6	p_7	p_8	p_9	p_{10}
r_1	0	0	0	0	0	0	0	0	0	0
r_2	0	0	0	0	0	0	0	0	0	0
r_3	0	0	0	0	0	0	0	0	0	0
r_4	0	0	0	0	0	0	0	0	0	1
r_5	0	0	0	0	0	0	0	0	1	1
r_6	0	0	0	0	0	0	0	1	1	1
r_7	0	0	0	0	0	0	1	1	1	1
r_8	0	0	0	1	1	1	1	1	1	1

Table 5.44 shows the movement of the particle (toward the inner/outer boundary of the Annulus) when it reaches a uniform velocity while moving freely with the fluid flow. A value of '0' shows the movement of the particle toward the inner boundary and a value of '1' shows the movement of the particle toward the outer boundary of the Annulus.

Again, we can see from Table 5.44 that when the radius of the particle is increased and is started away from the inner boundary, the particle moves toward the outer boundary (rotating boundary) of the Annulus as it reaches the uniform velocity. For smaller radii and the starting positions near the inner boundary the particle moves toward the inner boundary of the Annulus using $RE = 90$.

RE $= 100$:

Results for 10 different starting positions of the particle using 8 different radii of the particle are presented. The values for the radius of the particle used are $r_1 = 0.0325$, $r_2 = 0.035$, $r_3 = 0.0375$, $r_4 = 0.040$, $r_5 = 0.0425$, $r_6 = 0.045$, $r_7 = 0.0475$ and $r_8 = 0.050$.

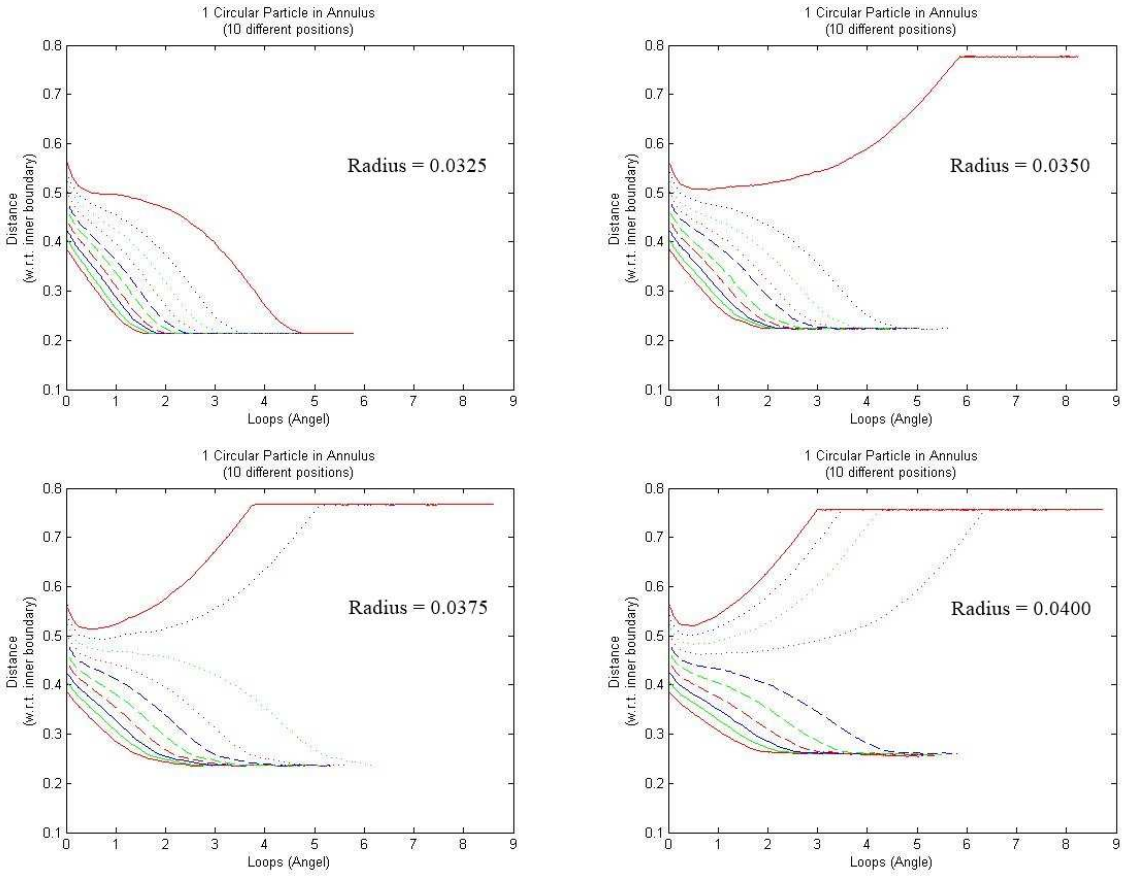

Figure 5.48: 1 circular particle moving in an Annulus

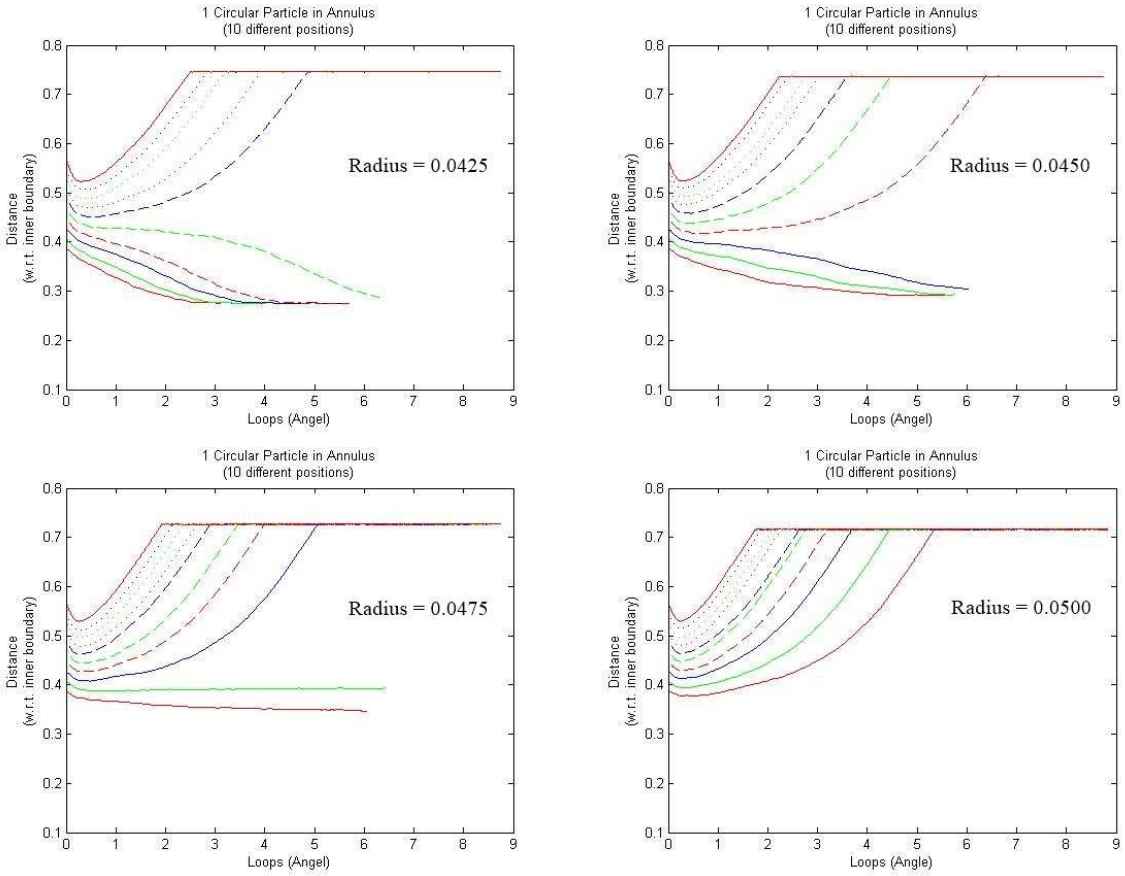

Figure 5.49: 1 circular particle moving in an Annulus

10 different lines (colored/dashed) show 10 different starting positions of the particle. The graphs show distance of the center of the particle from the inner boundary of the Annulus w.r.t. the number of loops the particle has revolved inside the Annulus.

We again present a table using 10 different starting positions against 8 different radii of the particle. The starting positions of the particle are varied inside the Annulus in the x-direction keeping the initial y-position of the particle fixed at $Y = 0$. Therefore, the starting x-positions of the particle are $p_1 = -0.345$, $p_2 = -0.350$, $p_3 = -0.355$, $p_4 = -0.360$, $p_5 = -0.365$, $p_6 = -0.370$, $p_7 = -0.375$, $p_8 = -0.380$, $p_9 = -0.385$ and $p_{10} = -0.390$. The values for the radii of the particle are $r_1 = 0.0325$, $r_2 = 0.035$, $r_3 = 0.0375$, $r_4 = 0.040$, $r_5 = 0.0425$, $r_6 = 0.045$, $r_7 = 0.0475$ and $r_8 = 0.050$.

Table 5.45: 1 circular particle moving in an Annulus ($RE = 100$)

Radius	Starting position of the particle									
	p_1	p_2	p_3	p_4	p_5	p_6	p_7	p_8	p_9	p_{10}
r_1	0	0	0	0	0	0	0	0	0	0
r_2	0	0	0	0	0	0	0	0	0	1
r_3	0	0	0	0	0	0	0	0	1	1
r_4	0	0	0	0	0	0	1	1	1	1
r_5	0	0	0	0	0	1	1	1	1	1
r_6	0	0	0	1	1	1	1	1	1	1
r_7	0	0	1	1	1	1	1	1	1	1
r_8	1	1	1	1	1	1	1	1	1	1

Table 5.45 shows the movement of the particle (toward the inner/outer boundary of the Annulus) when it reaches a uniform velocity while moving freely with the fluid flow. A value of '0' shows the movement of the particle toward the inner boundary and a value of '1' shows the movement of the particle toward the outer boundary of the Annulus.

Again, we can see from Table 5.45 that when the radius of the particle is increased and is started away from the inner boundary, the particle moves toward the outer boundary (rotating boundary) of the Annulus as it reaches the uniform velocity. For smaller radii and the starting positions near the inner boundary the particle moves toward the inner boundary of the Annulus using $RE = 100$.

Conclusion

From the results we conclude that as the *RE* is increased, the chances for the particle to move towards the outer boundary (rotating boundary) increases. Similarly, if the starting position of the particle is kept away from the inner boundary, again the chances for the particle to go toward the outer boundary increases. And finally, a large sized particle is more likely to go toward the outer boundary. We have shown through the tables some values of *RE*, radius of the particle and starting positions of the particle which are suitable for the particle to move on either boundary of the Annulus as the particle reaches the uniform motion.

These results can help in estimating the movement of the particles in a particle separator. We can easily find out that whether the particle will move towards the inner boundary or whether it will move towards the outer boundary for different particle sizes, different *RE* and different starting positions.

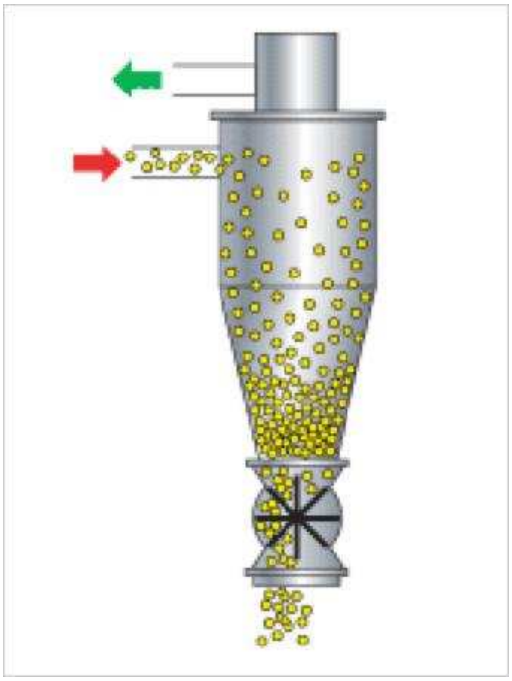

Figure 5.50: A simple cyclone separator (figure reprinted from [1])

Comparison between circular, square and elliptic shape particles

The movement of a circular, elliptical and square shaped particle in an Annulus is analyzed for each particle type separately. The particles are allowed to move freely with the fluid flow. The radius of the inner boundary and the outer boundary of the Annulus is 0.25 and 0.5 respectively. The outer boundary of the Annulus is moving with a constant speed of $v = 1.5$ and the inner boundary is kept fixed. The radius of the circle is $r_{circ} = 0.0375$, length of the semi-major axis of the ellipse is $l_{el} = 0.0375$ and the length of the diagonal of the square is $l_{sq} = 0.0375$. $RE = 100$ and the initial position for each particle is $(-0.375, 0)$. This comparison has been made to find the effect of the shape of the particle on its movement inside the Annulus.

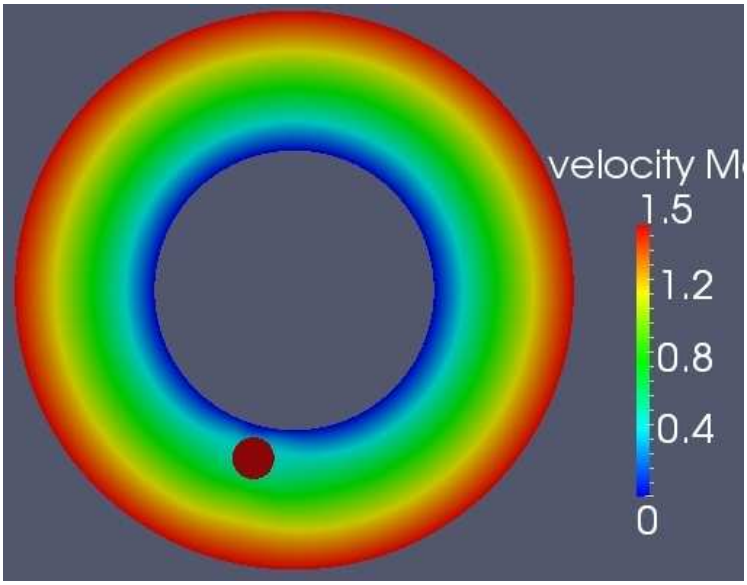

Figure 5.51: A circular particle moving inside an Annulus

The time-loops and time-speed graph of a circular particle is shown in Fig. 5.52:

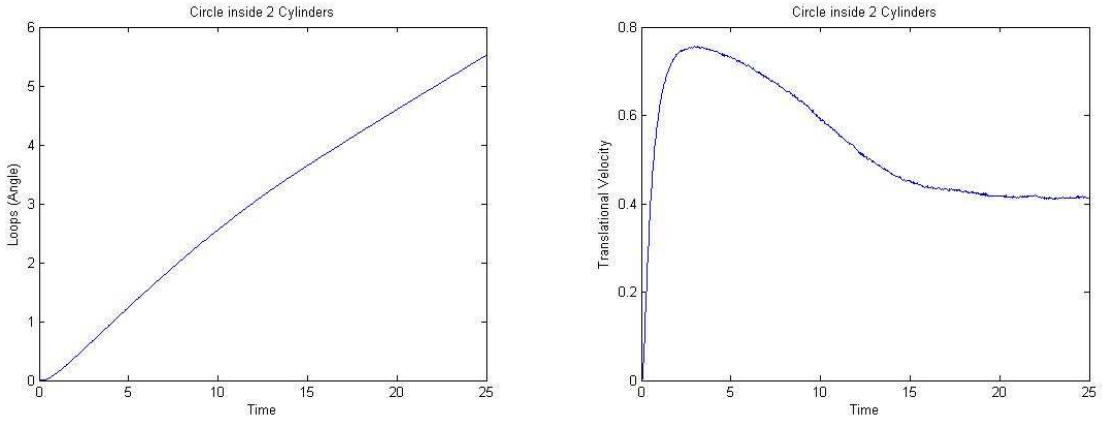

Figure 5.52: Loops and speed of a circular particle w.r.t. time

Figure 5.52 shows that the circular particle moves towards the inner boundary as it revolves around the Annulus and reaches a uniform motion.

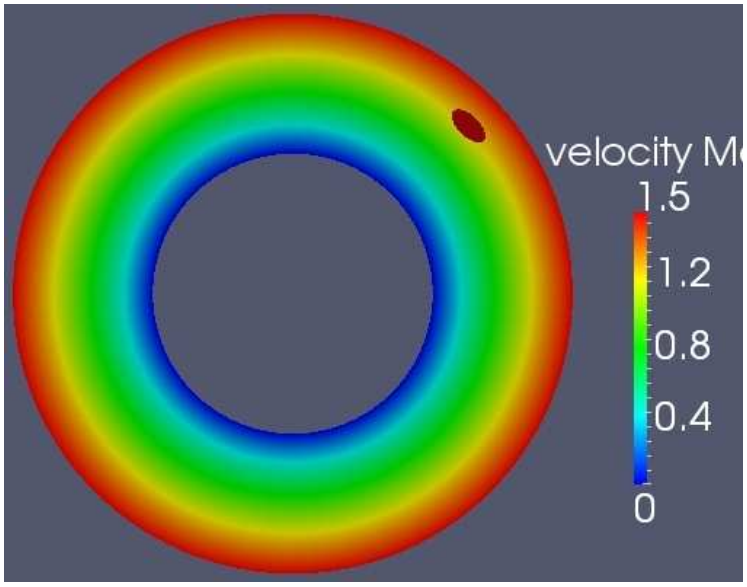

Figure 5.53: An elliptical particle moving inside an Annulus

The time-loops and time-speed graph of an elliptical particle is shown in Fig. 5.54:

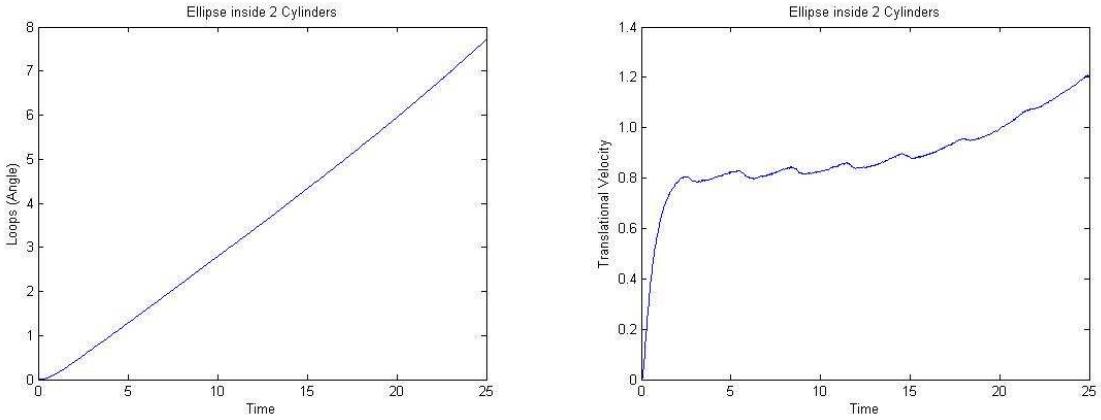

Figure 5.54: Loops and speed of an elliptical particle w.r.t. time

Figure 5.54 shows that the elliptical particle moves towards the outer boundary as it revolves around the Annulus. For the case of a circular particle, we have seen that the particle moved towards the inner boundary. It is important to note here that the total number of loops which the elliptical particle has revolved around the Annulus is more than the total number of loops which the circular particle has revolved.

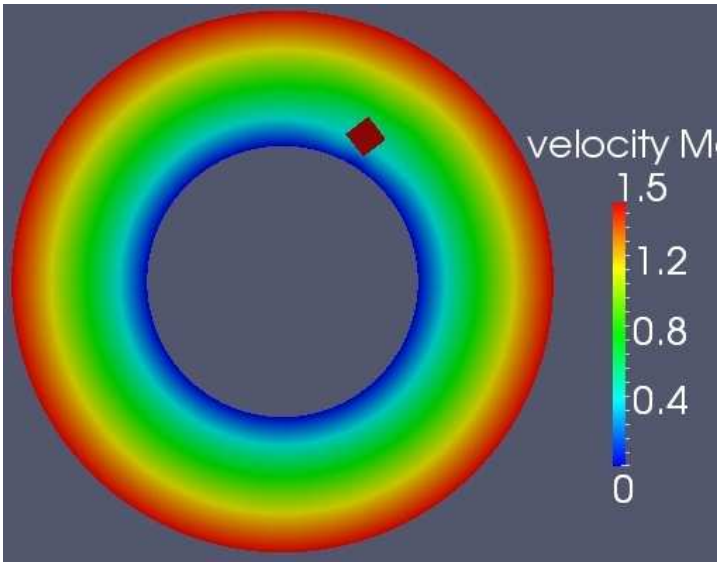

Figure 5.55: A square shaped particle moving inside an Annulus

The time-loops and time-speed graph of a square shaped particle is shown in Fig. 5.56:

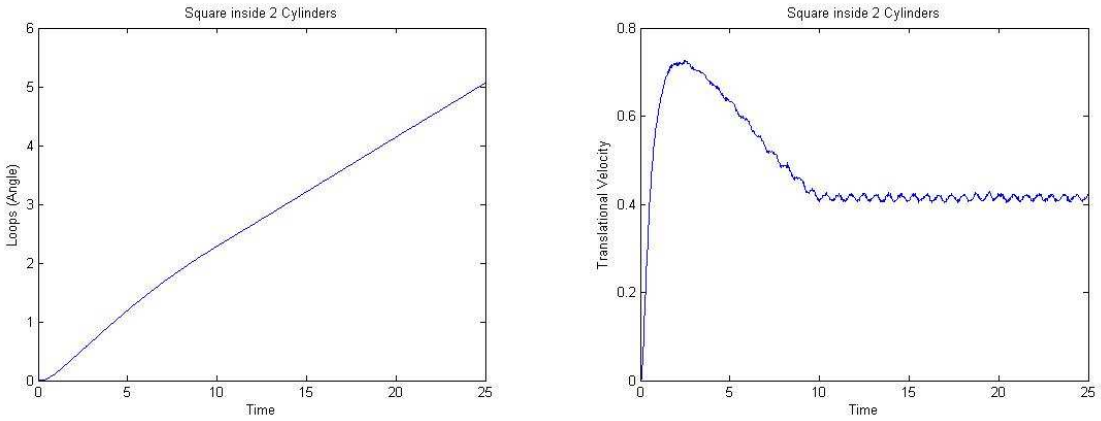

Figure 5.56: Loops and speed of a square shaped particle w.r.t. time

Figure 5.56 shows that the square shaped particle has also moved towards the inner boundary, like the circular particle, as it revolves around the Annulus. Interestingly, the square shaped particle has revolved through a smaller number of loops as compared to the number of loops the circular particle has revolved.

Conclusion

The comparison was made by keeping the same diameter for each particle. The circular particle as well as the square shaped particle moved towards the inner boundary but the elliptical particle moved towards the outer boundary of the Annulus. Additionally, we have noticed that the circular and the square shaped particle revolved through a smaller number of loops in the same time as compared to the elliptical particle during the motion inside the Annulus. We can only determine from these results that different shapes of the particle can show a different behavior of the particle movement in the Annulus keeping the same initial positions of the particle. These results have motivated us to start a race between two different shape particles inside an Annulus.

Different shape Particle's Race

A circular, elliptical and square shaped particle are allowed to move with the flow field inside an Annulus. Two different shape particles are introduced at the time in the annulus and their behavior is examined. The flow field is produced by giving an initial constant speed $v = 1.5$ to the outer boundary of the Annulus while the inner boundary is fixed. The radius of the inner boundary and the outer boundary of the Annulus is 0.25 and 0.5 respectively. $RE = 100$ and the two different shapes of the particle are kept at (-0.375) and $(0.375, 0)$ initially, opposite to each other, respectively.

A circle with radius = 0.0375 and an ellipse with semi-major axis = 0.0375 initiate the races.

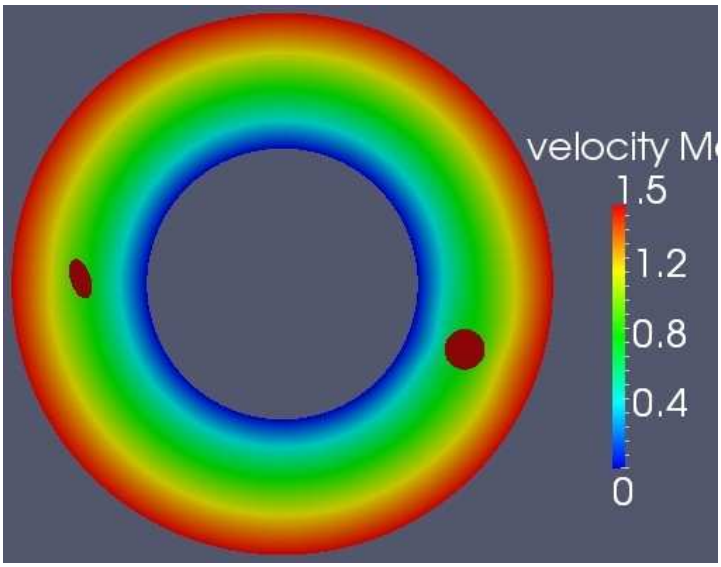

Figure 5.57: A circular and an elliptical particle moving in an Annulus

The time-loops and time-speed graph of two particles is shown in Fig. 5.58:

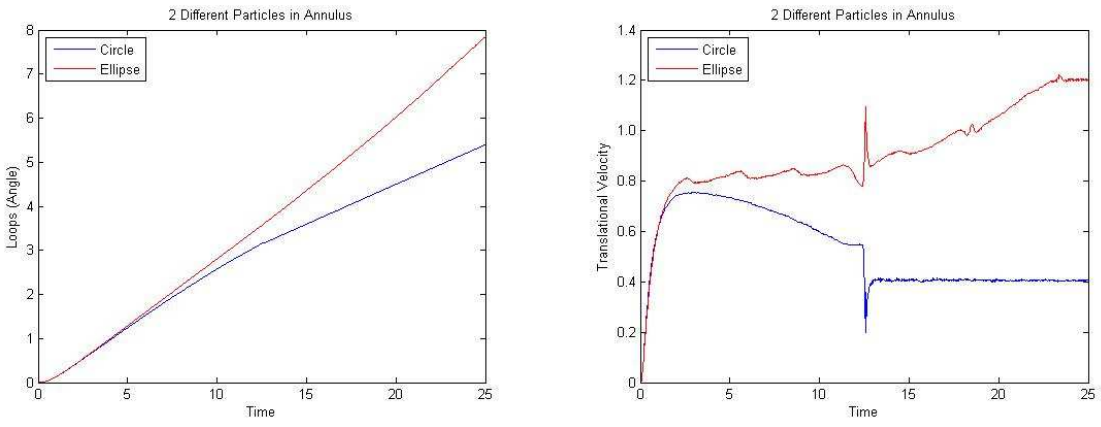

Figure 5.58: Loops and speed of 2 particles w.r.t time

Figure 5.58 (left) shows the number of loops the particles has revolved w.r.t time and the Figure 5.58 (right) show the speed of the particles w.r.t time.

We can see from the Figure 5.58 (left) that the circular particle revolves through a smaller number of loops and the elliptic particle revolves through more number of loops in the same time.

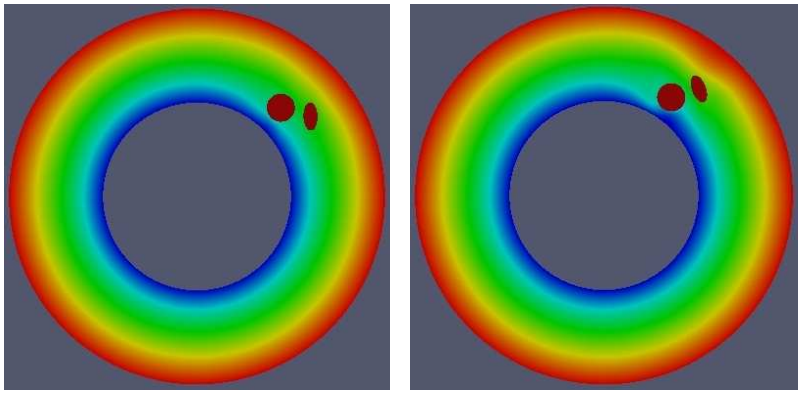

(a) t = 11.8 (b) t = 11.9

(c) t = 12.0 (d) t = 12.1

Figure 5.59: Elliptical particle crossing the circular particle

The elliptical particle crosses the circular particle during the motion and they also experience collision as can be seen from the fluctuation in the speed (see Figure 5.58 (right)).

A circle with radius = 0.0375 and a square with diagonal = 0.0375 initiate the races.

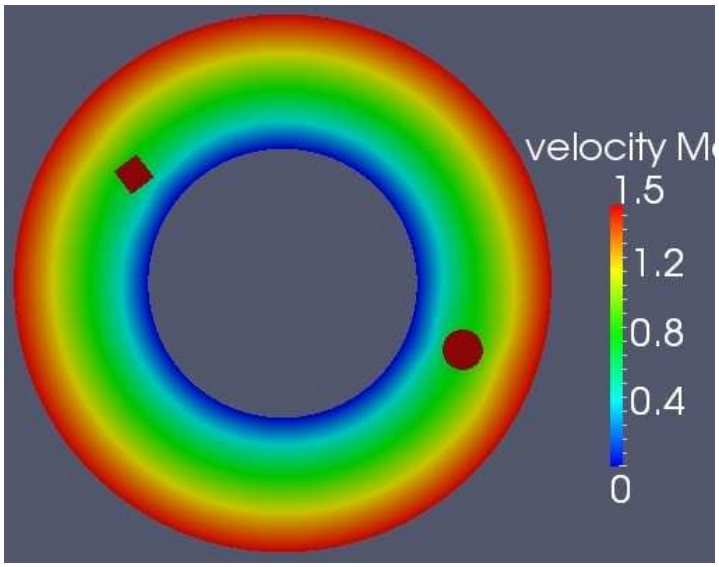

Figure 5.60: A circular and a square shape particle moving in an Annulus

The time-loops and time-speed graph of two particles is shown in Fig. 5.61:

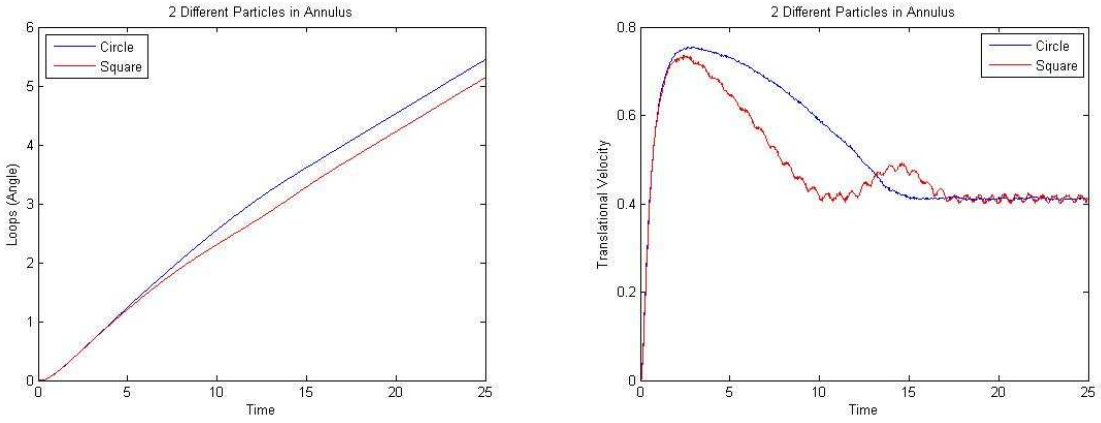

Figure 5.61: Loops and speed of 2 particles w.r.t time

We can see from the figure 5.61 (left) that the square shaped particle revolves through a smaller number of loops than the circular particle in the same time which shows that the square shaped particle moved with lesser speed inside the Annulus. Figure 5.61 (right) shows different speed with which the particles moved.

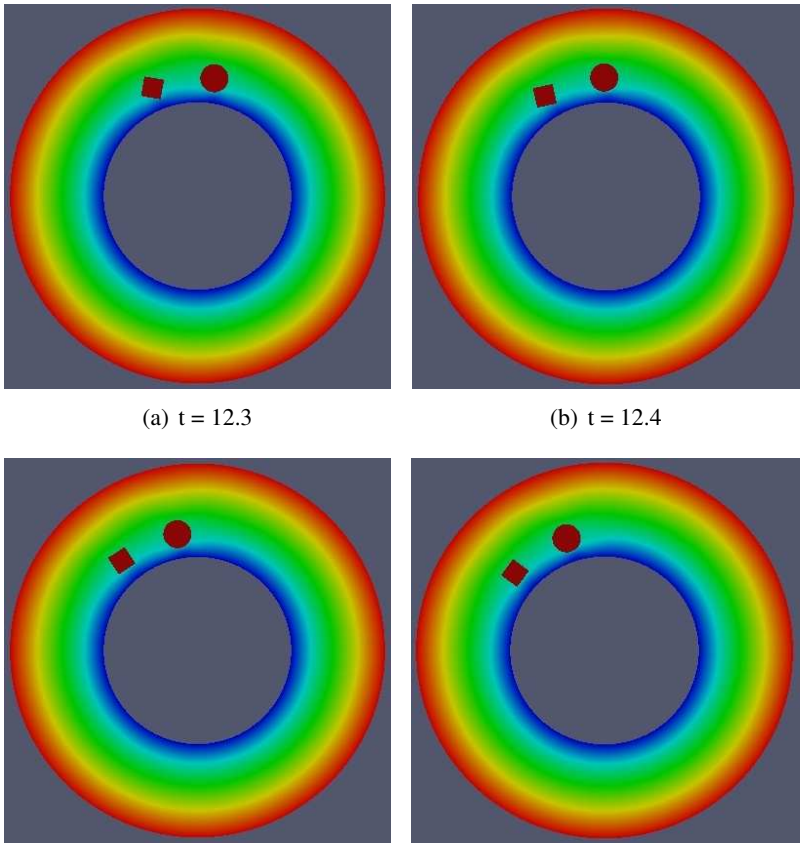

(a) t = 12.3 (b) t = 12.4

(c) t = 12.5 (d) t = 12.6

Figure 5.62: A circular and square shaped particle inside an Annulus

The circular particle moved faster initially but could not cross the square shaped particle as both particles are moving in the same line closer to the inner boundary. The particles also did not experience collision as shown in the Figure 5.61 (right).

An ellipse with semi-major axis = 0.0375 and a square with diagonal = 0.0375 initiate the races.

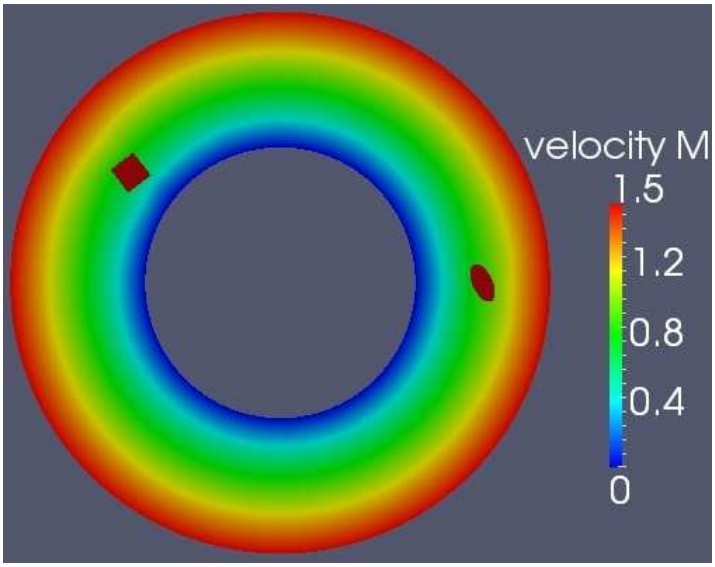

Figure 5.63: An elliptical and a square shape particle moving in an Annulus

The time-loops and time-speed graph of two particles is shown in Fig. 5.64:

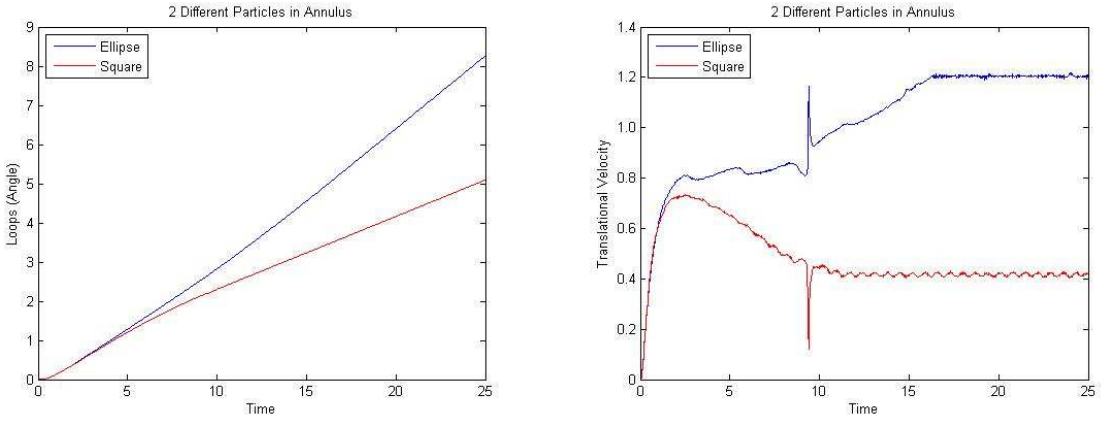

Figure 5.64: Loops and speed of 2 particles w.r.t time

Again, a big difference can be seen between the number of loops for the elliptical and square shaped particle. Figure 5.64 (left) shows that the square shaped particle revolves through a smaller number of loops than the elliptical shaped particle in the same time and the particles undergo the collision process as shown in the figure 5.64 (right). Also we can assume from the figure 5.64 (right) that the particles might have escaped the collision process a few times as the elliptical shaped particle passes the square shaped particle.

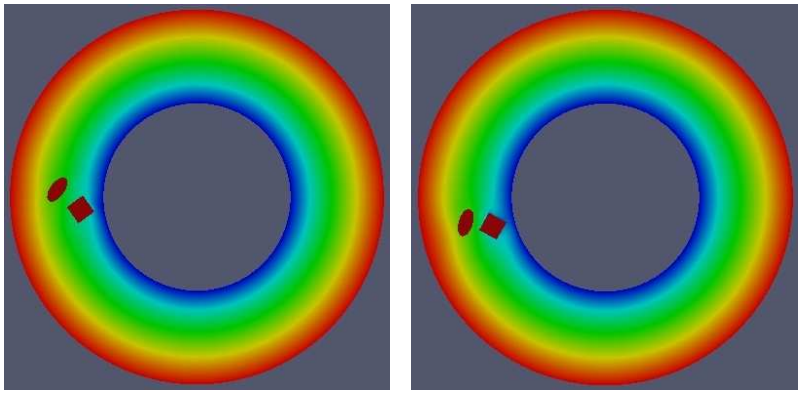

(a) t = 8.8 (b) t = 8.9

(c) t = 9.0 (d) t = 9.1

Figure 5.65: Elliptical particle crossing the square shaped particle

Again, the elliptical particle crosses the square shaped particle during the motion and they also experience collision as can be seen from the Figure 5.64 (right).

Conclusion

When the pair of a circular and a square shaped particle is allowed to move inside an Annulus, the difference between the speed at which both particles move is almost negligible. However, in the case of an ellipse and square shaped particle pair and the circle and ellipse shaped particle pair, the elliptical particle remained faster as compared to the other particles. The circular and square shaped particles moved toward the inner boundary of the Annulus while the elliptical particle moved towards the outer boundary. The elliptical particle undergoes the collision process as it crosses the circular and square shaped particle.

5.4.2. Particle-Laden Lid-Driven Cavity

Solid particles in an incompressible flow in a 2D lid-driven cavity are allowed to fall under the action of gravity and fluid forces. The objective of this benchmarking project is to see the motion of the particles in the cavity and the behavior/efficiency of the collision model used during the motion and collision of the particles in the cavity.

The computational domain is the unit square $\Omega = (0,1)^2$, the boundary conditions for $\mathbf{u} = (u,v)$ are given by $u(x,1) = 4x(1-x)$, $v(x,1) = 0$ on the moving lid and $u(x,y) = v(x,y) = 0$ elsewhere. The densities of the two phases are given by $\rho_f = 1.0$ and $\rho_s = 1.001$. The kinematic viscosity of the fluid is $\nu = 10^{-2}$, Reynolds number $Re = 100$, the gravitational acceleration constant equals $g = 980$.

At the beginning of the simulation, the fluid and particles are at rest. The particles are separated equidistantly in the cavity. Simulations are performed for $N = 100$, $N = 720$ and $N = 1225$ particles using diameter of each particle $d_p = 0.0564$ for the case of 100 particles and $d_p = 0.016$ for the case of 720 and 1225 particles.

Collision model 3 is used for these simulations which is based on a minimization procedure (section 3.3) and it computes the motion of rigid particles by the global computation of the forces acting on them.

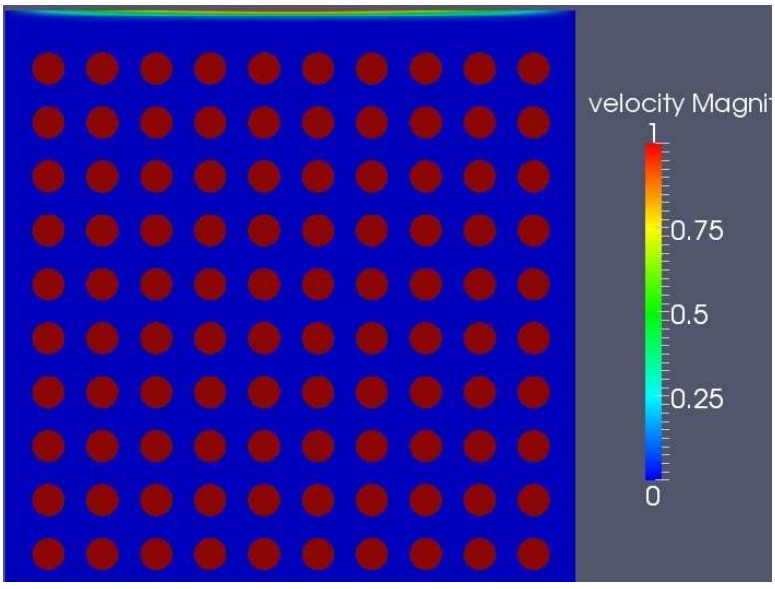

Figure 5.66: Initial configuration of 100 Particles in Lid Driven Cavity

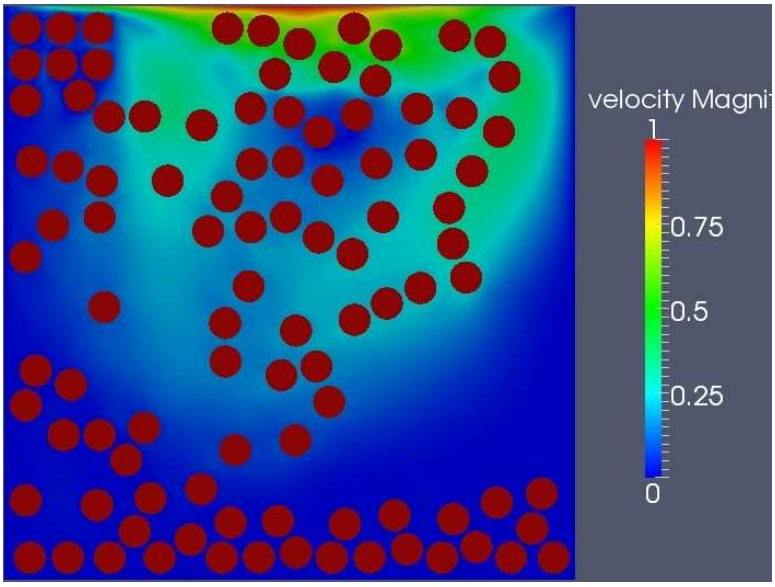

Figure 5.67: 100 Particles in Lid Driven Cavity at time $t = 20$

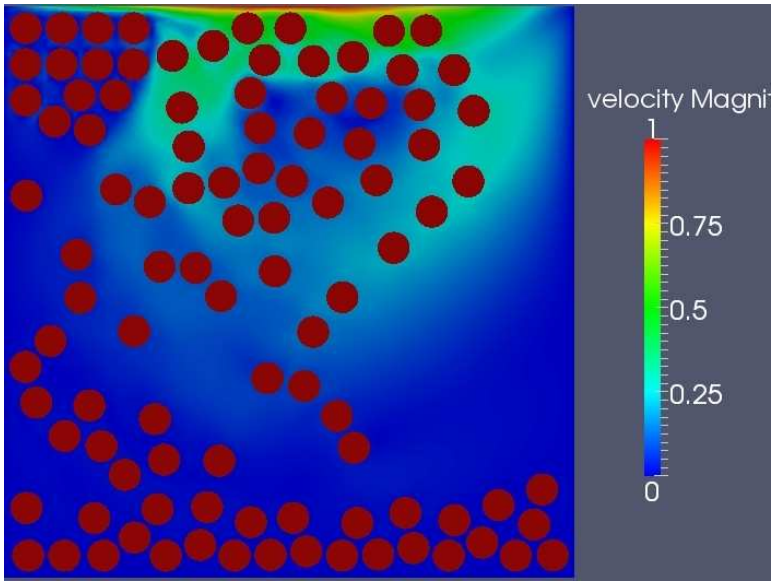

Figure 5.68: 100 Particles in Lid Driven Cavity at time $t = 25$

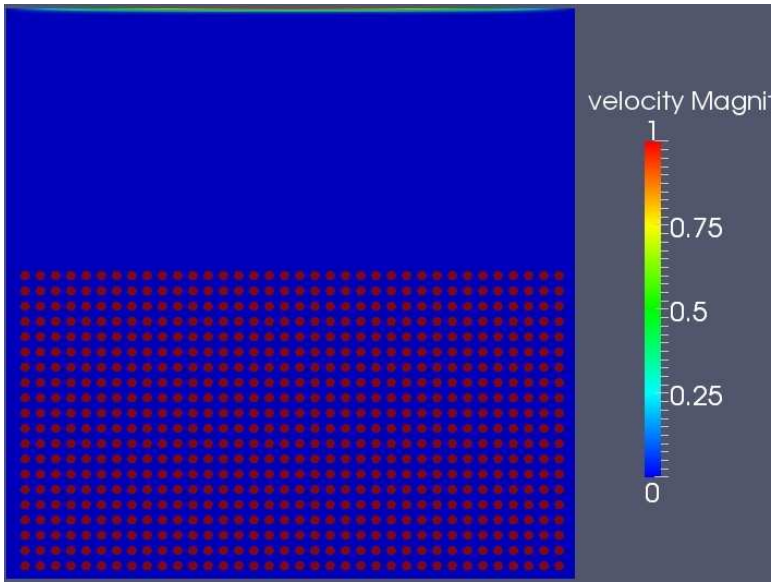

Figure 5.69: Initial configuration of 720 Particles in Lid Driven Cavity

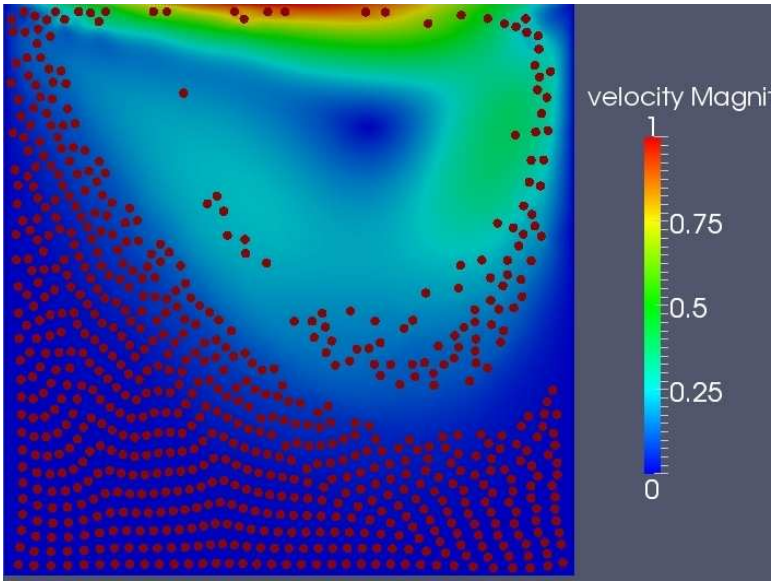

Figure 5.70: 720 Particles in Lid Driven Cavity at time $t = 10$

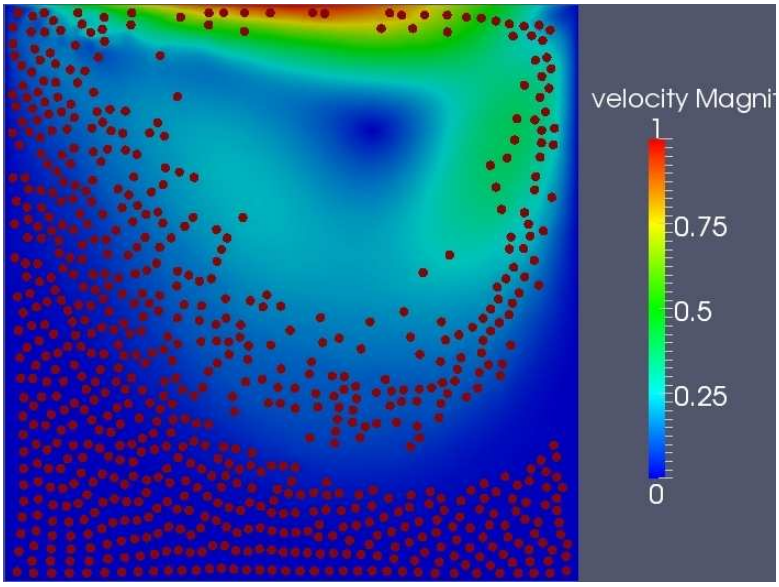

Figure 5.71: 720 Particles in Lid Driven Cavity at time $t = 20$

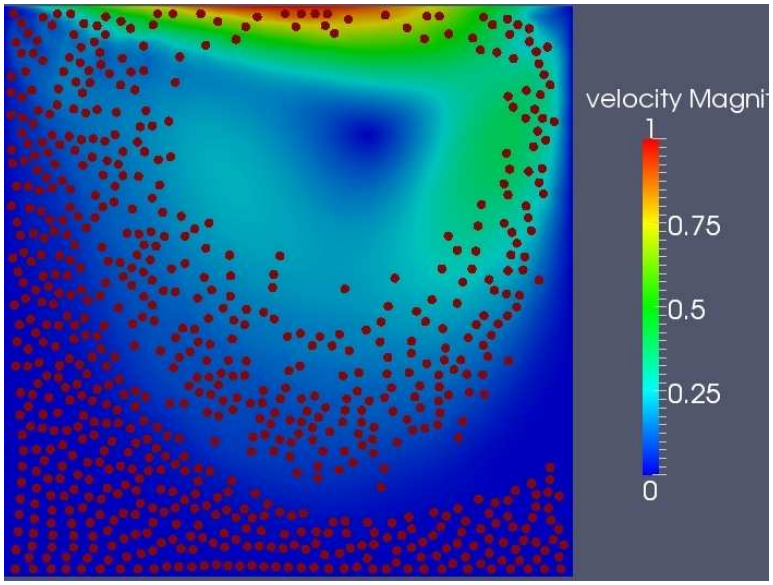

Figure 5.72: 720 Particles in Lid Driven Cavity at time $t = 30$

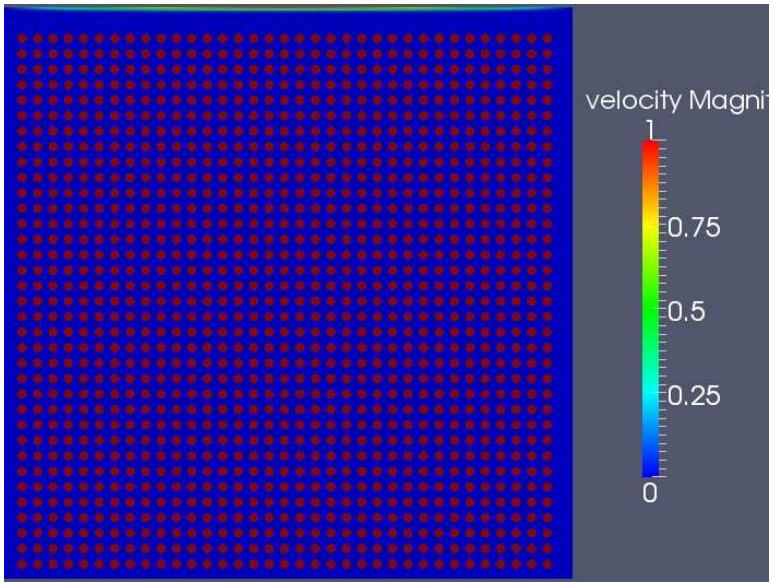

Figure 5.73: Initial configuration of 1225 Particles in Lid Driven Cavity

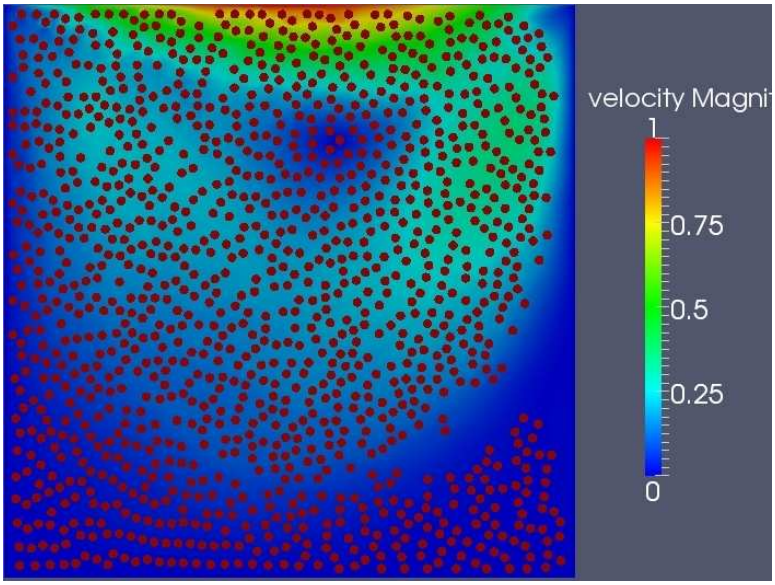

Figure 5.74: 1225 Particles in Lid Driven Cavity at time $t = 10$

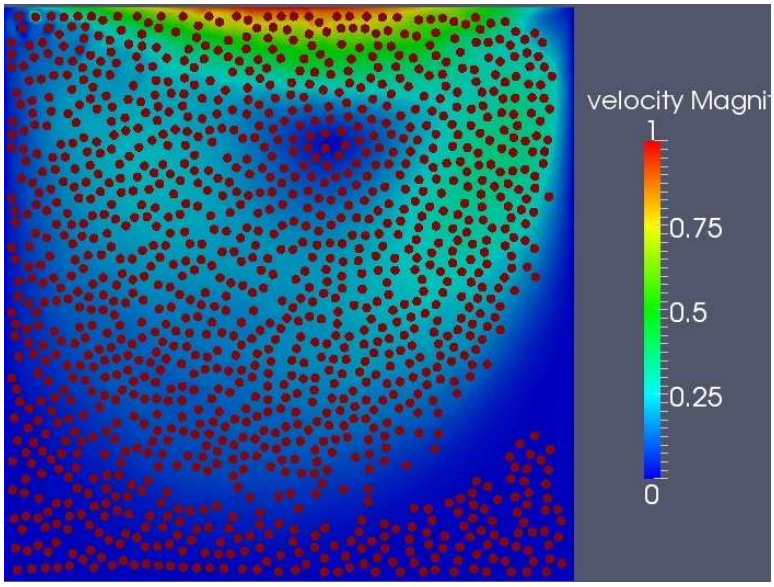

Figure 5.75: 1225 Particles in Lid Driven Cavity at time $t = 15$

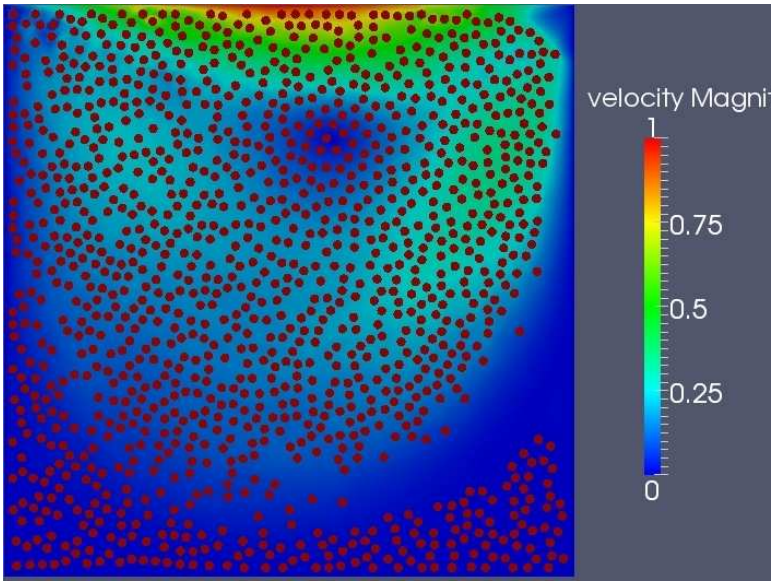

Figure 5.76: 1225 Particles in Lid Driven Cavity at time $t = 20$

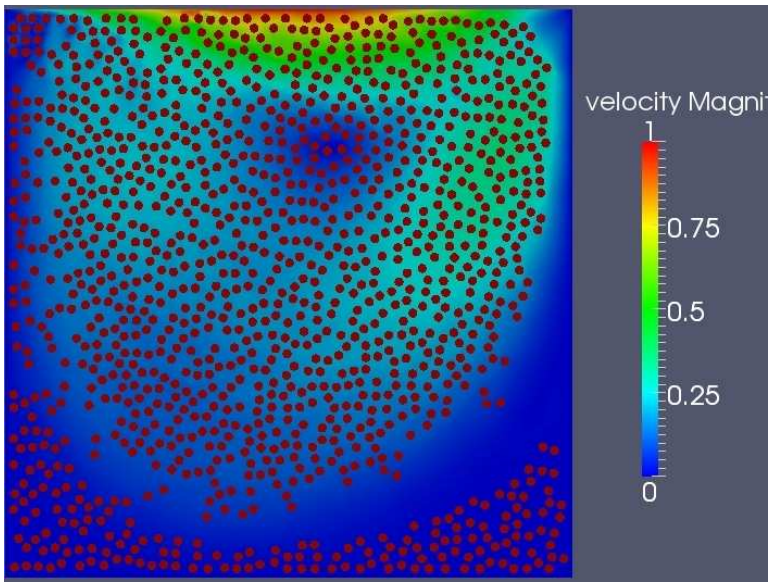

Figure 5.77: 1225 Particles in Lid Driven Cavity at time $t = 30$

Conclusion

We have simulated particles in a lid driven cavity. Different sizes for the particles as well as different number of particles were used for the three different configurations. From all the results it is clear that some of the particles settle down at the bottom of the cavity and the rest of the particles keep moving along with the flow field. A few particles are observed to be aggregated at the top left corner of the cavity.

6

Conclusion

In this work we have investigated different collision models in particulate flow. We have analyzed these collision models for their characteristics, efficiency and implementation coupled with the CFD. Initially, the collision models were tested in the absence of the fluid flow, more appropriately we considered dry particle collisions and later the routines for these collision models were integrated within our CFD code FEATFLOW for further tests and for the particulate flow simulations. The investigated models consist of different classes of collision models belonging to repulsive force models, lubrication models, minimization models (by minimizing the velocities of the approaching particles), sticky/gluey models and conservation of momentum models.

Two applications for the particulate flow have also been investigated, namely, particles in an Annulus (circular Couette flow) and particles in a lid driven cavity. Particles inside an Annulus are simulated which comprises of many tests for circular particles and later for particles of arbitrary/-general shapes which can be very useful in different applications such as the particle separator. Different properties and behavior of the particles depending on their size, shape and distance form the moving/rotating boundary of the Annulus are successfully concluded. Secondly, particles inside a lid driven cavity are simulated and their movement and behavior inside the lid driven cavity has been discussed. We came across a meaningful configuration for the particles in a lid driven cavity, after making a series of tests showing the (low) densities of the particles which kept moving in the fluid by applying a uniform velocity profile on the moving boundary of the cavity instead of settling down at the bottom.

The repulsive force collision model (Model 1) examined in our work depends on the distance between the centers of the colliding particles only whereas the lubrication model (Model 2), the collision model based on a minimization procedure (Model 3), the sticky or gluey particle model (Model 4) and the collision model based on conservation of linear momentum (Model 5) examined in the work depend on the velocities of the approaching particles as well as on the distance between the particles. The velocity based collision models have an advantage over the distance based collision models that they can give a better approximation for the new velocities of the colliding particles in particulate flow simulations. All these collision models are easy to implement and can be used in different situations for the particulate flow. Sub-time-steps can also be used to improve the efficiency of the collision models except the Model 3 and Model 4.

We have discussed a case during the tests for the particle collisions when there is no need for the collision model as we used a finer mesh and a small time step but this increases the simulation costs and makes it necessary to use a collision model such that the physical behavior of the particles in the fluid is as expected during the collision.

The aforementioned collision model based on a minimization procedure (Model 3) can avoid particle overlaps even for larger time steps as it is based on a minimization procedure which calculates the new velocities of the colliding particles in a global way. All the other collision models described in the thesis, except the sticky particle model (Model 4) which is an extension

of the Model 3), use the one by one iterative way for finding the forces on the particles. Moreover, Model 1 and Model 2 require the tuning of some parameters for the calculation of repulsive forces. Model 4, due to the sticking effect, can be used for the simulation of particle aggregates which occur in many natural processes. The collision model based on a minimization procedure (Model 3) has shown better results, as compared to the other collision models, derived from the tests carried out from the collision of two circular particles.

In the future work, the collision models may be improved by using a strategy to check particle collisions/overlaps discussed in section 3.7 which is more efficient in detecting the particle collisions accurately. Further detailed investigation of the collision models for the arbitrary shape particles is also desired. We wish to extend these collision models for the 3D particulate flow. Model 3 requires the investigation of a better solver for the solution of system of equations which can ensure a faster way for the simulation of a large number of particles. More detailed studies and tests are intended to analyze the behavior of the collision model 4 (sticky particle model).

Bibliography

[1] Cyclone separator. URL http://www.che.iitb.ac.in/online/labfacility/cyclone-separator/.

[2] D. J. Acheson. *Elementary fluid dynamics*. Clarendon Press Oxford University Press, Oxford New York, 1990. ISBN 0198596790.

[3] A.A. Adetayo, J.D. Litster, S.E. Pratsinis, and B.J. Ennis. Population balance modeling of drum granulation of materials with wide size distribution. *Powder Technology*, 82:37–49, 1995.

[4] A. M. ARDEKANI and R. H. RANGEL. Numerical investigation of particle-particle and particle-wall collisions in a viscous fluid. *Journal of Fluid Mechanics*, 596:437–466, 2008. DOI: 10.1017/S0022112007009688.

[5] K. Asakura, T. Asari, and I. Nakajima. Simulation of solid-liquid flows in a vertical pipe by a collision model. *Powder Technology*, 94(3):201 – 206, 1997. DOI: 10.1016/S0032-5910(97)03294-4.

[6] Richard Barrett, Michael Berry, Tony F. Chan, James W. Demmel, June Donato, Jack J. Dongarra, Victor Eijkhout, Roldan Pozo, Charles Romine, and Henk A. van der Vorst. *Templates for the Solution of Linear Systems: Building Blocks for Iterative Methods.* SIAM, second edition, November 1994.

[7] E. Bayraktar, O. Mierka, F. Platte, D. Kuzmin, and S. Turek. Numerical aspects and implementation of population balance equations coupled with turbulent fluid dynamics. *Computers & Chemical Engineering*, 35(11):2204 – 2217, 2011. DOI: 10.1016/j.compchemeng.2011.04.001.

[8] A. Berlemont, P. Achim, and Z. Chang. Lagrangian approaches for particle collisions: The colliding particle velocity correlation in the multiple particles tracking method and in the stochastic approach. *Physics of Fluids*, 13(10):2946–2956, 2001. DOI: 10.1063/1.1396845.

[9] S. F. Bockman. Generalizing the formula for areas of polygons to moments. *Am. Math. Monthly*, 96(2):131–132, February 1989. DOI: 10.2307/2323197.

[10] Y. Brenier and E. Grenier. Sticky particles and scalar conservation laws. *SIAM Journal on Numerical Analysis*, 35(6):2317–2328, 1998. DOI: 10.1137/S0036142997317353.

[11] S. C. Brenner and L. R. Scott. *The Mathematical Theory of Finite Element Methods.* Springer, second edition, 2002.

[12] Timothy J. Crowley, Edward S. Meadows, Evangelos Kostoulas, and Francis J. Doyle III. Control of particle size distribution described by a population balance model of semibatch emulsion polymerization. *Journal of Process Control*, 10(5):419 – 432, 2000. DOI: http://dx.doi.org/10.1016/S0959-1524(00)00017-2.

[13] C. Diaz-Goano, P. Minev, and K. Nandakumar. A lagrange multipliers/fictitious domain approach for particulate flow. In Svetozar Margenov, Jerzy Wasniewski, and Plamen Yalamov, editors, *Large-Scale Scientific Computing*, volume 2179 of *Lecture Notes in Computer Science*, pages 409–416. Springer Berlin Heidelberg, 2001. DOI: 10.1007/3-540-45346-6_43.

[14] Christophe Duchanoy and Thibauld R.G. Jongen. Efficient simulation of liquid-solid flows with high solids fraction in complex geometries. *Computers and Fluids*, 32(10):1453 – 1471, 2003. DOI: 10.1016/S0045-7930(02)00102-0.

[15] A. F. Fortes, D. D. Joseph, and T. S. Lundgren. Nonlinear mechanics of fluidization of beds of spherical particles. *Journal of Fluid Mechanics*, 177, 1987. DOI: 10.1017/S0022112087001046.

[16] Dominik Göddeke. *Fast and Accurate Finite-Element Multigrid Solvers for PDE Simulations on GPU Clusters*. PhD thesis, Technische Universität Dortmund, Fakultät für Mathematik, 2010.

[17] V. Girault and P. A. Raviart. *Finite element methods for Navier-Stokes equations.* Springer, 1986.

[18] R. Glowinski, T.W. Pan, T.I. Hesla, and D.D. Joseph. A distributed lagrange multiplier/fictitious domain method for particulate flows. *International Journal of Multiphase Flow*, 25(5): 755 – 794, 1999. DOI: 10.1016/S0301-9322(98)00048-2.

[19] R. Glowinski, T.W. Pan, T.I. Hesla, D.D. Joseph, and J. Periaux. A fictitious domain approach to the direct numerical simulation of incompressible viscous flow past moving rigid bodies: Application to particulate flow. *Journal of Computational Physics*, 169(2):363 – 426, 2001. DOI: 10.1006/jcph.2000.6542.

[20] Roland Glowinski. Finite element methods for incompressible viscous flow. In P.G. Ciarlet and J.L. Lions, editors, *Numerical Methods for Fluids (Part 3)*, volume 9 of *Handbook of Numerical Analysis*, pages 701 – 769. Elsevier, 2003. DOI: 10.1016/S1570-8659(03)09003-3.

[21] C.W Hirt, A.A Amsden, and J.L Cook. An arbitrary lagrangian-eulerian computing method for all flow speeds. *Journal of Computational Physics*, 14(3):227 – 253, 1974. DOI: 10.1016/0021-9991(74)90051-5.

[22] H.H. Hu. Direct simulation of flows of solid-liquid mixtures. *International Journal of Multiphase Flow*, 22(2):335 – 352, 1996. DOI: 10.1016/0301-9322(95)00068-2.

[23] H.H. Hu, D.D. Joseph, and M.J. Crochet. Direct simulation of fluid particle motions. *Theoretical and Computational Fluid Dynamics.*, 3:285–306, 1992.

[24] Reima Iwatsu, Katsuya Ishii, Tetuya Kawamura, Kunio Kuwahara, and Jae Min Hyun. Numerical simulation of three-dimensional flow structure in a driven cavity. *Fluid Dynamics Research*, 5(3):173 – 189, 1989. DOI: 10.1016/0169-5983(89)90020-8.

[25] V. John. Higher order finite element methods and multigrid solvers in a benchmark problem for the 3d navier-stokes equations. *Int. J. for Numerical Methods in Fluids*, 40:775–798, 2002.

[26] A. A. Johnson and T. E. Tezduyar. Simulation of multiple spheres falling in a liquid-filled tube. *Computer Methods in Applied Mechanics and Engineering*, 134:351–373, 1995.

[27] Aline Lefebvre. Numerical simulation of gluey particles. *ESAIM: Mathematical Modelling and Numerical Analysis*, pages 53–80, 2009. DOI: 10.1051/m2an/2008042.

[28] Stefan Luding. Introduction to discrete element methods. *European Journal of Environmental and Civil Engineering*, 12(7-8):785–826, 2008. DOI: 10.1080/19648189.2008.9693050.

[29] Dan B. Marghitu and Mihai Dupac. *Advanced Dynamics: Analytical and Numerical Calculations with MATLAB*. New York, Springer, 2012.

[30] B. Maury. Direct simulations of 2d fluid-particle flows in biperiodic domains. *Journal of Computational Physics*, 156(2):325 – 351, 1999. DOI: 10.1006/jcph.1999.6365.

[31] B. Maury. Characteristics ale method for the unsteady 3d navier-stokes equations with a free surface. *International Journal fo Computational Fluid Dynamics.*, 6:175–188, 1996.

[32] B. Maury. A time-stepping scheme for inelastic collisions. *Numerische Mathematik*, 102(4): 649–679, 2006. DOI: 10.1007/s00211-005-0666-6.

[33] Bertrand Maury. A many-body lubrication model. *J. for Comput. and Appl. Math*, 325(9): 1053 – 1058, 1997. DOI: 10.1016/S0764-4442(97)89104-5.

[34] B.K. Mishra and Raj K. Rajamani. The discrete element method for the simulation of ball mills. *Applied Mathematical Modelling*, 16(11):598 – 604, 1992. DOI: http://dx.doi.org/10.1016/0307-904X(92)90035-2.

[35] A. Munjiza, D.R.J. Owen, and N. Bicanic. A combined finite-discrete element method in transient dynamics of fracturing solids. *Engineering Computations*, 12:145 – 174, 1995. DOI: 10.1108/02644409510799532.

[36] Stanley Osher and Ronald P. Fedkiw. Level set methods: An overview and some recent results. *Journal of Computational Physics*, 169(2):463 – 502, 2001. DOI: http://dx.doi.org/10.1006/jcph.2000.6636.

[37] Abderrahim Ouazzi. *Finite element simulation of nonlinear fluids with application to granular material and powder*. PhD thesis, Technische Universität Dortmund, Fakultät für Mathematik, 2005.

[38] N.A. Patankar, P. Singh, D.D. Joseph, R. Glowinski, and T.W. Pan. A new formulation of the distributed lagrange multiplier/fictitious domain method for particulate flows. *Int. J. Multiphase Flow*, 26:1509–1524, 2000.

[39] S.B. Pillapakkam and P. Singh. A level-set method for computing solutions to viscoelastic two-phase flow. *Journal of Computational Physics*, 174(2):552 – 578, 2001. DOI: 10.1006/jcph.2001.6927.

[40] Alexander V Potapov, Melany L Hunt, and Charles S Campbell. Liquid-solid flows using smoothed particle hydrodynamics and the discrete element method. *Powder Technology*, 116 (2-3):204 – 213, 2001. DOI: 10.1016/S0032-5910(00)00395-8.

[41] M Razzaq, H Damanik, J Hron, A Ouazzi, and S Turek. Fem multigrid techniques for fluid–structure interaction with application to hemodynamics. *Applied Numerical Mathematics*, 62(9):1156–1170, 2012.

[42] Mudassar Razzaq. Finite element simulation techniques for incompressible fluid structure interaction with applications to bioengineering and optimization. 2011.

[43] Mudassar Razzaq, S Turek, J Hron, JF Acker, F Weichert, IQ Grunwald, C Roth, and M Wagner. *Numerical Simulation and Benchmarking of Fluid Structure Interaction with Application to Hemodynamics*. Techn. Univ., Fak. für Mathematik, 2009.

[44] Mudassar Razzaq, C Tsotskas, T Kipouros, M Savill, and J Hron. Multi-objective optimization of a fluid structure interaction benchmarking. *CMES: Computer Modeling in Engineering & Sciences*, 90(4):303–337, 2013.

[45] S. Kim S. and S. J. Karrila. *Microhydrodynamics: Principles and Selected Applications*. Butterworth-Heinemann, Boston, second edition, 1991. ISBN 0486442195.

[46] Yousef Saad. *Iterative Methods for Sparse Linear Systems.* SIAM, second edition, January 2000.

[47] A. Sarthou, S. Vincent, J. P. Caltagirone, and Ph. Angot. Eulerian-lagrangian grid coupling and penalty methods for the simulation of multiphase flows interacting with complex objects. *International Journal for Numerical Methods in Fluids*, 56(8):1093–1099, 2008. DOI: 10.1002/fld.1661.

[48] R.C. Senior and J.R. Grace. Integrated particle collision and turbulent diffusion model for dilute gas-solid suspensions. *Powder Technology*, 96(1):48 – 78, 1998. DOI: 10.1016/S0032-5910(97)03358-5.

[49] Hersir Sigurgeirsson, Andrew Stuart, and Wing-Lok Wan. Algorithms for particle-field simulations with collisions. *Journal of Computational Physics*, 172(2):766 – 807, 2001. DOI: 10.1006/jcph.2001.6858.

[50] P. Singh, T.I. Hesla, and D.D. Joseph. Distributed lagrange multiplier method for particulate flows with collisions. *International Journal of Multiphase Flow*, 29(3):495 – 509, 2003. DOI: 10.1016/S0301-9322(02)00164-7.

[51] Martin Sommerfeld. Validation of a stochastic lagrangian modelling approach for inter-particle collisions in homogeneous isotropic turbulence. *International Journal of Multiphase Flow*, 27(10):1829 – 1858, 2001. DOI: 10.1016/S0301-9322(01)00035-0.

[52] Jiyuan Tu, Guan Heng Yeoh, and Chaoqun Liu. *Computational Fluid Dynamics: A Practical Approach*. Elsevier/Butterworth-Heinemann, Amsterdam Boston, 2013. ISBN 978-0-08-098243-4.

[53] S. Turek. Featflow. finite element software for the incompressible navier-stokes equations: User manual, release 1.1. Technical report, 1998. URL `http://www.featflow.de/`.

[54] S. Turek. *Numerical Analysis of a New Time-stepping θ-scheme for Incompressible Flow Simulations*. Ergebnisberichte angewandte Mathematik. Univ. Dortmund, Fachbereich Mathematik, 2005. URL `http://books.google.de/books?id=qGbTtgAACAAJ`.

[55] Stefan Turek, Decheng Wan, and LiudmilaS. Rivkind. The fictitious boundary method for the implicit treatment of dirichlet boundary conditions with applications to incompressible flow simulations. In Eberhard Baensch, editor, *Challenges in Scientific Computing - CISC 2002*, volume 35 of *Lecture Notes in Computational Science and Engineering*, pages 37–68. Springer Berlin Heidelberg, 2003. DOI: 10.1007/978-3-642-19014-8_3.

[56] B. C. Vemuri, Y. Cao, and L. Chen. Fast collision detection algorithms with applications to particle flow. *Computer Graphics Forum*, 17(2):121–134, 1998. DOI: 10.1111/1467-8659.00233.

[57] Decheng Wan and Stefan Turek. Fictitious boundary and moving mesh methods for the numerical simulation of rigid particulate flows. *Journal of Computational Physics*, 222(1): 28 – 56, 2007. DOI: http://dx.doi.org/10.1016/j.jcp.2006.06.002.

[58] Decheng Wan and Stefan Turek. Direct numerical simulation of particulate flow via multigrid fem techniques and the fictitious boundary method. *International Journal for Numerical Methods in Fluids*, 51(5):531–566, 2006. DOI: 10.1002/fld.1129.

[59] Decheng Wan and Stefan Turek. An efficient multigrid-fem method for the simulation of solid-liquid two phase flows. *Journal of Computational and Applied Mathematics*, 203(2): 561 – 580, 2007. DOI: 10.1016/j.cam.2006.04.021.

[60] Decheng Wan, Stefan Turek, and Liudmila S. Rivkind. An efficient multigrid fem solution technique for incompressible flow with moving rigid bodies. In Miloslav Feistauer, Vit Dolejsi, Petr Knobloch, and Karel Najzar, editors, *Numerical Mathematics and Advanced Applications*, pages 844–853. Springer Berlin Heidelberg, 2004. DOI: 10.1007/978-3-642-18775-9_83.

[61] Frank Weichert, Lars Walczak, Denis Fisseler, Tobias Opfermann, Mudassar Razzaq, Raphael Münster, Stefan Turek, Iris Grunwald, Christian Roth, Christian Veith, et al. Simulation of intra-aneurysmal blood flow by different numerical methods. *Computational and mathematical methods in medicine*, 2013, 2013.

[62] John F. Wendt, editor. *Computational Fluid Dynamics*. Springer Berlin Heidelberg, 2009. DOI: 10.1007/978-3-540-85056-4.

[63] N. Zhang and Z. C. Zheng. A collision model for a large number of particles with significantly different sizes. *J. Phys. D: Appl. Phys*, 40:2603–2616, 2007.

[64] Y. Zhang and J.M. Reese. Continuum modelling of granular particle flow with inelastic interparticle collisions. *Chemical Engineering Research and Design*, 81(4):483 – 488, 2003. DOI: 10.1205/026387603765173745.

[65] Tarek Zohdi. *An introduction to modeling and simulation of particulate flows*. SIAM, Society for Industrial and Applied Mathematics, Philadelphia, PA, 2007. ISBN 9780898716276.